

**The stochastic movements of individual
streambed grains**

by

J. Kevin Pierce

B.S. Physics, West Virginia University 2013

M.Sc. Physics, University of British Columbia 2016

A THESIS SUBMITTED IN PARTIAL FULFILLMENT
OF THE REQUIREMENTS FOR THE DEGREE OF

Doctor of Philosophy

in

THE FACULTY OF ARTS

(Department of Geography)

The University of British Columbia

(Vancouver)

June 2021

© J. Kevin Pierce, 2021

Abstract

Bedload transport is the movement of coarse grains through river channels by bouncing, rolling, and sliding. Because coarse grains control river stability, predicting the rate of bedload transport is a fundamental problem in river science. This problem is usually approached with continuum mechanics, but this approach is questionable considering that coarse sediment grains rarely move in densities approximating a continuum.

An alternative approach describes bedload transport from the trajectories of individual grains using statistical physics. This approach has become increasingly popular in recent decades, but many fundamental issues prevent this approach from being widely adopted. In particular, the connection between individual particle trajectories and transport rates remains unclear, and particle trajectory models remain highly simplified. Feedbacks between topography and sediment transport remain challenging to analyze, and basic properties of bedload motions like downstream travel velocities remain incompletely understood. Buried particles cannot move downstream, but even this simple observation has not been comprehensively described in the statistical physics approach.

This thesis presents four projects completed in my PhD which overcome these issues to provide new understanding of bedload transport from a statistical point of view. First, I demonstrate how to calculate the sediment flux from the dynamics of individual grains, and I model the trajectories of grains alternating through motion and rest having fluctuating velocities in the motion state. This work links the sediment flux to the grain-scale dynamics and describes particle trajectories in unprecedented detail. Second, I include

feedbacks between local bed elevations and sediment transport, quantifying the interplay of bed elevation changes and sediment transport rates, and predicting how long particles can stay buried in the riverbed. Third, I incorporate this sediment burial process into a model of downstream sediment transport, predicting how grains move downstream when they can become buried. Finally, I concentrate on bedload dynamics at short timescales, predicting the movement velocities of bedload particles using methods adopted from granular physics. I conclude by summarizing these developments, discussing their implications for the statistical description of bedload transport, and suggesting how we can use this modelling progress to better understand landscapes.

Lay Summary

Predicting the flow rates of gravel through river channels is important to manage environmental issues involving rivers. Most approaches to predict gravel flow consider gravel as if it were a heavy fluid. This description oversimplifies the problem, since gravel flow is actually individual grains bouncing and rolling downstream, which is hardly like a fluid.

In this thesis, I consider gravel flow as the result of individual grains. Using physics and probability, I calculate how fast individual grains move downstream, then I demonstrate how to use their downstream movement paths to predict overall gravel flow rates. This research produces a more realistic description of gravel movement in rivers which helps us understand how rivers change through time.

Preface

This thesis is entirely the original research of Kevin Pierce, including all figures, writing, and calculations. The supervisory committee and especially the research supervisor Marwan Hassan provided guidance in the research. The thesis includes two published works, Chapters 3 and 4, available in *Journal of Geophysical Research: Earth Surface* and *Geophysical Research Letters* respectively, with Marwan Hassan as coauthor (*Pierce and Hassan, 2020a,b*). Chapters 2 and 5 will be submitted for publication subsequent to submission of the thesis.

Contents

Abstract	ii
Lay Summary	iv
Preface	v
Contents	vi
List of Tables	xii
List of Figures	xiii
Acknowledgments	xxii
1 Sediment transport and landscape evolution	1
1.1 Theories of individual particle movement	3
1.1.1 Motivation: tracers and basic understanding	5
1.1.2 Einstein's random walk model	5
1.1.3 Inclusion of the movement duration	8
1.1.4 The Newtonian approach	11
1.1.5 Mechanistic-stochastic models for the sediment velocity distribution	12
1.1.6 The definition of the flux	14
1.1.7 The scaling arguments of Bagnold	16
1.1.8 Einstein's probabilistic approach	17

1.1.9	Fusing Einstein and Bagnold: The erosion-deposition model	19
1.1.10	The nonlocal formulation	21
1.1.11	Landscape evolution	22
1.1.12	Fluctuations and scale dependence	23
1.1.13	Birth death models for bedload flucuations	24
1.1.14	Renewal theories for scale dependence	26
1.2	Summary	28
1.3	Outline of the thesis	28
1.3.1	Problem 1: The scale-dependent flux from individual particle dynamics	28
1.3.2	Problem 2: Feedbacks between sediment transport fluctuations and bed elevation change	29
1.3.3	Problem 3: The effect of sediment burial on downstream transport of sediment tracers	30
1.3.4	Problem 4: The control of particle-bed collisions over bedload particle velocity distributions	30
2	From particle dynamics to the sediment flux	31
2.1	Introduction	31
2.2	Description of motion-rest alternation with velocity fluctuations	33
2.2.1	Dynamical equation for grain-scale sediment transport	34
2.2.2	Derivation of the master equation for the sediment position distribution	35
2.3	Formalism for the downstream sediment flux	36
2.4	Results	40
2.4.1	Position probability distribution of sediment particles	40
2.4.2	The moments of particle position through motion-rest alternation	42
2.4.3	Calculation of the sediment flux	43
2.5	Discussion	44
2.5.1	Fluctuations and collective motions	46

2.5.2	Measuring the sediment flux	47
2.5.3	Limitations and next steps	48
2.6	Summary	48
3	Analysis of bed elevation change and sediment transport fluctuations	50
3.1	Stochastic model of bedload transport and bed elevations	53
3.2	Model solutions	57
3.2.1	Numerical study of the joint model	57
3.2.2	Approximate solutions of the joint model	59
3.3	Results	61
3.3.1	Probability distributions of bedload transport and bed elevations	61
3.3.2	Statistical moments of bed elevation and the particle activity	62
3.3.3	Collective entrainment and bedload activity fluctuations	65
3.3.4	Resting times of sediment undergoing burial	65
3.4	Discussion	68
3.4.1	Context of the research	68
3.4.2	New contributions	69
3.4.3	Next steps for research	70
3.5	Summary	72
4	Burial-induced three-range diffusion in sediment transport	73
4.1	Bedload trajectories as a multi-state random walk	76
4.1.1	Assumptions of the burial model	76
4.1.2	Governing equations	77
4.1.3	Joint probability distribution of particle position with burial	78
4.1.4	Downstream diffusion	80
4.1.5	Diffusion exponents and three range scaling	81
4.2	Discussion	83

4.2.1	Local and intermediate ranges with comparison to earlier work	83
4.2.2	Global and geomorphic ranges with next steps for research	85
4.3	Summary	86
5	Collisional Langevin model of bedload sediment velocity distributions	88
5.1	Introduction	88
5.2	Mechanistic description of particle velocities	91
5.2.1	Episodic collisions	92
5.2.2	Turbulent fluid forces	94
5.2.3	Langevin equation for collisional bedload transport	95
5.2.4	Chapman-Komogorov equation and particle-bed collision integral	96
5.3	Results	97
5.3.1	Derivation of the bedload velocity distribution	97
5.3.2	Exponential and Gaussian regimes: limits to earlier work	99
5.3.3	Comparison with experimental data	101
5.4	Discussion	102
5.4.1	Does the velocity distribution depend on particle size?	105
5.5	Summary	106
6	Summary and future work	107
6.1	Overall methodology of the thesis	108
6.1.1	Langevin and master equations	108
6.1.2	Idealized noises and their combinations	108
6.2	Key contributions	110
6.2.1	Calculation of the probability distribution of the sediment flux from micromechanics of particle transport	110
6.2.2	Inclusion of velocity fluctuations into Einstein's model of individual particle trajectories	110

6.2.3	Quantification of the control of bed elevation fluctuations over sediment transport fluctuations	111
6.2.4	Characterization of how sediment burial affects the downstream transport of sediment particles	112
6.2.5	Description of how particle-bed collisions control movement velocities of grains	112
6.3	Limitations and future research directions	113
6.3.1	Landscape dynamics and channel morphology	113
6.3.2	Grain size distributions	114
6.3.3	The full range of geophysical flows	114
6.4	Conclusion	115
	Bibliography	117
A	Calculations involved in dynamical sediment flux model	150
A.1	Derivation of the master equation for particle position	150
A.2	Solution for the position probability distribution	152
A.3	Calculation of the scale-dependent rate function $\Lambda(T)$	155
B	Calculations involved in the sediment burial model	158
B.1	Calculation of the distribution function	158
B.2	Calculation of the moments	161
B.3	Limiting behavior of the moments	162
C	Calculations involved in the bed elevation model	165
C.1	Numerical simulation algorithm	165
C.1.1	Times between transitions of any kind	165
C.1.2	Selection of transitions that occur	166
C.1.3	Pseudo code for the Gillespie SSA	167
C.2	Approximate solutions of the Master equation	168
C.2.1	Mean field solution of particle activity	168
C.2.2	Mean field solution of bed elevations	169
C.2.3	Closure equation approach for bed elevations	170

D Calculations involved in the Collisional Langevin model .	172
D.1 Derivation of Master Equation	172
D.2 Derivation of Steady-state solution	173
D.3 Calculation of the moments	174
D.4 Weak and strong collision limits	175

List of Tables

Table 3.1 Migration, entrainment, and deposition rates at $z(m) = 0$ from <i>Ancey et al.</i> (2008). Units are s^{-1} (probability/time). Bed elevation changes modulate these rates in accord with (3.2-3.5).	58
Table 4.1 Abbreviations used in the expressions of the mean (4.6), second moment (4.7) and variance (4.8) of bedload tracers.	81
Table 5.1 Parameters used to fit the distributions in figure 5.4. The first five columns involve data from the experiments for particle diameter d , shear velocity u_* , particle Reynolds number Re_p , Stokes number St , and Froude number Fr . The final two columns involve values that were tuned to fit the theoretical distribution 5.8 to the experimental data, the dissipation ε and the collision rate ν . Units are indicated in square brackets. One can see a generally increasing relationship between particle size and elasticity, and likewise a decreasing relationship between particle size and collision frequency.	103

List of Figures

Figure 1.1 Panel (a) indicates the representation of Einstein’s model as an idealized “white shot noise”, as indicated in eq. 1.2, while panel (b) shows the “stairstep” trajectories of sediment particles moving downstream through cycles of steps (which are instantaneous) and rests (which have mean duration $1/k_E$).	7
Figure 1.2 Panel (a) indicates the generalization of Einstein’s model to include the interval of sediment motion between entrainment and deposition, now represented with dichotomous noise eq. 1.7, while panel (b) shows the tilted stair-step trajectories of sediment particles moving downstream in cycles of motion at velocity V (with mean duration $1/k_D$) and rest (with mean duration $1/k_E$).	10
Figure 1.3 Panel (a) demonstrates the trajectory of a particle within the Fan et al model, where Coulomb friction impedes turbulent drag. Panel (b) shows the resulting exponential particle velocity distribution, having relatively large fluctuations with mode at $u = 0$. Panel (c) shows the analogous trajectory from the Ancey et al model, where turbulent Stokes drag generates the Gaussian velocity distribution seen in (d). The latter has relatively narrow and symmetric fluctuations, with a positive mode well above $u = 0$	14

- Figure 1.4 Particle fluxes can be defined with either a control volume V or a control surface S . Here, particles are shown moving from time $t - dt$ (faint white particles) to time t (grey particles). Each particle's velocity component u_i in the downstream direction is indicated. At the instant t , the surface definition of the flux 1.17 gives $q = \frac{1}{L}(u_7 + u_8)$, while the volume definition 1.18 gives $\Phi = \frac{1}{L}(u_1 + \dots + u_6)$, showing the non-equivalence of these two definitions. 15
- Figure 1.5 Einstein's conceptual picture (modified from *Yalin (1972)*). Particles move in discrete jumps of length ℓ from left to right through an array of adjacent control volumes. The bedload flux is the rate of particles crossing the surface S per unit width and time, collected from all upstream control volumes. 18
- Figure 1.6 The scale-dependent sediment flux is described as a renewal process. Panel (a) indicates the arrivals of particles at rate Λ , while panel (b) shows an ensemble of realizations of the sediment flux versus the observation time T . Note that different realizations of the flux converge toward the same value at large observation times, whereas at small observation times, uncertainty in the flux is large. This is observation-scale dependence. The nature of this convergence depends on the particle dynamics in an as yet unspecified way. 26

Figure 2.1 Panel (a) sketches a realization of the noise in equation 2.1, while panel (b) shows the trajectory derived from it (in blue) alongside other possible trajectories. Keys in panel (a) demonstrate the average movement time $1/k_D$ and rest time $1/k_E$, while the key in panel (b) shows the average movement velocity V . Velocity fluctuations produce tilted stair-step trajectories with unsteady slopes in the $x - t$ plane. This can be compared with figure 1.2 which does not include fluctuations. 34

Figure 2.2 The left panel indicates the configuration for the flux. The particle trajectories within are calculated from equation 5.3, demonstrating alternation between rest and motion with fluctuating velocity. Particles begin their transport with positions $-L \leq x \leq 0$ at $t = 0$, and as depicted in the right panel, the flux is calculated with the number of particles $N_>(T)$ which lie to the right of $x = 0$ at the observation time $t = T$, divided by T : $q(T) = N_>(T)/T$. The probability distribution of $q(T)$ is determined from all possible realizations of the trajectories and initial positions as N, L tend to infinity while the density of particles $\rho = N/L$ to the left of the control surface remains fixed. . 37

Figure 2.3 Panel (a) indicates the probability distribution of particle position (eq. 2.13) as it evolves through time. From the initial mixture of motion and rest states, particles advect downstream as they diffuse apart from one another due to differences in their velocities and transition times between motion and rest. Panel (b) shows the resulting particle diffusion (eq. 2.16). At timescales $t \ll 2D/V^2$, the diffusion is normal since the movement is approximately a standard Brownian diffusion process. For larger timescales, $2D/V^2 \ll t \ll \tau$, particles undergo ballistic diffusion similar to *Lisle et al.* (1998) as a result of some particles being stationary as others advect. Finally at times longer than the timescale $\tau = 1/k$ associated with entrainment and deposition, diffusion is again normal, formed of particles well-mixed among motion and rest states. All results are scaled by the mean hop length $\ell = V/k_D$ and the timescale $\tau = 1/k$ of the motion/rest alternation. In both plots, the lines are analytical results while the points are the results of Monte Carlo simulations based on evaluating cumulative transition probabilities on a small timestep (e.g. *Barik et al.*, 2006).

Figure 2.4 The mean sediment flux is plotted for different values of the Peclet number $Pe = V^2/(2k_D D)$, characterizing the relative strength of particle velocity fluctuations during motion. The flux is normalized by the prediction $q_0 = E\ell$ of the Einstein theory (sec. 1.1.8). For nonzero velocity fluctuations in the motion state (finite Pe), the Einstein limit is approached as the observation time T grows. Stronger velocity fluctuations (smaller Pe) slow the convergence to this limit. In all cases, satisfactory convergence of the mean flux is achieved when the observation time satisfies $T \gg 1/(k_D Pe)$, as expected by equation 2.19. Plotted lines are the analytical result eq. 2.18, while the points are the results of Monte Carlo simulations. 45

Figure 3.1 Definition sketch of a control volume containing n moving grains and m resting grains. Migration, entrainment, and deposition are represented by arrows, and the instantaneous bed elevation is depicted by dotted lines. The bed is displayed in a degraded state, where $m < 0$. The marginal distributions of n and m are indicated in the upper right panel, while the bottom panel is a realized time-series of bed elevations computed from m using (3.1). 54

Figure 3.2 Panel (a) presents the probability distribution of particle activity n and panel (b) presents the probability distribution of the relative number of particles m for a representative subset of simulations. These distributions represent different flows from table 3.1, distinguished by color, and different values of the active layer depth l (equivalently the coupling constant κ), distinguished by the marker style. The mean field theories (mft) of equations (3.10) and (3.13) are displayed as solid black lines. 62

Figure 3.3 Data from all simulations demonstrating that the active layer depth l characterizes bed elevation changes as posited in equation (3.6): $\sigma_m^2 \approx (l/z_1)^2$	63
Figure 3.4 The shifts between particle activity moments conditioned on instantaneous elevations and their over-all mean values. Panel (a) indicates the mean particle activity shift versus the bed elevation measured in units of $\sigma_z = l$. This shift displays asymmetric dependence on m at the flow conditions of the <i>Ancey et al.</i> (2008) experiments, and departures of the bedload transport mean can be as much as 60% when the bed is in a severely degraded state with $z \approx -3l$. The closure equation (3.12) is plotted in panel (a) Panel (b) demonstrates a more symmetrical variance shift with some dependence on flow conditions displaying shifts of up to 20% with bed elevations. These results indicate that bedload statistics measurements on short timescales could be severely biased by departures from the mean bed elevation.	64
Figure 3.5 The shift of the mean particle activity in panel (a) and its fluctuations in panel (b) with departures of the bed elevation from its mean. All simulations are at flow condition (g) from table 3.1 except λ and μ are modified to shift the fraction $f = \mu/\sigma$ of the over-all entrainment rate E due to collective entrainment. Clearly, collective entrainment drives strong departures of the bedload statistics away from the mean field model (3.10) at large departures from the mean bed elevation. Panel (b) shows particle activity fluctuations suppressed by 90% when $z \approx -3l$ and collective entrainment is the dominant process. When collective entrainment is absent, meaning $\mu/\sigma = 0$, this moment regulation effect vanishes: it is a consequence of collective entrainment.	66

Figure 3.6 Resting time statistics scale differently with transport conditions and the bed elevation variance. Panel (a) shows differing flow conditions at a fixed l value, while panel (c) shows fixed flow conditions at differing l . When scaled by T_0 (3.17), both types of difference collapse in the tails of the distributions, as shown in panels (b) and (d). In panels (b) and (d), the black dotted lines indicate a power law decay of the collapsed tails having parameter $\alpha \approx 1.18$. 67

Figure 4.1 Joint distributions for a grain to be at position x at time t are displayed for the choice $k_1 = 0.1$, $k_2 = 1.0$, $v = 2.0$. Grains are considered initially at rest ($\theta_1 = 1$, $\theta_2 = 0$). The solid lines are the analytical distribution in equation (4.5), while the points are numerically simulated, showing the correctness of our derivations. Colors pertain to different times. Units are unspecified, since the aim is to demonstrate the general characteristics of $p(x, t)$. Panel (a) shows the case $\kappa = 0$ – no burial. In this case, the joint distribution tends toward Gaussian at large times (Einstein, 1937; Lisle *et al.*, 1998). Panel (b) shows the case when grains have rate $\kappa = 0.01$ to become buried while resting. Because of burial, the joint distribution tends toward a more uniform distribution than Gaussian. 79

Figure 4.2 Panel (a) sketches conceptual trajectories of three grains, while panel (b) depicts the variance (4.8) with mean motion time 1.5 s, resting time 30.0 s, and movement velocity 0.1 m/s – values comparable to laboratory experiments transporting small (5 mm) gravels (*Lajeunesse et al.*, 2010; *Martin et al.*, 2012). The burial timescale is 7200.0s (two hours), and grains start from rest ($\theta_1 = 1$). The solid line is equation (4.8), and the points are numerically simulated. Panel (b) demonstrates four distinct scaling ranges of σ_x^2 : local, intermediate, global, and geomorphic. The first three are diffusive. Three crossover times τ_L , τ_I , and τ_G divide the ranges. Within each range, a slope key demonstrates the scaling $\sigma_x^2 \propto t^\gamma$. Panel (a) demonstrates that different mixtures of motion, rest, and burial states generate the ranges. At local timescales, grains usually either rest or move; at intermediate timescales, they transition between rest and motion; at global timescales, they transition between rest, motion, and burial; and at geomorphic timescales, all grains bury. Additional slope keys in the local and global ranges of panel (b) illustrate the effect of initial conditions and rest/burial timescales on the diffusion, while the additional slope key within the geomorphic range demonstrates the expected scaling when burial is not permanent, as discussed in section 4.2. 82

Figure 5.1 Definition sketch of rarefied sediment transport with turbulent fluid drag and particle-bed collision forces. During saltation, pre-collisional streamwise velocities u are transformed to postcollisional velocities $\varepsilon u < u$ 93

- Figure 5.2 Left and right panels are paired. Left panels show velocity realizations as gray traces. Velocities are calculated from Monte Carlo simulations. Individual realizations are singled out as black traces. Particle-bed collisions imply sudden downward-velocity jumps. Flow forces generate fluctuating positive accelerations between collisions. Right panels show simulated histograms of particle velocities and exact solutions from equation 5.8. As elasticity ε varies, the particle velocity distributions interpolate between exponential (inelastic) and Gaussian (elastic) forms. 100
- Figure 5.3 The particle velocity distribution approaches an exponential distribution in (a) as particle-bed collisions become extremely elastic ($\varepsilon \rightarrow 1$), and it approaches a Gaussian in (b) as they become extremely inelastic ($\varepsilon \rightarrow 0$). On the abscissa, the mean sediment velocity is standardized by its mean \bar{u} and standard deviation σ_u 101
- Figure 5.4 This figure compares the available experimental data on velocity distributions and the theoretical velocity distribution 5.8 with parameters ν , ε , and D treated as calibration parameters. In all cases there is good agreement, indicating that the model is capable of the range of distributions exhibited by the experimental data. 104

Acknowledgments

Attending university long enough to earn a PhD is an unbelievable privilege, and I only had access to it thanks to an incredible amount of guidance and support.

Most of all, to mom Calisa Pierce, dad Jim Pierce, my sisters Kelsey and Kim, and my grandmother Wilma Steele, you've formed all of the best parts of my personality and guided me toward this point, and it's impossible to explain how thankful I am for that. Regarding family I will also always be thankful for my great aunt Alice who graciously paid for my undergraduate education.

Thanks to my early teachers who put in the extra care to keep me on track, Jonathan Ramey, Damon Spurlock, Linda Mendez, Linda Afzhalirhad, Phyllis Adkins, Brandon Willard, Marty Ojeda, and Red Hamlin among many others.

Thanks also to my professors at Southern WV Community College who fostered my way of thinking and provided many of the tools I used for the research in this thesis. At SWVCC, I'd like to thank especially Mindy Saunders, Tex Wood, Anne Klein, Charles Wood, Don Saunders, and George Trimble. Mindy built my math and physics foundation with her incredibly effective teaching, Anne showed me there's invisible order in everything, and Tex demonstrated that art will always lead science. SWVCC was a personal transformation and a great privilege.

At WVU, I'd like to thank Alan Bristow, Tudor Stanescu, and Leo Golubovic in particular. Alan and Tudor, thank you for providing my first opportunities in research. Leo, you are the key person in my development

as a researcher. Every time I solve a challenging problem with some Bessel functions or contour integrals, I think “Dr. Golubovic would like this one!” I’ll be successful if I can one day be as influential an educator as you’ve been.

To my extended cohort at WVU physics, Payne, Megat, Collins, Scott, Dustin, Rice, Wolfe, Samet, Craig, April, Evan, Larry, Robert, Stephen, Rick, Matt, Caleb, John, and all of you others, thanks for the collaboration and the hilarious times. I’ll never forget Scott’s quaternions, Samet’s olympiad problems, or Megat’s power tower magic (which still blows my mind). I hope the lounge is still happening, that its residents by some miracle still have 24 hour access into the building, that some barefoot Megat-like character is still gaming in the corner, that they have some Andrew Rice imitator for comic relief, and that an esteemed graduate student like Payne still finds time to stoop to the lounge-residents’ level. May the lounge live on forever!

Now we come to Marwan Hassan. Some time ago now I wandered into your office saying I liked rivers and wanted to describe sediment transport with statistical physics. I realize now when I said “statistical physics” your eyes lit up with visions of Einstein, Nakagawa, Yano, and so many other names I now know well. I was lucky to use the right trigger words. Marwan, thanks for taking the risk on me, for all of the guidance, for lending me hundreds of books and papers, for giving me freedom to explore ideas, and most of all for showing me that it’s ok (and implicitly expected) to be human in science.

My friends in geography have also been great. Thanks to the whole extended research family: Shawn, Matteo, Conor, Nisreen, Yinlue, Alex, Kyle, Leo, Dave, Tobias, Katie, Maria, Elli, Jiamei, Xingyu, Niannian, and Emma, plus the outsider Eaton-ites, Will, Dave, Rose, and Anya. In particular thanks to Shawn for all of the shared speculations, and Matteo and Conor – friendships forged through suffering! We’ll have to keep in touch and form productive research collaborations once Matteo returns from retirement.

Thank you Rui Ferreira and Brett Eaton! Rui, you welcomed me to

Portugal, offered me guidance in the laboratory, and educated me on turbulence and hydraulics. Your kindness, physics knowledge, and wide-ranging interests beyond physical science are inspiring. Thanks for the thoughtful comments and advice on my PhD. I'm not forgetting what I owe you! I will always be impressed at your concise way of speaking and unbounded kindness. Brett, you were the first person to welcome me to UBC, and I'll always appreciate your effort to teach me how to write, interpret flume experiments, and understand simplified modelling in light of real world complexity. Although I'm not sure if I understood your lessons as well as you would have liked, I still have a list of your favorite books on my computer, and they're a first task for as soon as I'm done. Maybe they'll bring me closer to your way of thinking.

I'd be amiss not to mention David Furbish. Before I started my PhD, when I was still exclusively a physics kid, I attended Furbish's colloquium in Geography at Marwan's invitation. At the end I asked a vague question about whether Langevin equations might be useful for describing sediment transport, and the answer was "absolutely yes". Now I have a thesis on it. David later recruited me into a lovely series of meetings where we discussed gases with adhesion, moon craters, entropy, soft matter, martian hillslopes, the social impacts of disinformation, and a whole range of questions in natural philosophy. David, Rachel, Sarah W, Sarah Z, Nakul, Tyler, Erika, and Shawn, thanks sincerely for letting me board the spaceship.

Among UBC Geographers I'd like to thank Nina Hewitt in particular. It was always a pleasure and sometimes a sigh of relief to TA your courses, which are so uniquely organized and student-focused. UBC Geography is a much greater department with you in it.

Finally, Mary! My PhD has not been great in terms of work-life balance. Thanks for sticking it out, putting up with my late bedtimes, early wakeups, the rambling science jargon, and all of the social events I skipped. It's time! I'm done. I'm ready for an extensive tour of the gap and some beautiful Queensland beaches with your family, featuring SPF110 and an incredibly giant umbrella. I hope to take up still-lives with Marianne's coaching. After that, we're a step closer to settling what colour cat we're gonna get. I'm

personally now leaning toward white.

Completing a PhD looks like a personal achievement, but it's really not. It's an expression of 30 years of influence and guidance from other people at every stage, my parents, my sisters, my grandmother, and a huge network of teachers and mentors. Thank you all for every part of it.

Chapter 1

Sediment transport and landscape evolution

Landscapes evolve when water, wind, and ice, driven by gravity, erodes down slopes produced by tectonics. Channels initiate along faults and depressions wherever climatic conditions are suitable, incising networks in the landscape and transferring sediments from uplands to lowlands. Earth's biota colonize these networks which form conduits for migration, transmitting water, genetic information, and organic material alike, while biota and chemical decomposition convert sediments to soils, staging the joint evolution of life and landscapes which has occurred across geological time.

Human impacts on these old patterns have become severe, in what has been characterized as an environmental and social crisis (*Slagmaker et al.*, 2021). Research demonstrates unprecedented recent shifts in ancient climatic (*Sivan et al.*, 2004; *Slater et al.*, 2021), denudational (*Hooke*, 2000; *Szabo et al.*, 2010), and biotic patterns (*Walther et al.*, 2002; *Willis and Bhagwat*, 2009), requiring effective aquatic habitat restoration, contaminant management, and engineering strategies more than ever before.

In this context river geomorphology as a scientific discipline has shifted toward more quantitative methods that enable concrete predictions about the natural world (*Church*, 2005, 2010). Sediment transport in river channels is especially amenable to this quantitative approach since it is mechanisti-

cally the result of fluid and granular physics. Sediment moves in different modes depending on the relative importance of the fluid forces against the weight of grains (*Bagnold*, 1956). When particles are coarse, as in gravel-bed rivers, the fluid forces are relatively weak and particles move as “bedload”, by bouncing, rolling, and sliding along the bed surface (*Kalinske*, 1947). In bedload transport conditions, fluid turbulence and the irregular bed surface adopt particular control over the sediment dynamics (*Ferreira et al.*, 2015).

Bedload transport exerts unique influence over channel morphology and stability (*Church*, 2006; *Recking et al.*, 2016), in part because the coarsest grains in a river provide a partially-immobile skeleton upon which sedimentary deposits can develop (*Eaton et al.*, 2020; *Hassan et al.*, 2007). A longstanding problem in river science is therefore to determine the bedload flux, or the rate of coarse sediment movement. Unfortunately, existing approaches to compute the bedload flux are inadequate, and predictions often deviate from measured values by orders of magnitude (*Barry et al.*, 2004; *Bathurst*, 2007; *Gomez and Church*, 1989; *Recking et al.*, 2012). Given that the problem has been researched intensively for over a century now (*Gilbert*, 1914), it is clear that new research strategies are needed (*Ancey*, 2020a; *Ancey and Pascal*, 2020).

Predicting bedload fluxes is challenging because transport is not always well correlated to average characteristics of the flow and bed material. Local fluxes can range through orders of magnitude as details of turbulent fluctuations and bed organization vary, while average characterizations of flow and sediment remain constant (*Charru et al.*, 2004; *Hassan et al.*, 2007; *Sumer et al.*, 2003; *Venditti et al.*, 2017). The same turbulence and sediment organization details which correlate with the bedload flux are also modified by it. Turbulent impulses drive sediment motion (*Amir et al.*, 2014; *Celik et al.*, 2014; *Shih et al.*, 2017; *Valyrakis et al.*, 2010), but moving sediment affects turbulent flow characteristics (*Liu et al.*, 2016; *Santos et al.*, 2014; *Singh et al.*, 2010). The surface arrangement and consolidation of grains (*Dwivedi et al.*, 2012; *Miller and Byrne*, 1966; *Paintal*, 1971) affects sediment mobility, but transport rearranges grains and consolidates the bed (*Allen and Kudrolli*, 2018; *Charru et al.*, 2004; *Kirchner et al.*, 1990; *Masteller et al.*,

2019; *Pretzlav et al.*, 2020). Bedload fluxes are in cyclical feedback with their controls (*Jerolmack and Mohrig*, 2005), and this challenges us to step beyond descriptions based on averaged values (*Ancey*, 2020b).

The approach taken in this thesis is to consider bedload transport as an aggregate result of many individual transported grains whose movements have probabilistic characteristics. This departs from the traditional strategy of correlating transport rates to the average flow and sedimentary characteristics (*Meyer-Peter and Müller*, 1948; *Parker*, 1990; *Wilcock*, 2001). Because the trajectories of individual grains are governed by Newtonian mechanics, this approach brings powerful tools to the problem, but it is nonetheless complicated because the forces driving and resisting sediment motion vary through space and time due to fluid turbulence and the erratic interactions of moving particles with the bed.

To address these complications, I develop in this thesis a handful of new bedload transport models using methods adopted from statistical physics. To provide context and motivation, the thesis begins by reviewing earlier approaches to bedload transport which my work is most related to, rephrasing works as necessary during this review to indicate common themes and show continuity with my own developments which follow in subsequent chapters.

1.1 Theories of individual particle movement

A basic problem in sediment transport theory is to predict the downstream movement of individual particles. At first glance, this seems an elementary problem in general physics, but numerous challenges appear. Particles moving as bedload are driven downstream by a turbulent fluid flow, but the exact relationships between the fluid flow and the applied forces are not exactly known (*Maxey and Riley*, 1983; *Schmeeckle et al.*, 2007). Downstream movement is resisted by frictional encounters (skidding, pivoting, colliding) between moving particles and the bed, but since the bed is a granular surface, its geometry is difficult to characterize (*Gordon et al.*, 1972), and the role of bed interactions is challenging to describe (*Niño and García*, 1998; *Sekine and Kikkawa*, 1992).

Entrainment and deposition provide an additional layer of complexity. Moving particles that encounter the bed with sufficiently low velocities can settle into pockets which protect them from the flow (*Miller and Byrne*, 1966) and cause deposition (*Charru et al.*, 2004). These pockets are not permanent shelter because rearrangement of the surrounding bed by entrainment of neighboring particles or subsurface creep (*Frey*, 2014; *Houssais et al.*, 2016) can re-expose particles to the flow, and sufficiently strong turbulent fluctuations (*Cameron et al.*, 2020) can overcome shelter even if its geometry is not disturbed (*Celik et al.*, 2014; *Valyrakis et al.*, 2010). As a result, particles generally alternate through sequences of entrainment and deposition, but the exact times at which these alternations occur is difficult to characterize (*Einstein*, 1937).

Particles at rest on the bed surface can also become covered by other transported particles (*Yang and Sayre*, 1971). These buried particles cannot move again until those burying them have been transported away (*Nakagawa and Tsujimoto*, 1981), generating long periods of immobility (*Ferguson and Hoey*, 2002; *Hassan and Church*, 1994).

Individual trajectories of particles therefore involve a number of contributing processes which occur over different characteristic timescales, from seconds to years (*Pretzlav et al.*, 2021), and each of these processes has so far evaded any exact description.

Nikora et al. (2001a, 2002) provided a conceptual framework which helps to organize this complexity. Nikora et al divided the downstream tractors of individual particles into three timescales, or “ranges”, termed local, intermediate, and global. The local range refers to the period of motion between subsequent interactions with the bed, when the particles accelerate downstream within the turbulent flow. The intermediate range reflects particle motions through sequences of bed encounters, when particles alternately accelerate and decelerate. The global range refers to particle trajectories through sequential entrainment and deposition events as they cycle between motion and rest. *Hassan and Bradley* (2017) added an additional range, referred to as “geomorphic”, to reflect the even longer period over which particles become buried within the subsurface or embedded among sedimen-

tary deposits (*Bradley*, 2017). This set of timescales – local, intermediate, global, and geomorphic – are used below to organize the literature describing trajectories of individual grains.

1.1.1 Motivation: tracers and basic understanding

An early motivation to understand individual particle motions was to predict the efficiency of sediment transport measurements (*Ettema and Mutel*, 2004), and this motivation still drives a great deal of research into individual particle motions today (*Hassan and Bradley*, 2017; *Pretzlav et al.*, 2021). A common technique to estimate sediment transport is to seed a stream with tracer stones and track their progress downstream (*Einstein*, 1937; *Pretzlav et al.*, 2021; *Takayama*, 1965). In principle, tracers provide a proxy for the population of grains in a stream, so one can estimate tracer velocities of tracers, then multiply by an estimate of the number of grains available for motion to calculate the overall sediment flux (*Ferguson and Hoey*, 2002; *Wilcock and McArdell*, 1997). In practice, challenges arise due to the distinct behavior of tracers over the local, intermediate, global, and geomorphic timescales. Apparently, tracer velocities depend on the observation time, in a phenomenon which has been called “advectional slowdown” (*Ferguson and Hoey*, 2002; *Haschenburger*, 2011, 2013; *Pelosi et al.*, 2014). This obscures the relationship between measured tracer velocities and actual sediment fluxes, exposing a need for further research into how exactly individual particle motions depend on observation scale and what processes generate advectional slowdown.

1.1.2 Einstein’s random walk model

Einstein was probably the first to model the movements of individual particles through streams (*Einstein*, 1937). Watching painted tracers move through a flume, Einstein came to the conclusion that the movement characteristics of any one particle could not be predicted, so he turned to probabilistic methods to characterize their transport.

Einstein’s key insight was to represent particle motions as an alternat-

ing sequence of movements and rests having random characteristics. As his interest was on the global range of particle motion when many motion-rest alternations have occurred, and because the duration of particle motions is usually short compared to rests, Einstein made the approximation that individual motions (between entrainment and deposition) are mathematically instantaneous. With this approximation, the downstream movement of sediment becomes an alternate cycle of instantaneous steps of random length, separated by rests of random duration. Implicitly, this picture of sediment trajectories assumes that movement velocities are infinite.

Einstein's experiments indicated that both step lengths and resting times were well-described by exponential distributions, and the focus of his PhD was to find the probability density $P(x, t)$ that a particle had travelled a net distance x after a time t has elapsed. In the course of this research, Einstein formulated an example of what is now called the continuous time random walk, but this was not formalized until much later (*Montroll, 1964*).

Einstein's assumptions imply that if the position of a single sediment particle at a given time is $x(t)$, the assumptions of infinite movement velocity, random resting durations, and random movement distances between entrainment and depositon (step lengths) can be written

$$\dot{x}(t) = \mu(t), \quad (1.1)$$

where $\dot{x} = dx/dt$, and $\mu(t)$ is a white shot noise (*Van Den Broeck, 1983*), which is essentially a sequence of pulses having random heights with mean height ℓ (the mean step length), and random locations in time with mean separation $1/k_E$ (the mean resting time, interpreted as the reciprocal of the entrainment rate k_E). A particular realization of this pulsed noise can be written

$$\mu(t) = \sum_{i=1}^{N(t)} s_i \delta(t - t_i). \quad (1.2)$$

Here $N(t)$ is the number of particle entrainments in time t which is a Poisson random variable, distributed as $P(N) = e^{-k_E t} (k_E t)^N / N!$. The t_i are distributed according to $P(t) = k_E \exp(-k_E t)$, and the s_i are step lengths dis-

tributed according to $P(s) = \ell^{-1} \exp(-s\ell^{-1})$. Figure 1.1 panel (a) sketches the pulsed noise $\mu(t)$, and panel (b) sketches the resulting global range bed-load sediment trajectories as a sequence of steps and rests.

Equation 1.1 is a kind of dynamical equation representing how the position of a sediment grain evolves through time (*Kubo et al.*, 1978), similar to Newtonian mechanics (*Goldstein*, 1997) but with random driving term (equation 1.2).

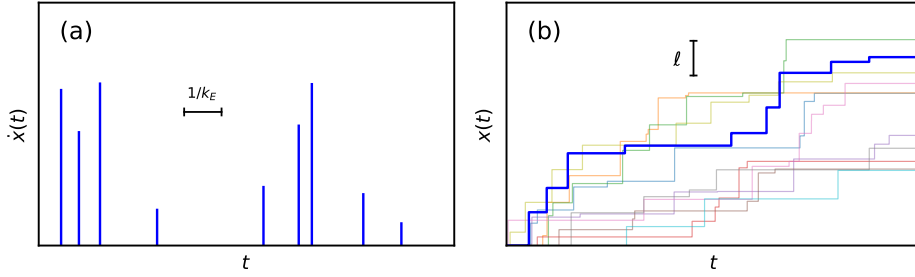


Figure 1.1: Panel (a) indicates the representation of Einstein's model as an idealized “white shot noise”, as indicated in eq. 1.2, while panel (b) shows the “stairstep” trajectories of sediment particles moving downstream through cycles of steps (which are instantaneous) and rests (which have mean duration $1/k_E$).

The governing equation of the distribution $P(x, t)$ to find the particle at x can be calculated as an ensemble average of $\delta(x - x(t))$ over all possible realizations of the noise (*Moss and McClintock*, 1989; *Risken*, 1984). Different methods exist to compute such averages (*Balakrishnan*, 1993; *Hanggi*, 1978, 1984; *Van Den Broeck*, 1983), but whatever the approach, the governing equation for the distribution comes out as

$$(\ell \partial_x \partial_t + k_E \ell \partial_x + \partial_t) P(x, t) = 0. \quad (1.3)$$

This equation can be solved by standard methods (series solutions or transform calculus) (*Arfken*, 1985; *Prudnikov et al.*, 1992) to reproduce the original result of *Einstein* (1937) for the probability distribution of position of

a sediment particle:

$$P(x, t) = \left[\delta(x)e^{-k_E t} + e^{-k_E t - x/\ell} \sqrt{\frac{k_E t}{\ell x}} \mathcal{I}_1\left(2\sqrt{\frac{k_E t}{\ell}}\right) \right] \theta(x)\theta(t) \quad (1.4)$$

Here, \mathcal{I}_ν is a modified Bessel function of order ν . The probability distribution eq. 1.4 fully characterizes the downstream movement of an individual particle alternating randomly through steps and rests.

This distribution displays both advection and diffusion. Advection occurs because particles move downstream. Diffusion occurs because step lengths and instants when entrainment events occur vary from one particle to the next.

One can calculate all moments of the position by multiplying eq. 1.3 by x^n and integrating over space. This gives the mean position of the particle

$$\langle x(t) \rangle = k_E \ell t. \quad (1.5)$$

This equation indicates that in Einstein's model, sediment grains move with effective velocity $V_{\text{eff}} = k_E \ell$ given by the product of the entrainment rate and mean step length.

The rate at which particles spread apart due to differences in their trajectories can be represented by the variance of position, $\sigma_x^2 = \langle x^2 \rangle - \langle x \rangle^2$. This gives

$$\sigma_x^2(t) = 2k_E \ell^2 t, \quad (1.6)$$

so particles in Einstein's model spread apart as a normal diffusion process $\sigma_x^2 = 2D_{\text{eff}} t$ (*Sokolov*, 2012), with an effective diffusivity $D_{\text{eff}} = k_E \ell^2$.

1.1.3 Inclusion of the movement duration

Einstein's model provides an adequate description of global range particle transport when the period of interest is much larger than the timescales of individual particle movements (local and intermediate ranges) and much smaller than the timescales over which particles become embedded in sedimentary deposits (geomorphic range).

The advent of high speed camera experiments produced new insight into the local and intermediate ranges of bedload motion (*Abbott and Francis*, 1977; *Drake et al.*, 1988; *Francis*, 1973) which *Einstein* (1937) never intended for his model to describe. In the local range, particles move with a fluctuating velocity due to the variable drag of the turbulent flow (*Fathel et al.*, 2015; *Lajeunesse et al.*, 2010) and changes in the particle's height within the flow profile (*van Rijn*, 1984; *Wiberg and Smith*, 1985). In the intermediate range, particle-bed collisions impart additional variability to sediment velocities (*Gordon et al.*, 1972; *Martin*, 2013). Einstein's instantaneous movement assumption obscures the timescales over which these processes occur.

Studies by *Lisle et al.* (1998), and *Lajeunesse et al.* (2017) generalized the Einstein theory to include intermediate timescales. They approximated particle velocities as constant (neglecting fluctuations), and assumed that the movement times are exponentially distributed random variables just like resting times, but this time characterized by a deposition rate k_D , whose reciprocal is the average period of time a particle spends in motion between entrainment and deposition. The analogue of Einstein's model equation 1.1 with a finite movement velocity V can be written

$$\dot{x} = V\eta(t), \quad (1.7)$$

This noise is displayed in figure 1.2 panel (a). Some particle trajectories produced by equation 1.7 are displayed in figure 1.2 panel (b).

The governing equation of the position probability distribution $P(x, t) = \langle \delta(x - \int_0^t V\eta(t')dt') \rangle$ becomes (*Balakrishnan*, 1993)

$$(\partial_t^2 + V\partial_x\partial_t + k_E V\partial_x + k\partial_t)P(x, t) = 0, \quad (1.8)$$

where k_E and k_D are the entrainment and deposition rates, V is the particle velocity during the motion state, and $k = k_E + k_D$. This partial differential equation is called an asymmetric telegrapher's equation (*Rossetto*, 2018), and although the symmetric analogue of this equation is well-studied (*Masoliver and Lindenberg*, 2017; *Weiss*, 2002), the asymmetric problem is not

often encountered.

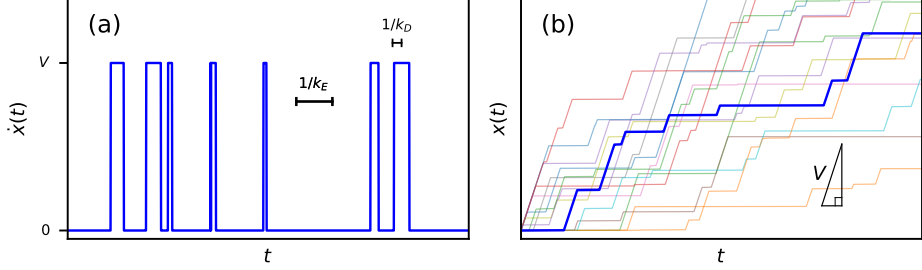


Figure 1.2: Panel (a) indicates the generalization of Einstein’s model to include the interval of sediment motion between entrainment and deposition, now represented with dichotomous noise eq. 1.7, while panel (b) shows the tilted stair-step trajectories of sediment particles moving downstream in cycles of motion at velocity V (with mean duration $1/k_D$) and rest (with mean duration $1/k_E$).

For the initial condition that particles have a probability k_E/k to start in motion, reflecting steady state conditions as far as alternation between motion and rest are concerned (e.g. *Ancey et al.*, 2006), the solution of equation 1.8 is (*Lisle et al.*, 1998)

$$P(x, t) = e^{-\chi - \tau} \left[\frac{k_E}{V} \delta(\tau) + \frac{k_E}{V} \sqrt{\frac{\chi}{\tau}} \mathcal{I}_1(2\sqrt{\chi\tau}) + \frac{k_D}{V} \mathcal{I}_0(2\sqrt{\chi\tau}) + \frac{k_E k_D}{kV} \sqrt{\frac{\tau}{\chi}} \mathcal{I}_1(2\sqrt{\chi\tau}) + \frac{k_E k_D}{kV} \delta(\chi) \right] \theta(\chi) \theta(\tau), \quad (1.9)$$

where $\chi = k_D x/V$ and $\tau = k_E(t - x/V)$ are shorthand notations. Incorporating the duration of sediment motion, the mean position of the sediment grain remains linear in time: $\langle x(t) \rangle = k_E V t / k$, representing movement with an effective velocity $V_{\text{eff}} = k_E V / k$, which is the fraction of time spent in motion (k_E/k) (*Ancey et al.*, 2006) multiplied by the velocity during the motion state. In contrast, the variance develops a two range scaling. Computing σ_x^2 provides

$$\sigma_x(t)^2 = \frac{2k_E k_D V^2}{k^3} \left(t + \frac{1}{k} e^{-kt} - \frac{1}{k} \right), \quad (1.10)$$

which is a non-trivial result. At short times, for $t \ll 1/k$, equation 1.10 shows diffusion $\sigma_x^2 \sim t^2$, which is a faster “ballistic” rate of spreading than the Einstein model predicts (*Sokolov*, 2012). At long times ($t \gg 1/k$), the diffusion becomes normal again ($\sigma_x^2 = 2D_{\text{eff}}t$), with an effective diffusion constant $D_{\text{eff}} = k_E k_D V^2 / k^3$. The rapid spreading of particles at short timescales occurs because some are completely stationary while others move with velocity V .

The eventual transition to normal diffusion occurs because particles eventually become well-mixed among motion and rest states. An analogous diffusion phenomenon is described in *Taylor* (1920).

In this trajectory model, both intermediate and global ranges are adequately represented, but local and geomorphic are not, the former since fluctuations of the velocity between entrainment and deposition have been neglected, and the latter since particle burial was not incorporated.

1.1.4 The Newtonian approach

Some authors have modelled local and intermediate ranges of individual particle trajectories by writing approximate Newtonian equations for the dynamics of individual particles and integrating them numerically. Early efforts applied time-averaged fluid forces linked to the logarithmic mean flow velocity profile (*van Rijn*, 1984; *Yalin*, 1963), and later efforts included collision models to modify particle velocities upon bed contact (*Niño and García*, 1998; *Sekine and Kikkawa*, 1992; *Wiberg and Smith*, 1985).

Researchers eventually included realistic granular interactions in many-particle simulations of bedload transport using the discrete element method (*Cundall and Strack*, 1979; *Jiang and Haff*, 1993). The early works utilizing this approach used a two dimensional domain with a highly simplified “slab” flow model (*Jiang and Haff*, 1993), while later works have included synthetic turbulence to drive particles (*Maurin et al.*, 2015; *McEwan and Heald*, 2001; *Schmeeckle and Nelson*, 2003) or clever reduced-complexity representations of the flow (*Clark et al.*, 2015, 2017).

The state of the art within this category of sediment transport models is

to include two-way coupling between particles and the fluid flow. The latter is modelled either by large eddy simulation or direct numerical simulation of the Navier-Stokes equations, while particles provide the boundary condition for the flow (*Elghannay and Tafti*, 2018; *González et al.*, 2017; *Ji et al.*, 2013; *Schmeeckle*, 2014; *Vowinckel et al.*, 2014; *Youse et al.*, 2020). These computational physics models produce impressive insight into the underlying granular and fluid physics mechanisms producing bed load transport (*Frey and Church*, 2011), but analytical models are nevertheless desired for further insight into the problem.

1.1.5 Mechanistic-stochastic models for the sediment velocity distribution

Another category of models have described bedload particle velocities using Langevin equations (*Ancey and Heyman*, 2014; *Fan et al.*, 2014), whereby the particles dynamics are driven by Gaussian white noise (*Kubo et al.*, 1978).

Experimental studies on bedload velocities have provided two major conclusions for the shape of the particle velocity distribution. One subset of observations shows that bedload velocities follow exponential distributions (*Fathel et al.*, 2015; *Furbish et al.*, 2012a; *Lajeunesse et al.*, 2010), and another subset shows Gaussian distributions (*Ancey and Heyman*, 2014; *Heyman et al.*, 2016; *Martin et al.*, 2012).

Fan et al. (2014) set out to describe exponential-distributed bedload particle velocities (u) with the Langevin equation

$$\dot{u}(t) = -\Delta \text{sgn}(u) + F + \sqrt{2D}\xi(t). \quad (1.11)$$

This equation drives the particle velocity by a fluid drag $F + \sqrt{2D}\xi(t)$, where F is a constant, D is a diffusivity that characterizes the magnitude of drag fluctuations, and $\xi(t)$ is a Gaussian white noise with unit variance and vanishing mean (*Gardiner*, 1983). This drag is resisted by a heuristic particle friction term $-\Delta \text{sgn}(u)$, introduced as a proxy for particle-bed collisions. The “Fokker-Planck equation” governing the probability distribution $P(u, t)$

of the particle velocity can be derived from equation 1.11 as (*Risken*, 1984; *Van Kampen*, 2007)

$$\frac{\partial}{\partial t} P(u, t) = -\Delta \frac{\partial}{\partial u} [\text{sgn}(u)P] + D \frac{\partial^2 P}{\partial u^2}, \quad (1.12)$$

implying that the steady-state velocity distribution ($\partial_t P(x, t) = 0$) provided by equation 1.11 is

$$P(u) = \frac{\Delta^2 - F^2}{2\Delta D} \exp\left(-\frac{-\Delta|u| + Fu}{D}\right). \quad (1.13)$$

This is the (two-sided) exponential distribution observed in one subset of experiments.

Ancey and Heyman (2014) formulated a Langevin equation to describe the Gaussian velocity distributions observed in the other subset of experiments. They wrote for the streamwise velocity

$$t_r \dot{u}(t) = -(U - u) + \sqrt{2D} \xi(t), \quad (1.14)$$

where U is the mean velocity of particles, D characterizes the magnitude of velocity fluctuations, and $\xi(t)$ is again a Gaussian white noise with vanishing mean and unit variance. The timescale t_r is a relaxation time over which velocity fluctuations decay. This time, the Fokker-Planck equation is

$$\frac{\partial}{\partial t} P(u, t) = -\frac{\partial}{\partial u} \left[\frac{U - u}{t_r} P \right] + \frac{D}{t_r^2} \frac{\partial^2 P}{\partial u^2}, \quad (1.15)$$

and the steady state solution becomes

$$P(u) = \sqrt{\frac{t_r}{2\pi D}} \exp\left(-\frac{t_r(u - U)^2}{2D}\right), \quad (1.16)$$

which is the Gaussian velocity distribution from the other subset of the experiments. These two models of bedload velocity distributions are summarized in figure 1.3. Although these descriptions describe two end-member sediment velocity distributions, Gaussian and exponential, the underlying mechanical reason why bedload transport has shown multiple velocity dis-

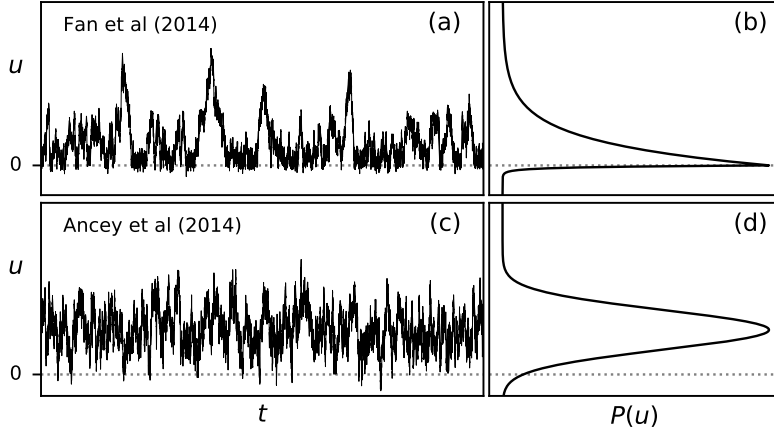


Figure 1.3: Panel (a) demonstrates the trajectory of a particle within the Fan et al model, where Coulomb friction impedes turbulent drag. Panel (b) shows the resulting exponential particle velocity distribution, having relatively large fluctuations with mode at $u = 0$. Panel (c) shows the analogous trajectory from the Ancey et al model, where turbulent Stokes drag generates the Gaussian velocity distribution seen in (d). The latter has relatively narrow and symmetric fluctuations, with a positive mode well above $u = 0$.

tributions remains an open question, and other distributions have been reported besides exponential and Gaussian (e.g. *Houssais and Lajeunesse*, 2012; *Liu et al.*, 2019). A comprehensive model of the full range of bedload transport observations is a desirable target.

1.1.6 The definition of the flux

Perhaps a surprising summary of bedload transport research is that no one definition of the sediment flux has even been agreed upon despite over a century of research (*Ballio et al.*, 2018). Today, there are two main complementary definitions of the bedload flux.

The first definition is reminiscent of continuum mechanics and formulates

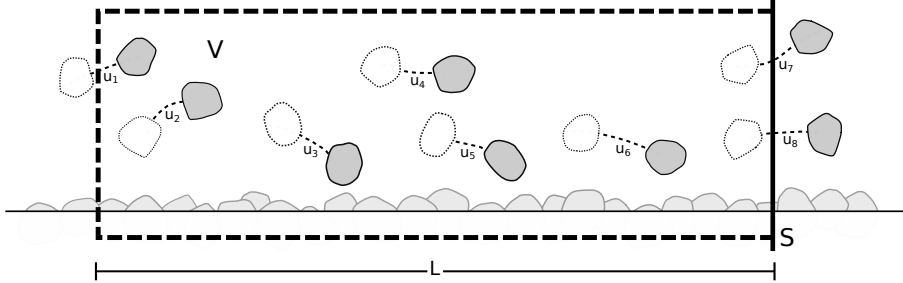


Figure 1.4: Particle fluxes can be defined with either a control volume V or a control surface S . Here, particles are shown moving from time $t - dt$ (faint white particles) to time t (grey particles). Each particle's velocity component u_i in the downstream direction is indicated. At the instant t , the surface definition of the flux 1.17 gives $q = \frac{1}{L}(u_7 + u_8)$, while the volume definition 1.18 gives $\Phi = \frac{1}{L}(u_1 + \dots + u_6)$, showing the non-equivalence of these two definitions.

the flux as a kind of current of sediment across a control surface S (*Ballio et al.*, 2014; *Furbish et al.*, 2012a; *Heyman et al.*, 2016):

$$q = \int_S c(\mathbf{x}, t) \mathbf{u} \cdot d\mathbf{S}. \quad (1.17)$$

This definition involves the concentration c of particles in space and their velocities at the instant they cross the control surface, which is a somewhat elusive quantity since bedload particles are not a continuous field (*Heyman et al.*, 2016).

The second definition formulates the downstream flux in terms of the number of particles moving within a control volume V :

$$\Phi = \frac{1}{L} \sum_{i \in V} u_i. \quad (1.18)$$

Here, the flux is evaluated as a sum over all downstream velocities of particles within the volume (of which there are a fluctuating number), and the division by the downstream length of the control volume is incorporated to count only

that proportion of particles near the downstream boundary of the volume. These two definitions, q defined with a surface and Φ defined with a volume, are generally not equivalent (*Ancey and Pascal*, 2020).

1.1.7 The scaling arguments of Bagnold

One of the most influential formulations of the bedload flux is due to *Bagnold* (1956, 1966), who derived a formula for the mean sediment flux using an energy balance approach. Bagnold understood sediment transport as a process which converts flow energy to heat via the effective friction (*Bagnold*, 1954) of grains against the bed as they move downstream through a succession of collisions (*Bagnold*, 1973). He assumed that the flow power P_f available to move sediment in a volume scales as $P_f \propto \tau - \tau_c$, where τ is the average bed shear stress and τ_c is the threshold shear stress at which particles first begin to move. Considering that the average volumetric flux of particles is Φ , and particles move with mean velocity proportional to the fluid velocity near the bed, Bagnold hypothesized that the power P_g required to sustain particle motion in a volume scales as $P_g \propto \Phi/\tau^{1/2}$. Balancing flow energy against frictional dissipation ($P_f = P_g$) then provides Bagnold's sediment transport formula

$$\Phi = k(\tau - \tau_c)\tau^{1/2}, \quad (1.19)$$

which has shown good correspondence with laboratory data at large transport rates, given careful calibration of the constant factors k and τ_c .

The large shear stress limit $\Phi \sim \tau^{3/2}$ of Bagnold's formula is shared in common with many other empirical formulas describing the mean downstream flux of bedload (e.g. *Meyer-Peter and Müller*, 1948; *Parker*, 1990; *Wilcock and Crowe*, 2003; *Yalin*, 1972). A distinguishing feature of Bagnold's formula is its derivation from mechanistic reasoning, although many of Bagnold's assumptions have since turned out to be incorrect. Bagnold's assumption that the power available to move sediment scaled with the excess shear stress leads to unphysical results over arbitrarily sloping beds (*Seminara et al.*, 2002), and the flow power dissipated by sediment transport shows only a weak correlation the sediment flux (*Ancey et al.*, 2008),

while Bagnold assumed they were directly proportional. These issues have been hinted when calibrating Bagnold's formula to data, where the parameters k and τ_c take on unphysical values at low transport rates (*Niño and Garcia*, 1996). Bagnold's formulation also faces the notorious challenge of defining the critical shear stress τ_c for the initiation of sediment transport (*Allen and Kudrolli*, 2018; *Clark et al.*, 2017; *Houssais et al.*, 2015; *Kirchener et al.*, 1990; *Paintal*, 1971). The difficulties with Bagnold's approach led to many revisions of his theory, often based on more carefully incorporating the properties of individual particle motions into the sediment transport energy budget (*Engelund and Fredsoe*, 1976; *Luque and van Beek*, 1976; *Martin and Church*, 2000; *Niño and García*, 1998).

1.1.8 Einstein's probabilistic approach

Among these revisions of Bagnold, one category shows a return to the probabilistic ideas of Einstein (*Ancey et al.*, 2006; *Parker et al.*, 2003). *Einstein* (1937) formulated his original model of individual particle trajectories in terms of entrainment and deposition rates using the idealization of grains moving downstream through a sequence of instantaneous steps. Later, *Einstein* (1942, 1950) calculated the sediment flux with these same probabilistic ideas, providing an alternative to Bagnold's scaling approach. The conceptual picture that Einstein considered is depicted in figure 1.5.

Einstein partitioned the channel into a sequence of identical control volumes V , and calculated the average rate at which particles cross a control surface by aggregating the contributions from each upstream control volume. Each control volume has downstream length ℓ which is also the average particle step length. Denoting by P_n the probability that an individual grain undergoes at least n jumps of length ℓ in a time interval T , meaning it travels at least a distance $n\ell$, and considering that there is a density ρ of particles at rest on the bed, it follows that on average $\rho\ell P_n$ particles will displace a distance $n\ell$ or more from within each control volume during the time interval T . As a result, since grains crossing S in a time T could have come from any upstream location, the number of grains crossing S in T is

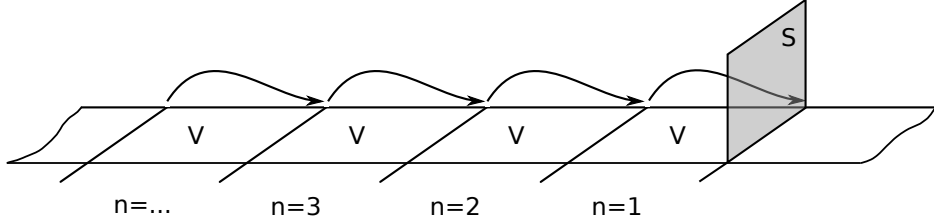


Figure 1.5: Einstein’s conceptual picture (modified from Yalin (1972)). Particles move in discrete jumps of length ℓ from left to right through an array of adjacent control volumes. The bed-load flux is the rate of particles crossing the surface S per unit width and time, collected from all upstream control volumes.

a sum over all control volumes: $\sum_{n=1}^{\infty} \rho\ell P_n$. Dividing by the time T to get the average rate of grains crossing S provides the mean flux:

$$q = \frac{\rho\ell}{T} \sum_{n=1}^{\infty} P_n. \quad (1.20)$$

The final quantity to evaluate is P_n , the probability a particle entrains *at least* n times in a time T .

Einstein originally constructed this probability by assuming that each particle had n independent entrainment opportunities in the period T , each with probability p , so that $P_n = p^n$, giving $q \propto p/(1 - p)$ by a geometric series, but this approach has been criticized by Yalin (1972) and others (Armanini, 2017; Armanini *et al.*, 2015; Cheng, 2004; Paintal, 1971). Some authors have argued convincingly that instead, one should calculate P_n as an exceedance probability. The central critique is that there is a distinct difference between *exactly* and *at least* n entrainment events in T .

If the entrainment rate of an individual grain is k_E (probability per unit time), then the probability that it entrains *exactly* n times in time T , denoted by p_n (distinct from P_n) is a Poisson distribution (Cox and Miller,

1965):

$$p_n = \frac{(k_E T)^n}{n!} e^{-k_E T}. \quad (1.21)$$

This implies that the probability that it entrains *at least* n times is $P_n = \sum_{i=n}^{\infty} \frac{(k_E T)^i}{i!} e^{-k_E T}$, so Einstein's mean sediment flux across the control surface (eq. 1.20) becomes

$$q = \frac{\rho \ell}{T} \sum_{n=1}^{\infty} \sum_{l=n}^{\infty} = \frac{\rho \ell}{T} \sum_{n=1}^{\infty} n \frac{(k_E T)^n}{n!} e^{-k_E T} = \rho k_E \ell. \quad (1.22)$$

Noticing that ρk_E is the entrainment rate of a single grain multiplied by the density of grains available for entrainment on the bed, we can summarize the Einstein theory as

$$q = E \ell, \quad (1.23)$$

where the quantity $E = \rho k_E$ is different the “areal entrainment rate”  representing the number of grains entrained per unit streambed area (*Furbish et al., 2012a; Wilcock and McArdell, 1997*).

Einstein's formulation requires expressions of the single particle entrainment rate k_E and step length ℓ in terms of the flow and sediment characteristics. Although Einstein and many followers have attempted to formulate these connections (e.g. *Einstein, 1950; Grass, 1970; Paintal, 1971*), there are still no comprehensive solutions. Linking Einstein's entrainment and deposition rates to the grain scale mechanics remains an active area of research (e.g. *Dey and Ali, 2018; Tregnaghi et al., 2012*).

1.1.9 Fusing Einstein and Bagnold: The erosion-deposition model

One uniquely successful strategy to relate Einstein's model to flow and sediment characteristics was developed by *Charru* (2006); *Charru et al.* (2004). This “erosion-deposition model” phrases sediment transport as a mass balance within a control volume using Einstein's entrainment rate E and the complementary deposition rate D . These model parameters are related to flow and sediment properties using scaling relations obtained from exper-

iments (*Charru*, 2006; *Charru et al.*, 2004; *Lajeunesse et al.*, 2010, 2015; *Seizilles et al.*, 2014), in what can be characterized as a mixture of the Einstein and Bagnold strategies.

The erosion-deposition model is

$$\partial_t \gamma + \partial_x V \gamma = E - D. \quad (1.24)$$

In this equation, γ is the “particle activity”, which is the number of moving particles per unit area (*Furbish et al.*, 2012a), V is the ensemble averaged movement velocity of sediment grains (which in unsteady conditions may depend on space and time), E is the areal entrainment rate (the number of particles transitioning into motion per unit area and time), and D is the areal deposition rate (the number of particles coming to rest on the bed per unit area and time).

Scaling arguments provide relations for E , D , and V in terms of the fluid shear stress τ , particle size d , particle settling velocity V_s , and critical shear stress τ_c :

$$E = \alpha_1 \frac{\tau - \tau_c}{d^3 V_s}, \quad (1.25)$$

$$D = \alpha_2 \frac{\gamma V_s}{d}, \quad (1.26)$$

$$V = \alpha_3 + \alpha_4(\sqrt{\tau} - \sqrt{\tau_c}). \quad (1.27)$$

The constant coefficients α_i are calibrated in experiments.

Equation 1.24 indicates that the mean flux in steady transport conditions is the implicit solution to the equation $E = D$. Using the scaling relations 1.25 and 1.27 provides the mean particle activity

$$\gamma = \frac{\alpha_1}{\alpha_2} \frac{\tau - \tau_c}{d^2 V_s^2}. \quad (1.28)$$

Expressing the mean flux as $\Phi = \gamma V$, the relationship between flux and bed shear stress becomes

$$\Phi = \frac{\alpha_1}{\alpha_2 d^2 V_s^2} (\tau - \tau_c) [\alpha_3 + \alpha_4(\sqrt{\tau} - \sqrt{\tau_c})]. \quad (1.29)$$

This recovers the Bagnold scaling $\Phi \propto \tau^{3/2}$ at large bed shear stresses.

1.1.10 The nonlocal formulation

Einstein's model of the bedload flux is inherently nonlocal in that it aggregates particle motions from all upstream locations (*Martin et al.*, 2012; *Schumer et al.*, 2009; *Tucker and Bradley*, 2010). Originally *Nakagawa and Tsujimoto* (1976) and later *Parker et al.* (2002) formalized this by writing the sediment flux in an explicitly nonlocal form:

$$q(x, t) = \int_0^\infty dx' F(x', t) E(x - x', t). \quad (1.30)$$

In this equation, motions are considered instantaneous, and $F(x, t)$ is the probability that a particle entrained at $t = 0$ steps at least a distance x before deposition at time t .

Furbish et al. (2012a, 2017) generalized the Parker model to include a finite duration of motion. They wrote

$$q(x, t) = \int_0^\infty dx' \int_0^\infty dt' F(x', t') E(x - x', t - t'), \quad (1.31)$$

where $F(x, t)$ represents the probability density that just-entrained particles move at least a distance x in time t before deposition. In general, this approach can handle non-uniform conditions by including space and time dependence in E and F .

For a simple example of the Furbish et al formalism, consider that particles move with a constant velocity V and have a deposition rate k_D . Then the probability density that a particle moves *exactly* a distance x in time t is $f(x, t) = \delta(x - Vt)k_D \exp(-k_D t)$, so the probability that it moves *at least* a distance x in t is

$$F(x, t) = \int_x^\infty \delta(x - Vt)k_D \exp(-k_D t) dx = \theta(Vt - x)k_D \exp(-k_D t). \quad (1.32)$$

Considering uniform conditions with a density ρ_s of particles available for motion on the bed surface, each having entrainment rate k_E , the areal en-

trainment rate can be expressed as $E = \rho_s k_E$, and equation 1.31 provides a mean flux

$$q = \rho_s k_E \int_0^\infty dx' \int_0^\infty dt \theta(Vt - x) k_D \exp(-k_D t) = \rho_s k_E V / k_D. \quad (1.33)$$

Since $1/k_D$ is the average time spent in motion, V/k_D is the average step length ℓ , and equation 1.33 provides another perspective on Einstein's central result $q = E\ell$, but with the added ability to describe unsteady conditions (Furbish *et al.*, 2012a).

1.1.11 Landscape evolution

Exner (1925) was probably the first to write a mathematical formula linking sediment transport to topographic change. He wrote

$$(1 - \phi) \frac{\partial z}{\partial t}(\mathbf{x}, t) = -\nabla q(\mathbf{x}, t). \quad (1.34)$$

This equation links the temporal evolution of the land elevation z at a location $\mathbf{x} = (x, y)$ to spatial gradients in the sediment flux q . The parameter ϕ is the bed porosity.

Nakagawa and Tsujimoto (1976) and *Tsujimoto* (1978) developed an alternative statement of the Exner equation using Einstein's entrainment and deposition rates. According to their formulation, spatial gradients in the sediment flux arise due to local discrepancies in entrainment and deposition rates:

$$\partial_x q(x, t) = E - D. \quad (1.35)$$

In combination with equation 1.34, this expression of the sediment flux implies (*Fathel et al.*, 2015; *Furbish et al.*, 2012a, 2017; *Parker et al.*, 2002) by which topographic evolution can be described with Einstein's rates:

$$(1 - \phi) \partial_x z(x, t) = D - E. \quad (1.36)$$

In a nonlocal framework, as in equation 1.31, sediment deposition can be interpreted as the eventual result of entrainment from all upstream locations,

giving

$$(1 - \phi)\partial_x z(x, t) = \int_0^\infty dx' \int_0^\infty dt' E(x', t') F(x', t') - E(x, t). \quad (1.37)$$

This “entrainment form of the Exner equation” (*Furbish et al.*, 2017) phrases topographic change from a stochastic interpretation of sediment transport.

The major limitation of these approaches are that they assume landscapes are continuous. This can be interpreted as an average over the detailed configurations of individual grains (*Coleman and Nikora*, 2009). This averaging process is expected to obscure the relevant landscape evolution processes whenever individual grains are large compared to the scales of interest (e.g. *Shobe et al.*, 2021).

1.1.12 Fluctuations and scale dependence

Sediment transport rates always fluctuate (*Hoey*, 1992; *Kuhnle and Southard*, 1988; *Recking et al.*, 2012), even under the most controlled laboratory conditions available (*Ancey et al.*, 2006; *Roseberry et al.*, 2012). At short timescales, fluctuations arise from the intermittent arrivals of individual grains (*Ballio et al.*, 2018; *Böhm et al.*, 2004). At moderate timescales they emerge from waves of moving grains (*Heyman et al.*, 2014) or the episodic entrainment of clusters of grains (*Papanicolaou et al.*, 2018; *Strom et al.*, 2004). At the longest timescales, they originate from migrating bedforms (*Guala et al.*, 2014) or cycles of aggradation and degradation in pools (*Dhont and Ancey*, 2018). These mechanisms generally occur in conjunction with other sources of bedload transport fluctuations like grain size sorting (*Cudden and Hoey*, 2003; *Iseya and Ikeda*, 1987), flow discharge variations (*Mao*, 2012; *Redolfi et al.*, 2018; *Wong and Parker*, 2006), and sediment supply perturbations (*Elgueta-Astaburuaga and Hassan*, 2019; *Lisle et al.*, 1993; *Madej et al.*, 2009).

Despite widespread acceptance that sediment transport rates always fluctuate, we still have relatively little understanding of how to describe these fluctuations. *Hamamori* (1962) was probably the first to calculate a probability distribution for the sediment flux, but this subject fell into relative

obscurity for a long period, until it was revisited by *Nikora et al.* (1997), *Ancey et al.* (2006), and others.

Recognition that sediment transport rates fluctuate requires careful interpretation of sediment transport measurements. In practice, sediment transport measurements always involve time or space averaging, whether measurements are obtained by light tables (*Chartrand et al.*, 2018), impact sensors (*Rickenmann and McArdell*, 2007), computer vision techniques (*Roseberry et al.*, 2012), or sediment traps (*Papangelakis and Hassan*, 2016).

This averaging process in conjunction with transport fluctuations introduces scale-dependence to sediment transport measurements, whereby averaged characteristics depend on the averaging timescale (*Ancey and Paschal*, 2020; *Campagnol et al.*, 2012; *Turowski*, 2010). A fundamental question raised by scale-dependence is how large averaging windows must be for sediment flux measurements to converge. To date, very few mathematical models have addressed this issue.

1.1.13 Birth death models for bedload flucuations

The prevalence of large bedload fluctuations motivated *Ancey et al.* (2006, 2008) to revisit Einstein’s assumptions to develop a model of the bedload flux as a random process. They derived the probability distribution of the flux by counting the number of moving particles in a control volume, considering that this number changes through time as a result of particles migrating into the volume from upstream, entraining, depositing, and migrating out of the volume to downstream.

To obtain realistically-wide fluctuations in particle activity, they introduced a positive feedback called “collective entrainment”, whereby the entrainment rate of grains increases in proportion to the number of moving grains in the volume (*Ancey et al.*, 2008; *Heyman et al.*, 2013).

Their governing equations are completely analogous to a stochastic population model (*Cox and Miller*, 1965; *Pielou*, 1977) where arrivals of moving particles to the volume is “birth” and departure is “death”. They formulated the probability distribution $P(n, t)$ of the number of moving grains in

the control volume at time t as

$$\begin{aligned}\partial_t P(n, t) = & [\lambda + (n - 1)\mu] P(n - 1, t) \\ & - [n + 1]\alpha P(n + 1, t) - [\lambda + n(\alpha + \mu)] P(n, t),\end{aligned}\quad (1.38)$$

whose terms describe particle birth (entrainment and migration in) at rate λ , collective entrainment at rate μ , and particle death (deposition and migration out) at rate α . The final term encodes the possibility that n stays constant. These coupled equations (one for each $n = 0, 1, \dots$) can be solved by generating functions (*Cox and Miller*, 1965), providing the steady-state distribution

$$P(n) = \frac{\Gamma(r + n)}{\Gamma(r)n!} p^r (1 - p)^n,\quad (1.39)$$

where $r = \lambda/\mu$ and $p = 1 - \mu/\alpha$. This is a negative binomial distribution, which is a wide-tailed generalization of the Poisson distribution.

From eq. 1.39, the mean number of moving particles is $\langle n \rangle = \lambda/(\alpha - \mu)$, and the variance is

$$\sigma_n^2 = \frac{\lambda\alpha}{(\alpha - \mu)^2}.\quad (1.40)$$

Owing to the collective entrainment process, particle activity fluctuations can be arbitrarily wide: $\sigma_n/\langle n \rangle = \sqrt{\alpha/\lambda}$, whereas in the absence of collective entrainment ($\mu = 0$), the strength of fluctuations is always pinned to a fixed value, as the distribution 1.39 limits to a Poisson distribution where the mean and variance are equal (*Ancey et al.*, 2006).

The probability distribution of the bedload flux can be computed by the control volume form eq. 1.18 given the probability distribution of particle velocities $P(u)$ under the assumption that velocity and activity are independent. Writing $P_k(u)$ as the probability distribution for the sum of k independent particle velocities ($u = u_1 + \dots + u_k$), the sediment flux probability distribution $P(\Phi)$ becomes (e.g. *Ancey and Heyman*, 2014)

$$P(\Phi) = L \sum_{k=0}^{\infty} P_k(L\Phi) P(n = k).\quad (1.41)$$

A limitation of this approach is that in reality, entrainment and deposition modify the bed elevation, which in turn modifies the rates of entrainment and deposition (Sawai, 1987; Wong *et al.*, 2007). This highlights a need to evaluate bed elevation change in birth-death models.

1.1.14 Renewal theories for scale dependence

The final bedload transport model to summarize calculates the sediment flux probability distribution from an “inter-arrival time distribution” representing the statistics of times between subsequent arrivals of particles to a control surface (Ancey, 2020a; Heyman *et al.*, 2013; Turowski, 2010).

The sediment flux distribution obtained from these approaches shifts depending on the observation time T over which crossing events are observed, so approaches based on inter-arrival times explicitly model scale dependence. In statistics, the problem of counting probabilistic arrival events is called renewal theory (Cox, 1962).

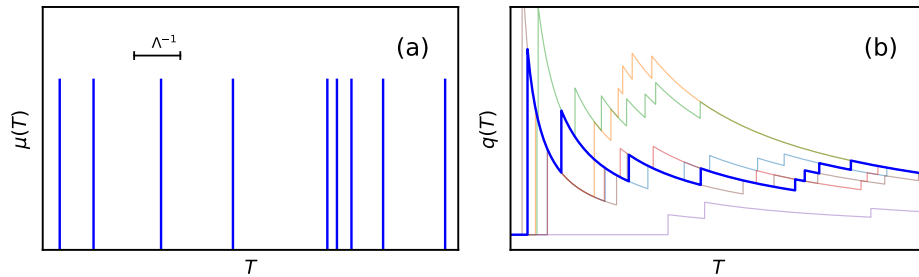


Figure 1.6: The scale-dependent sediment flux is described as a renewal process. Panel (a) indicates the arrivals of particles at rate Λ , while panel (b) shows an ensemble of realizations of the sediment flux versus the observation time T . Note that different realizations of the flux converge toward the same value at large observation times, whereas at small observation times, uncertainty in the flux is large. This is observation-scale dependence. The nature of this convergence depends on the particle dynamics in an as yet unspecified way.

Earlier studies have considered different arrival time distributions to cal-

culate the probability distribution of the time-averaged sediment flux, but only the simplest exponential case is reviewed here. The exponential inter-arrival time distribution is $P(t) = \Lambda \exp(-\Lambda t)$, so the rate of particle arrivals is Λ . In this case, the flux averaged over a period T can be represented with a Poisson pulse noise, similar to the particle position in the Einstein model of section 1.1.2:

$$q(T) = \frac{1}{T} \int_0^T dt' \mu(t'). \quad (1.42)$$

Here, the noise is

$$\mu(t) = \sum_{i=1}^{N(t)} \delta(t - t_i), \quad (1.43)$$

as indicated in figure 1.6 panel (a). In this equation, $N(t)$ is Poisson distributed with rate Λ . The flux in eq. 1.42 is a random variable as indicated in figure 1.6 panel (b). Its probability distribution $P(q|T)$, which is contingent on the observation time T , can be derived by evaluating $P(q|T) = \langle \delta(q - \int_0^T \mu(t') dt' / T) \rangle$. This equation entails an average over all possible realizations of the noise in eq. 1.43, producing (*Van Kampen, 2007*)

$$P(q|T) = \sum_{l=0}^{\infty} \frac{(\Lambda T)^l}{l!} e^{-\Lambda T} \delta(q - \frac{l}{T}), \quad (1.44)$$

which is a scale-dependent Poisson distribution for the sediment flux across the control surface.

The mean flux derived from this renewal scheme – $\langle q(T) \rangle = \int_0^\infty dq P(q|T)$ – is

$$\langle q(T) \rangle = \Lambda, \quad (1.45)$$

which is independent of the observation scale, while the magnitude of bedload transport fluctuations scales with $1/T$:

$$\sigma_q(T)^2 = \frac{\Lambda^2}{T}. \quad (1.46)$$

Even this simple model gives a non-trivial conclusion that the relative uncertainty in a measurement of bedload transport depends on the observation

time: $\sigma_q(T)/\langle q(T) \rangle \propto T^{-1/2}$. Our uncertainty in a sediment transport measurement diverges as the observation time becomes short.

A limitation of renewal approaches to calculate the flux is that they do not obviously relate to the dynamics of individual particles. In renewal models as they are phrased now, the inter-arrival time distribution is not based on the underlying mechanics of particle transport.

1.2 Summary

This literature review has indicated that successful bedload transport descriptions have been developed to describe individual particles and bedload fluxes, although many limitations are left in need of further research attention.

All of the works reviewed so far are either mean field models that do not include fluctuations, or stochastic models that calculate probability distributions for the quantities of interest. The common thread of all of these models is that they take advantage of various devices to side-step the complex interplay of turbulence and granular physics which ultimately control bedload transport.

In the case of mean field models, the devices are heuristic scaling arguments and semi-empirical formulas, while in the case of stochastic models, they are simplified dynamical equations driven by idealized noises, like sequences of pulses, alternating switches, and erratic fluctuations. This thesis applies the latter methodology to many of the limitations highlighted in the review. An outline of the problems to be addressed follows below.

1.3 Outline of the thesis

1.3.1 Problem 1: The scale-dependent flux from individual particle dynamics

The original model by *Einstein* (1937) described particle trajectories as a sequence of instantaneous steps. This model was subsequently improved  to include a finite duration of motion at constant velocity (*Lajeunesse et al.*,

2017; *Lisle et al.*, 1998).

In reality, particle velocities fluctuate during movements due to turbulence and particle-bed collisions, so there is a need to go one step further and account also for velocity fluctuations of moving particles in Einstein-type models.

In addition, although the scale-dependent sediment flux has been calculated from renewal models (*Ancey*, 2020a; *Turowski*, 2010), these approaches are not based on the dynamics of individual particles in transport, so it remains unclear how the sediment flux distribution and its scale dependence originate from the transport characteristics of individual grains.

Chapter 2 introduces a new model of individual bedload trajectories that includes velocity fluctuations in the motion state. The chapter also demonstrates how these trajectories can be used to calculate the scale-dependent probability distribution of the bedload flux. This joins together and extends studies from *Einstein* (1937) to *Ancey* (2020b) to develop new understanding of individual particle motions and the scale-dependent sediment flux.

1.3.2 Problem 2: Feedbacks between sediment transport fluctuations and bed elevation change

Birth-death models calculate the flux probability distribution assuming that entrainment and deposition do not change the local bed elevation (*Ancey and Heyman*, 2014; *Heyman et al.*, 2013), but this assumption violates conservation of mass.

Bed elevation changes produce sediment burial, and although sediment burial is known to affect tracer particle motions at geomorphic timescales (*Ferguson and Hoey*, 2002; *Hassan and Bradley*, 2017), our understanding of how long sediment can remain buried is limited.

Chapter 3 generalizes the model of *Ancey et al.* (2008) to include bed elevation changes in order to evaluate the effect of bed elevation change on bedload transport fluctuations and to study how the timescales of sediment burial relate to the movement characteristics of individual grains.

1.3.3 Problem 3: The effect of sediment burial on downstream transport of sediment tracers

Modelling sediment transport as an alternating sequence of motion and rest intervals implicitly assumes that particles are either moving or resting on the bed surface. Although this provides a useful description of bedload transport across local and intermediate timescales, it requires modification to describe for global and geomorphic timescales. At longer timescales, particle burial moderates the downstream movements of grains (*Hassan and Bradley, 2017*), but burial has not yet been incorporated into Einstein-type models of particle trajectories.

Chapter 4 generalizes the model of *Lisle et al. (1998)* and *Lajeunesse et al. (2017)* to include sediment motion, rest, and burial. This provides the first description of sediment trajectories over local, intermediate, global, and geomorphic timescales.

1.3.4 Problem 4: The control of particle-bed collisions over bedload particle velocity distributions

Finally, the Langevin models of *Fan et al. (2014)* and *Ancey and Heyman (2014)* describe the velocity distributions of sediment moving downstream in the local and intermediate ranges between entrainment and deposition. These models produce two different end-member sediment velocity distributions, and no mathematical models have been developed that describe the full range of distributions observed in experiments.

Chapter 5 presents a stochastic Langevin model including episodic particle-bed collisions formulated by analogy with the theory of granular gases (*Brilliantov and Poschel, 2004*). The episodic representation improves on the static Coulomb-like friction representing collisions in earlier models. The improved model is demonstrated to describe all of the different bedload velocity distributions which have been reported in experiments.

Chapter 2

From particle dynamics to the sediment flux

2.1 Introduction

A relatively weak flow shearing a bed of sediment entrains individual particles into a state of motion controlled by turbulent forcing and intermittent collisions with other grains at rest on the bed, generating wide fluctuations in the sediment velocity (*Fathel et al.*, 2015; *Heyman et al.*, 2016). Bed load particles move downstream until they are disentrained when they happen to encounter sufficiently sheltered pockets on the bed surface to interrupt their motions (*Charru et al.*, 2004; *Gordon et al.*, 1972). Eventually, the bed around them rearranges and destroys this shelter, or turbulent fluctuations overcome the shelter (*Celik et al.*, 2014; *Valyrakis et al.*, 2010), and particles are once again entrained. Bed load transport is thus a kind of itinerant motion, characterized by alternation between fluctuating movements and periods of rest. This process is difficult to describe mathematically given the technicality of the required physics.

To date, descriptions of bed load transport have therefore simplified the problem in various ways to enable progress. The foundational work is due to Einstein, who considering  load motions as instantaneous so he could describe bed load transport as an alternating sequence of “steps” and

rests having random length and duration (*Einstein*, 1937), in a pioneering application of the continuous time random walk (*Montroll*, 1964). Einstein concluded that particles move downstream with a mean velocity $\langle u \rangle = k_E \ell$, where k_E is the rate at which an individual bed particle entrains into motion, and ℓ is the mean length of each downstream step. Later, Einstein applied these ideas to calculate the mean downstream flux due to the movements of many such particles (*Einstein*, 1950). Einstein reasoned that if the density of resting particles on the bed is ρ_b , the overall areal entrainment rate of particles can be written $E = \rho_b k_E$, giving a mean sediment flux $\langle q \rangle = \rho_b \langle u \rangle = E\ell$.

Many researchers have since refined Einstein's approach to provide more realistic descriptions of individual particle motions than his instantaneous step model. One set of efforts has neglected the particle deposition process to calculate the downstream velocity distributions of moving particles using mechanistic equations with noise terms representing turbulent fluid forces and particle-bed collisions (*Ancey and Heyman*, 2014; *Fan et al.*, 2014). Another set of works have described particles alternating between motion and rest considering that motions occur with a constant velocity (*Lajeunesse et al.*, 2017; *Lisle et al.*, 1998). No models have yet been formulated which describes particles alternating between motion and rest with motions having realistic fluctuating velocities, even though this is how bedload particles actually move.

Parallel to these efforts to better describe individual particle trajectories, a complementary set of studies have developed stochastic formulations of the sediment flux which improve on the mean field description provided by Einstein (*Ancey*, 2020a; *Furbish et al.*, 2012b; *Turrowski*, 2010). Sediment fluxes generally exhibit wide fluctuations due to variations in the number of moving particles and their velocities (*Ancey et al.*, 2006; *Böhm et al.*, 2005; *Furbish et al.*, 2012b), the migration of bedforms and sediment waves (*Guala et al.*, 2014; *Recking et al.*, 2012), and a host of other processes (*Dhont and Ancey*, 2018). Because these fluctuations occur over disparate timescales, measurements of mean sediment fluxes depend on the timescale over which they are collected, a phenomenon called scale dependence (*Ancey*, 2020a;

Dhont and Ancey, 2018; Saletti et al., 2015; Singh et al., 2009; Turowski, 2010). To date, very few models have calculated the probability distribution of the bed load sediment flux due to individual particle motions (*Ancey and Heyman, 2014; Ancey et al., 2008*), and among these, even fewer have described any observation-scale dependence of the flux (*Ancey and Pascal, 2020; Turowski, 2010*). Among those that do, none have yet formulated the sediment flux in terms of the downstream trajectories of individual grains.

This survey provides context for the two problems addressed in this chapter. First, we lack the capability to describe individual sediment trajectories through motion and rest including velocity fluctuations in the motion state; and second, we need more understanding of how to connect individual particle trajectories through motion and rest to the overall downstream sediment flux, including its probability distribution and the dependence of its statistical moments on the observation time.

Here, I develop a new statistical physics-based formalism which addresses both of these problems by describing individual particle trajectories with a stochastic Langevin equation. This dynamical equation describes alternation between motion and rest at random intervals while particles in motion have velocity that fluctuates around a mean value. Using the probability distribution of particle position generated by this model, I construct a formalism to derive analytically the probability distribution of the sediment flux. This distribution exhibits observation-scale dependence as a result of velocity fluctuations among moving particles. Below, I develop the new formalism in sec. 2.2, solve it in sec. 2.4, and discuss the implications of my results and future research ideas in secs. 2.5 and 2.6.

2.2 Description of motion-rest alternation with velocity fluctuations

The starting point for this analysis is an idealized one-dimensional domain, infinite in extent, populated with sediment particles on the surface of a sedimentary bed. Particles are set in motion by the turbulent flow and move downstream until they deposit, and the cycle repeats. The downstream

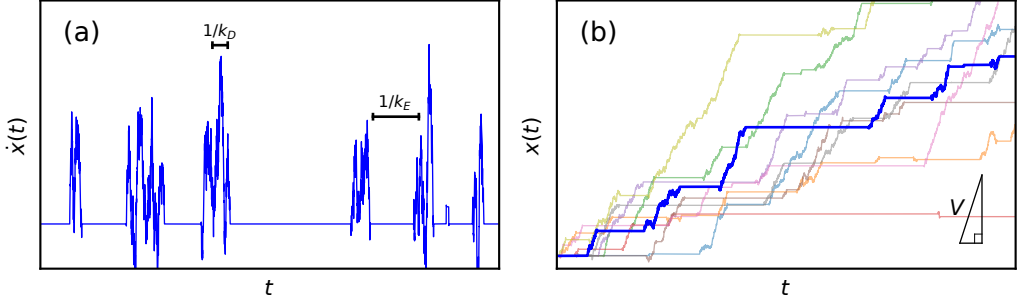


Figure 2.1: Panel (a) sketches a realization of the noise in equation 2.1, while panel (b) shows the trajectory derived from it (in blue) alongside other possible trajectories. Keys in panel (a) demonstrate the average movement time $1/k_D$ and rest time $1/k_E$, while the key in panel (b) shows the average movement velocity V . Velocity fluctuations produce tilted stair-step trajectories with unsteady slopes in the $x - t$ plane. This can be compared with figure 1.2 which does not include fluctuations.

coordinate is x , so that \dot{x} describes a velocity in the downstream direction. The flow is considered weak enough that interactions among moving grains are very rare, although interactions between moving particles and the bed may be common, characteristic of rarefied transport conditions (e.g. *Furbish et al.*, 2017; *Kumaran*, 2006). Particles are considered to have similar enough shapes and sizes so as to have nearly identical mobility characteristics. These conditions allow for all particles to be described as independent from one another but governed by the same underlying dynamical equations.

2.2.1 Dynamical equation for grain-scale sediment transport

From these assumptions, the first target is to write an equation of motion for the individual sediment particle encompassing two features. First, particles should alternate between motion and rest. The entrainment transition rate from rest to motion occurs with probability per unit time (or rate) k_E , while the deposition transition from motion to rest occurs with rate k_D . Second,

particles in motion should move with mean velocity V as their instantaneous velocities jitter around this mean value due to turbulent drag and particle-bed collisions.

The simplest equation of motion including these features is

$$\dot{x}(t) = [V + \sqrt{2D}\xi(t)]\eta(t). \quad (2.1)$$

Here $\xi(t)$ is a Gaussian white noise having zero mean and unit variance representing velocity fluctuations among moving particles. $\eta(t)$ is a dichotomous noise which takes on values $\eta = 1$, representing motion (with mean duration $1/k_D$), and $\eta = 0$, representing rest (with mean duration $1/k_E$). Some trajectories produced by this equation are sketched in figure 2.1. In this equation, V is the mean particle velocity describing the overall downstream drift of moving particles, while D is a diffusivity [units L^2/T^3] describing velocity fluctuations among moving particles. The transition rate from $\eta = 0$ to $\eta = 1$ is k_E , and the transition rate from $\eta = 1$ to $\eta = 0$ is k_D . The notation $k = k_E + k_D$ is a shorthand used throughout the thesis.

The Langevin equation 2.1 is a generalization of the model by *Lisle et al.* (1998) and *Lajeunesse et al.* (2017), presented in section 1.1.3, to include velocity fluctuations in the motion state protocol. It is similar to the “randomly flashing diffusion” developed by Luczka and coworkers in physics (*Luczka et al.*, 1992; *Luczka et al.*, 1993, 1995), although it is not clear if these models relate mathematically. Equation 2.1 describes the downstream movement of particles alternating through motion and rest with velocity fluctuations in the motion state. This dynamical equation provides a more realistic description of bed load trajectories than earlier works in the Einstein paradigm (sec. 1.1).

2.2.2 Derivation of the master equation for the sediment position distribution

The solution of equation 2.1 for a given realization of the two noises $\eta(t)$ and $\xi(t)$ gives one possible trajectory of a particle. The probability distribution $P(x, t)$ that a particle which started at position $x = 0$ at time $t = 0$ has

travelled to position x by time t can be formulated as an average over the ensemble of all possible trajectories.

This probability distribution of position is formed as $P(x', t) = \langle \delta(x' - x(t)) \rangle_{\eta, \xi}$, where $x(t)$ is the formal solution of eq. 2.1 and the average is over both noises. This symbolic equation is not directly useful as taking averages over both noises is a challenging mathematical problem (*Hanggi*, 1978). This calculation is completed in the appendix in section A.1, providing the master equation

$$(\partial_t^2 + V\partial_x\partial_t + k_E V\partial_x + k\partial_t - D\partial_x^2\partial_t - k_E D\partial_x^2)P(x, t) = 0 \quad (2.2)$$

for the probability distribution of position. The master equation 2.2 is a diffusion-like equation governing the probability distribution of position for individual particles alternating between motion and rest, with the movement velocity being a fluctuating quantity.

One can see in particular that taking the entrainment rate k_E very large, meaning that particles are very often moving, implies an advection-diffusion equation $(\partial_t + V\partial_x - D\partial_x^2)P = 0$ for the position, characteristic of a particle moving downstream with Gaussian velocity fluctuations (*Ancey and Heyman*, 2014). Otherwise, there is a possibility that the particle is at rest and the advection-diffusion process interrupted, giving rise to the additional terms in eq. 2.2, a structure reminiscent of equation 1.8 from simpler motion-rest models.

2.3 Formalism for the downstream sediment flux

The probability distribution of the sediment flux can be calculated using the probability distribution of particle position $P(x, t)$ provided as the solution of equation 2.2. This method is modified from the approach recently developed by Banerjee and coworkers in physics (*Banerjee et al.*, 2020). This generalizes the nonlocal formulation (1.1.10) to provide the probability distribution of the flux, and it reframes the renewal approach (sec. 1.1.14) to in terms of the mechanics of individual particles in transport.

The basic idea, as depicted in Figure 2.2, is to initially distribute N

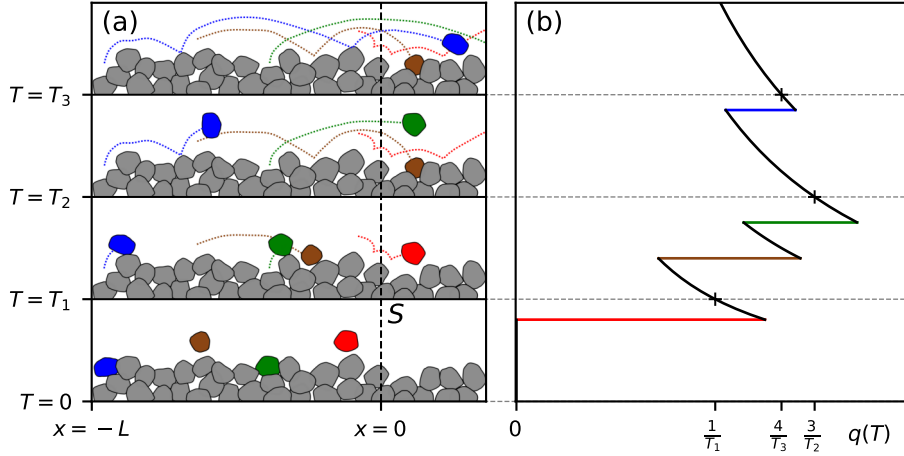


Figure 2.2: The left panel indicates the configuration for the flux. The particle trajectories within are calculated from equation 5.3, demonstrating alternation between rest and motion with fluctuating velocity. Particles begin their transport with positions $-L \leq x \leq 0$ at $t = 0$, and as depicted in the right panel, the flux is calculated with the number of particles $N_>(T)$ which lie to the right of $x = 0$ at the observation time $t = T$, divided by T : $q(T) = N_>(T)/T$. The probability distribution of $q(T)$ is determined from all possible realizations of the trajectories and initial positions as N, L tend to infinity while the density of particles $\rho = N/L$ to the left of the control surface remains fixed.

particles in all states of motion along a domain of length L at some random initial locations x_i to the left of $x = 0$. Later, the number of particles N and the size L of the domain will be limited to infinity such that their ratio $\rho = N/L$ remains constant. This limit will provide a configuration similar to the one constructed in the nonlocal formation (sec. 1.1.10).

From this initial configuration, particles move downstream through time according to equation 2.1. The flux is calculated as the average rate of particles crossing to the right of the control surface (at $x = 0$) after the sampling time T . This time-averaged flux is

$$q(T) = \frac{1}{T} \sum_{i=1}^N I_i(T). \quad (2.3)$$

In this equation, the $I_i(T)$ are indicator functions which equal 1 if the i th particle has passed the control surface ($x = 0$) at the observation time T and 0 otherwise. All particles which have not crossed the control surface (or which have crossed and then crossed back) contribute nothing to the flux.

The probability distribution of the flux is then the average of equation 2.3 across all possible initial configurations of particles and their trajectories

$$P(q|T) = \left\langle \delta \left(q - \frac{1}{T} \sum_{i=1}^N I_i(T) \right) \right\rangle. \quad (2.4)$$

These averages are again most easily conducted in Laplace space. Taking the Laplace transform over q (i.e. forming the characteristic function of $P(q|T)$) obtains

$$\tilde{P}(s|T) = \left\langle \exp \left(\frac{s}{T} \sum_{i=1}^N I_i(T) \right) \right\rangle \quad (2.5)$$

$$= \prod_{i=1}^N \left\langle \exp \left(-\frac{s}{T} I_i(T) \right) \right\rangle \quad (2.6)$$

$$= \prod_{i=1}^N \left[1 - (1 - e^{-s/T}) \langle I_i(T) \rangle \right] \quad (2.7)$$

This progression relies on the independence of averages for each particle (so the average of a product is the product of averages) and the observation that $e^{aI} = 1 - (1 - e^a)I$ because I is either 0 or 1.

The average over initial conditions and possible trajectories for the i th particle involved in this characteristic function can be written

$$\langle I_i(t) \rangle = \frac{1}{L} \int_L^0 dx' \int_0^\infty dx P(x - x', t) \quad (2.8)$$

where $P(x, t)$ is the position probability distribution which solves equation

2.2. Equation 2.8 describes the probability that the *i*th particle is found to the right of control surface by time T provided it started at a random location somewhere to the left. These $\langle I_i(t) \rangle$ are the components of the flux that depend on the particle dynamics.

Inserting equation 2.8 into equation 2.7 and taking the limits $L \rightarrow \infty$ and $N \rightarrow \infty$ as the density of particles $\rho = N/L$ remains constant, producing the configuration of the nonlocal formulation in section 1.1.10, provides

$$\tilde{P}(s|T) = \lim_{N \rightarrow \infty} \left(1 - \frac{1}{N} (1 - e^{-s/T}) \Lambda(T) \right)^N \quad (2.9)$$

$$= \exp \left[- (1 - e^{-s/T}) \Lambda(T) \right]. \quad (2.10)$$

where $\Lambda(T) = \rho \int_0^\infty dx \int_0^\infty dx' P(x + x', T)$ is a rate *function*, similar to the rate constant in the renewal process models of section 1.1.14, except that it is now formulated in terms of individual particle trajectories via the probability distribution of particle position $P(x, t)$, which itself originates from the Langevin equation 2.1 governing the particle dynamics.

Equation 2.10 is the characteristic function of a Poisson distribution (*Cox and Miller*, 1965). Expanding in $e^{-s/T}$ and inverting the Laplace transform provides a key equation of this chapter, the probability distribution of the flux held contingent on the sampling time T :

$$P(q|T) = \sum_{l=0}^{\infty} \frac{\Lambda(T)^l}{l!} e^{-\Lambda(T)} \delta(q - \frac{l}{T}). \quad (2.11)$$

This equation implies that the mean flux is $\langle q(T) \rangle = \int_0^\infty q P(q|T) dq = \Lambda(T)/T$. Similarly the variance is $\sigma_q^2(T) = \Lambda(T)/T^2$. For the case when $\Lambda(T)$ is proportional to the observation time ($\Lambda \propto T$), these formulas become identical to the renewal theory approach reviewed in section 1.1.14. This correspondence demonstrates that the renewal approach can be formulated equivalently by considering the dynamics of individual particles as a starting point.

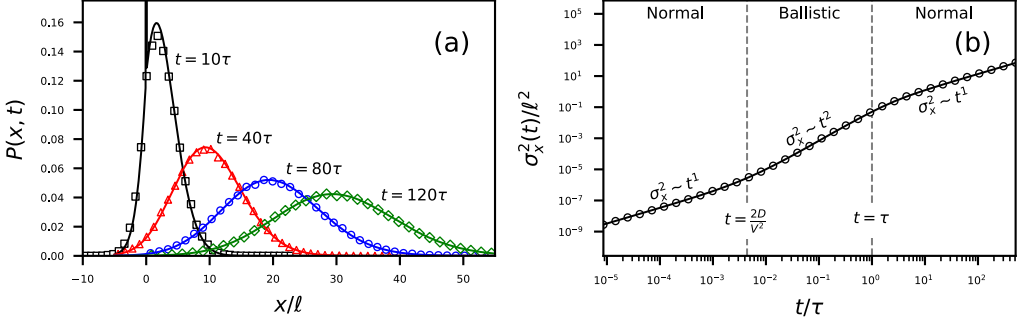


Figure 2.3: Panel (a) indicates the probability distribution of particle position (eq. 2.13) as it evolves through time. From the initial mixture of motion and rest states, particles advect downstream as they diffuse apart from one another due to differences in their velocities and transition times between motion and rest. Panel (b) shows the resulting particle diffusion (eq. 2.16). At timescales $t \ll 2D/V^2$, the diffusion is normal since the movement is approximately a standard Brownian diffusion process. For larger timescales, $2D/V^2 \ll t \ll \tau$, particles undergo ballistic diffusion similar to *Lisle et al.* (1998) as a result of some particles being stationary as others advect. Finally at times longer than the timescale $\tau = 1/k$ associated with entrainment and deposition, diffusion is again normal, formed of particles well-mixed among motion and rest states. All results are scaled by the mean hop length $\ell = V/k_D$ and the timescale $\tau = 1/k$ of the motion/rest alternation. In both plots, the lines are analytical results while the points are the results of Monte Carlo simulations based on evaluating cumulative transition probabilities on a small timestep (e.g. *Barik et al.*, 2006).

2.4 Results

2.4.1 Position probability distribution of sediment particles

The master equation 2.2 describes the evolution of the probability distribution of position through time. The solution of this equation should be some combination of the *Einstein* (1937) theory for particle transport (sec-

tion 1.1.2) with the Gaussian solution of the advection-diffusion equation (*Morse and Feshbach*, 1953b).

Because the master equation is second order in time, it requires initial conditions for both P and $\partial_t P$. Considering that particles start at rest in a mixture of motion and rest states, with a fraction k_E/k starting in motion and a fraction k_D/k starting in rest, these conditions derive from the initial state

$$P(x, 0) = \lim_{t \rightarrow 0} \frac{k_E}{k} \sqrt{\frac{1}{4\pi Dt}} \exp \left[-\frac{(x - Vt)^2}{4Dt} \right] + \frac{k_D}{k} \delta(x) \quad (2.12)$$

which gives $P(x, 0) = \delta(x)$ and $\partial_t P(x, 0) = \frac{k_E}{k} [D\delta''(x) - V\delta'(x)]$ (c.f. *Weiss*, 2002).

The master equation 2.2 is solved by transform calculus in section A.2 of the appendix, providing

$$\begin{aligned} P(x, t) &= [-\varphi D\partial_x^2 + V\varphi\partial_x + k + \delta(t) + \partial_t] \\ &\times \int_0^t \mathcal{I}_0 \left(2\sqrt{k_E k_D u(t-u)} \right) e^{-k_E(t-u)-k_D u} \\ &\times \sqrt{\frac{1}{4\pi Du}} \exp \left[-\frac{(x - Vu)^2}{4Du} \right] du, \end{aligned} \quad (2.13)$$

where $\varphi = k_D/k$ is the probability the particle starts at rest. This equation generalizes the earlier result 1.9 for alternation between motions and rests to include velocity fluctuations within the motion state.

The distribution 2.13 is shown evolving through time in figure 2.3 panel (a), where the advection and diffusion characteristics of equation 2.2 are both evident. The integral in equation 2.13 encodes the earlier expectation of Einstein model-like behavior mixed with a Gaussian propagator, in that it convolves the Bessel probability that the particle has been in motion for a period u out of a time t with the Gaussian probability that a particle has travelled a distance x in time u within the motion state. The prefactors of this integral term can be understood as adapting this distribution to the initial conditions.

2.4.2 The moments of particle position through motion-rest alternation

The moments of position produced by equation 2.13 could be derived by integrating it directly, but this is difficult. Instead, the moments can be calculated directly from the master equation 2.2 (*Cox and Miller*, 1965).

Multiplying equation 2.2 by x^l and integrating over all x provides

$$\begin{aligned} \partial_t^2 \langle x^l \rangle - Vl \partial_t \langle x^{l-1} \rangle - k_E Vl \langle x^{l-1} \rangle + k \partial_t \langle x^l \rangle \\ - Dl(l-1) \partial_t \langle x^{l-2} \rangle - k_E Dl(l-1) \langle x^{l-2} \rangle = 0. \end{aligned} \quad (2.14)$$

For $l = 1$, this equation generates the mean position $\langle x \rangle(t) = k_E Vt/k$, which is unaffected by diffusion (since Gaussian velocity fluctuations are symmetric). The case $l = 2$ provides the second moment, implying the variance of position is

$$\sigma_x(t)^2 = \frac{2k_E k_D V^2}{k^3} \left(t + \frac{1}{k} e^{-kt} - \frac{1}{k} \right) + 2 \frac{k_E D}{k} t. \quad (2.15)$$

This equation describes a non-trivial multi-scale diffusion phenomenon, whereby the rate at which particles spread apart from one another depends on how long their dynamics have been ongoing.

Provided that $2D/V^2 \ll k_D/k^2$, series expansion of 2.15 in t and $1/t$ reveals three different scaling behaviors:

$$\sigma_x^2 \sim \begin{cases} t, & t \ll \frac{2Dk}{V^2 k_D}, \\ t^2, & \frac{2Dk}{V^2 k_D} \ll t \ll \frac{1}{k}, \\ t, & t \gg \frac{1}{k}. \end{cases} \quad (2.16)$$

Note in the physical condition when $k \approx k_D$, which is generally satisfied for bedload transport since motions are typically short compared to rests (*Hasan et al.*, 1991; *Wu et al.*, 2019a), the above condition for existence of three ranges becomes $Pe \gg 1$, where $Pe = V^2/(2k_D D)$ is a Peclet number (e.g. *Heyman et al.*, 2014). This Peclet number measures the relative importance of advection and diffusion to the downstream movements of particles.

The large Peclet limit ($Pe \gg 1$) is the physically-relevant condition for bedload transport, where velocity fluctuations are typically small compared to mean downstream movement velocities, so that particles very rarely move upstream (e.g. *Fathel et al.*, 2015). This limit also generates the three-range diffusion exemplified by equation 2.16, so we should expect bedload particles to spread apart with three different scaling ranges depending on how long they have been observed (c.f. *Nikora et al.*, 2001a, 2002). Figure 2.3 panel (b) sketches this three-range diffusion.

Below, this anomalous diffusion behavior (c.f. *Sokolov*, 2012) is shown to affect the rate constant $\Lambda(t)$ in the sediment flux. As a result of these multi-scale particle dynamics, the sediment flux becomes scale-dependent in a richer way than the renewal model of section 1.1.14.

2.4.3 Calculation of the sediment flux

From the formalism in section 2.3, the central parameter of the sediment flux distribution is the rate function

$$\Lambda(t) = \rho \int_0^\infty dx_i \int_0^\infty dx P(x + x_i, t). \quad (2.17)$$

This represents the number of particles crossing $x = 0$ at the observation time T given they started somewhere to left of $x = 0$ at $T = 0$.

Using the probability distribution of position 2.13, the integrals in equation 2.17 are performed in section A.3 of the appendix, providing the rate function

$$\begin{aligned} \Lambda(t) = \rho \int_0^t & \mathcal{I}_0\left(2\sqrt{k_E k_D u(t-u)}\right) e^{-k_E(t-u)-k_D u} \\ & \times \left[\sqrt{\frac{D}{\pi u}} \left([\bar{\partial}_t + k]u - \frac{k_D}{2k} \right) e^{-V^2 u/4D} \right. \\ & \left. + \frac{V}{2} \left([\bar{\partial}_t + k]u - \frac{k_D}{k} \right) \operatorname{erfc}\left(-\sqrt{\frac{V^2 u}{4D}}\right) \right] du. \end{aligned} \quad (2.18)$$

In this equation, the notation $\bar{\partial}_t$ means that the partial time derivative

acts from the left of all terms in which it is involved, as in $f(t)\tilde{\partial}_t g(t) = \partial_t[f(t)g(t)]$.

This is an intricate result for the rate function in the sediment flux distribution 2.11. This mathematical complexity may not be surprising given that equation 2.1 involves two interacting diffusion processes. As displayed in figure 2.4, as a result of eq. 2.18 the mean sediment flux takes on a non-trivial scale-dependence, characterized by a decay toward the Einstein prediction $q_0 = \rho k_E V/k = E\ell$ as the observation time becomes much larger than $1/(k_D Pe)$.

Further insight into the rate constant of the sediment flux distribution can be gained by investigating extreme cases of the observation time. As shown in appendix section A.3, equation 2.18 takes on relatively simple forms at extreme values of T :

$$\Lambda(T) = \begin{cases} \frac{\rho k_E}{k} \sqrt{\frac{DT}{\pi}} & T \ll (k_D Pe)^{-1} \\ \frac{\rho k_E V T}{k} & T \gg (k_D Pe)^{-1}. \end{cases} \quad (2.19)$$

Since the mean flux is $\langle q(T) \rangle = \Lambda(T)/T$, the condition on the observation time so that the flux converges to the Einstein value $q_0 = \rho k_E V/k = E\ell$ can be expressed as $T \gg (k_D Pe)^{-1}$. It is related to the Peclet number and is proportional to the time particles spend in motion ($1/k_D$). As a result, when particle velocity fluctuations during motions become large comparable to the mean particle velocity, equation 2.19 indicates that the flux becomes slow to converge to the Einstein result.

2.5 Discussion

This chapter has generalized the earlier descriptions of individual sediment trajectories (e.g. *Lajeunesse et al.*, 2017; *Lisle et al.*, 1998) to include velocity fluctuations in the motion state.

Using results from this generalized model as an example, I demonstrated how to calculate the sediment flux probability distribution, phrasing earlier renewal theory approaches (sec. 1.1.14) more directly in terms of the underlying particle dynamics (e.g. *Ancey*, 2020a; *Turowski*, 2010). This method

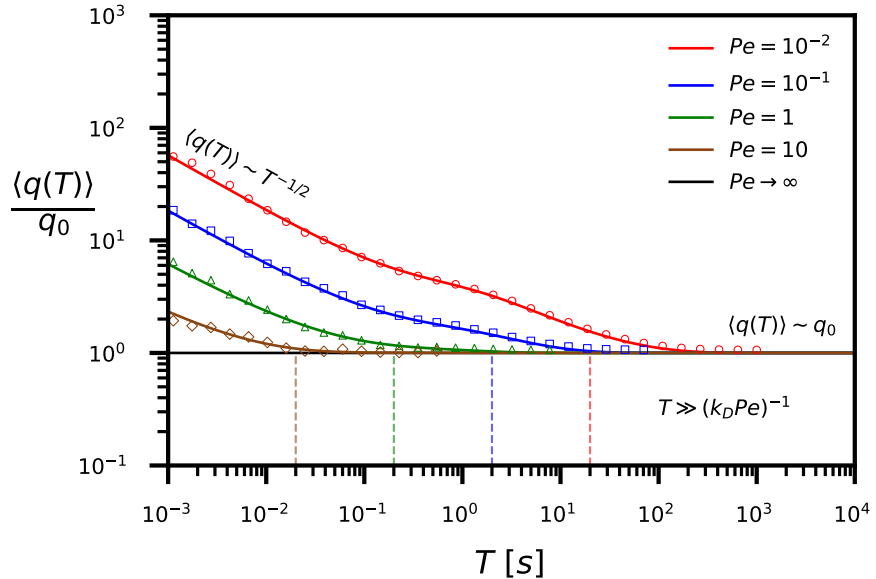


Figure 2.4: The mean sediment flux is plotted for different values of the Peclet number $Pe = V^2/(2k_D D)$, characterizing the relative strength of particle velocity fluctuations during motion. The flux is normalized by the prediction $q_0 = E\ell$ of the Einstein theory (sec. 1.1.8). For nonzero velocity fluctuations in the motion state (finite Pe), the Einstein limit is approached as the observation time T grows. Stronger velocity fluctuations (smaller Pe) slow the convergence to this limit. In all cases, satisfactory convergence of the mean flux is achieved when the observation time satisfies $T \gg 1/(k_D Pe)$, as expected by equation 2.19. Plotted lines are the analytical result eq. 2.18, while the points are the results of Monte Carlo simulations.

can also be viewed as a generalization of the nonlocal formulation (sec. 1.1.10) developed by *Furbish et al.* (2012b); *Parker et al.* (2002) to describe sediment flux probability distributions, rather than just mean values.

2.5.1 Fluctuations and collective motions

The sediment flux probability distribution in equation 2.11 represents a Poisson distribution with an observation scale-dependent rate. Poisson distributions have relatively thin tails, meaning their fluctuations are typically small (*Ancey et al.*, 2006). In reality, sediment flux distributions are only Poissonian at high transport rates, whereas in other conditions they have wide tails representing the possibility of extremely large transport fluctuations (*Ancey et al.*, 2008; *Dhont and Ancey*, 2018; *Saletti et al.*, 2015; *Turowski*, 2010) which appear as bursts (e.g. *Goh and Barabási*, 2008) in the sediment flux timeseries (*Benavides et al.*, 2021; *Heyman et al.*, 2013; *Singh et al.*, 2009). This highlights a need to generalize the mechanistic theory of the sediment flux I developed here to produce wider transport rate fluctuations.

Descriptions of sediment transport based on population dynamics in a control volume have produced realistically-wide fluctuations by incorporating a positive feedback between the number of moving particles and the particle entrainment rate called collective entrainment (*Ancey and Heyman*, 2014; *Ancey et al.*, 2008). This feedback generates waves of moving particles (*Ancey and Heyman*, 2014; *Heyman et al.*, 2015) and produces non-exponential inter-arrival time distributions (*Heyman et al.*, 2013) which imply wide-tailed flux distributions when incorporated in the renewal theory (e.g. *Ancey*, 2020a; *Turowski*, 2010).

Collective entrainment has been attributed to particle-particle interactions such as small granular avalanches and collision-induced entrainment (e.g. *Pähztz et al.*, 2020), and to fluid-particle interactions, such as large eddies entraining particles en masse as they sweep downstream (*Ancey and Heyman*, 2014; *Cameron et al.*, 2020; *Lee and Jerolmack*, 2018).

Particle-particle interactions would be challenging to include in a mechanistic model for the sediment flux like I developed here. The dynamical

equation 2.1 would generalize to $\dot{x}_i(t) = F_i(x_i, t) + \sum_{j \neq i} G_{ij}(\{x_j\}, t)$, where the F_i are the driving terms unique to each particle, while the G_{ij} are some (generally stochastic) terms representing interactions between the i th and j th particles (Goldstein, 1997).

The resulting joint distribution of particle positions and velocities – $P(x_1, v_1, \dots, x_{N(t)}, v_{N(t)}, t)$ – might be formulated by analogy to the theory of reaction diffusion systems (Cardy, 2008; Pechenik and Levine, 1999), non-ideal gases (Brilliantov and Poschel, 2004; Chapman and Cowling, 1970), or other interacting particle models available in physics literature (Escaff et al., 2018; Hernández-García and López, 2004).

A generalization of the model developed in this chapter to include collective motions should be capable of producing realistically-wide sediment transport fluctuations. Such a development will be a challenging next step for research. The present chapter only lays the groundwork.

2.5.2 Measuring the sediment flux

Figure 2.4 indicates that the sediment flux described by equation 2.18 converges when $T \gg (k_D Pe)^{-1}$ to its eventual value $q = E\ell$ predicted by the Einstein theory. Because particles move for durations $1/k_D$ on average, the variance of velocity among moving particles can be written $\sigma_V^2 = 2D/k_D$. In terms of this quantity, the convergence condition is $T \gg \sigma_V^2/(k_D V^2)$, now phrased in terms of easily measurable quantities – the velocity of particles, the average time spent in motion, and the magnitude of velocity fluctuations.

This simple result provides the minimal time required to resolve mean sediment transport rates in terms of measurable properties of particle motions. For example, in the experiments of Martin et al. (2012), this condition implies convergence times of approximately $T \gg 15s$. With wide sediment velocity fluctuations and long particle movement periods, the required observation timescale could become large. In this case, mean sediment flux timeseries obtained with light tables and acoustic sensors (Mendes et al., 2016; Tsakiris et al., 2014; Zimmermann et al., 2008) would require careful interpretation.

2.5.3 Limitations and next steps

It has long been recognized that many processes lend variability to the sediment flux, like bedform migration (*Guala et al.*, 2014; *Hamamori*, 1962), particle sorting processes  or entrainment of clusters (*Papanicolaou et al.*, 2018; *Strom et al.*, 2004). Understanding these processes has been a challenging problem, in part because different sources of fluctuations mix within measured transport signals (e.g. *Dhont and Ancey*, 2018; *Hoey*, 1992; *Saletti et al.*, 2015; *Singh et al.*, 2009).

Although the present model has analyzed independent particles, so it does not include these processes, we can wonder if better understanding fluctuations due to single-particle sources will aid understanding of more complex collective sources. An attempt to subtract the signature of individual particle dynamics from spectra of bedload transport may be a useful step to understand more complex morphological sources of sediment transport variability in channels. A comprehensive understanding of the linkage between individual particle dynamics and sediment fluxes, as I have worked toward here, would provide a foundation for such a subtraction process.

2.6 Summary

This chapter introduced a two-noise stochastic dynamical equation to describe individual bedload trajectories for particles alternating between motion and rest states. The motion state included velocity fluctuations, providing the first analytical model of this type.

The probability distribution of the bedload sediment flux was calculated from these particle dynamics, and the resulting flux distribution was demonstrated to adopt scale-dependence from the underlying dynamics of individual particles. The observation timescales over which sediment flux observations converge were expressed in terms of the mean particle movement velocity and the typical magnitude of its fluctuations, characterized by a Peclet number.

These results generalize the bedload trajectory models of *Einstein* (1937), *Lisle et al.* (1998), and *Lajeunesse et al.* (2017) to include fluctuating move-

ment velocities. This work also builds a particle dynamics framework underneath earlier renewal models of the sediment flux probability distribution (*Ancey, 2020a; Lajeunesse et al., 2010*).

Finally, the work further quantifies the dependence of the sediment flux on the observation scale and provides guidance as to the measurement times required to resolve sediment transport without ambiguity, at least in the idealized conditions in which the model was developed. The next step is to include collective motions to produce wider sediment transport fluctuations.

Chapter 3

Analysis of bed elevation change and sediment transport fluctuations

The transport characteristics of coarse grains moving under a turbulent flow ultimately control a wide set processes within rivers, including the export of contaminants (*Macklin et al.*, 2006; *Malmon et al.*, 2005), the success of ecological restoration efforts (*Gaeuman et al.*, 2017), and the response of channel morphology to disturbances (*Hassan and Bradley*, 2017). Although the displacements of individual grains are a mechanical consequence of forces imparted from the flow, bed, and other grains (*González et al.*, 2017; *Vowinckel et al.*, 2014; *Wiberg and Smith*, 1985), accurately characterizing these forces within natural channels is practically impossible, especially considering the intense variability these forces display (*Celik et al.*, 2010; *Dwivedi et al.*, 2011; *Schmeeckle et al.*, 2007). In response, researchers have developed a stochastic concepts of bedload transport (*Einstein*, 1937), whereby the erosion and deposition of individual grains are modelled as the random results of undetermined forces (*Ancey et al.*, 2006; *Einstein*, 1950; *Paintal*, 1971).

Essentially two types of bedload transport model have been developed from this concept. The first type provides the probabilistic dynamics of a

small population of tracer grains as they transport downstream (*Einstein*, 1937; *Hubbell and Sayre*, 1964; *Lajeunesse et al.*, 2017; *Martin et al.*, 2012; *Nakagawa and Tsujimoto*, 1976; *Wu et al.*, 2019a), while the second provides the statistics of the number of moving grains (“the particle activity”) within a control volume (*Ancey et al.*, 2006; *Einstein*, 1950; *Furbish et al.*, 2012b). In the first type, individual displacements are considered to result from alternate step-rest sequences, where step lengths and resting times are random variables following statistical distributions (*Einstein*, 1937). Differences between the random-walk motions of one grain and the next imply a spreading apart of tracer grains as they transport downstream: bedload tracers undergo diffusion.

Resting time distributions have been carefully studied in relation to these models because the predicted diffusion characteristics are critically dependent on whether the distribution has a light or heavy tail (*Bradley*, 2017; *Martin et al.*, 2012; *Weeks and Swinney*, 1998). Resting times have puzzled researchers because early experiments showed exponential distributions (*Einstein*, 1937; *Hubbell and Sayre*, 1964; *Nakagawa and Tsujimoto*, 1976; *Yano*, 1969), while later experiments showed heavy-tailed power-law distributions (*Bradley*, 2017; *Liu et al.*, 2019; *Martin et al.*, 2012; *Olinde and Johnson*, 2015; *Pretzlav*, 2016; *Voepel et al.*, 2013). A predominant hypothesis is that power-law distributed resting times originate from buried grains (*Martin et al.*, 2014; *Voepel et al.*, 2013). This permits surface grains to retain exponential resting times. Conceptually, when grains rest on the surface, material transported from upstream can deposit on top of them, preventing entrainment until its removal, driving up resting times and imparting a heavy tail to the distribution.

Martin et al. (2014) have provided the only direct support for this hypothesis by tracking grains through complete cycles of burial and exhumation in a narrow flume. They observed heavy-tailed resting times of buried grains and described their results with a mathematical model similar to an earlier effort by *Voepel et al.* (2013). Both of these models treat bed elevation changes as a random walk and interpret resting times as return periods from above in the bed elevation time-series (*Redner*, 2007). Each describes

resting time distributions from different experiments, but they rely on different random walk models, and their treatment of bed elevations as a process independent of sediment transport is questionable at first glance, since bedload transport is the source of bed elevation changes (*Wong et al.*, 2007), while neither model explicitly describes bedload transport. Models of sedimentary bed evolution incorporating sediment transport processes might enhance understanding of sediment resting times.

The second type of stochastic model prescribes rates (probabilities per unit time) to the erosion and deposition events of individual grains within a control volume to calculate the particle activity (*Einstein*, 1950). These approaches aim at a complete statistical characterization of the bedload flux (*Fathel et al.*, 2015; *Furbish et al.*, 2012b, 2017; *Heyman et al.*, 2016), including probability distributions (*Ancey et al.*, 2006, 2008), spatial and temporal characteristics of its fluctuations (*Dhont and Ancey*, 2018; *Heyman*, 2014; *Roseberry et al.*, 2012), and the dependence of these statistical characteristics on the length and time scales over which they are observed (*Saletti et al.*, 2015; *Singh et al.*, 2009, 2012). A recent surge in research activity has generated rapid progress in this subject. For example, *Ancey et al.* (2006) demonstrated that a constant erosion rate as originally proposed by *Einstein* (1950) was insufficient to develop realistically large particle activity fluctuations, so they added a positive feedback between the particle activity and erosion rate they called “collective entrainment” (*Ancey et al.*, 2008; *Heyman et al.*, 2013, 2014; *Lee and Jerolmack*, 2018). While this feedback was deemed necessary to model realistic activity fluctuations, the implications of collective entrainment for the bed topography have not been fully explored.

In this work, I present the first stochastic model coupling the erosion and deposition of individual bedload grains to local bed elevation changes. This model extends the birth-death model approach reviewed in section 1.1.13 to describe the interplay between the bedload flux and the bed elevation within a control volume. This new model evaluates the effect of collective entrainment on bed elevation change, and it allows for investigations of the residence times of particles buried in the bed subsurface. The model has two

major assumptions: First, bedload erosion and deposition are characterized by probabilities per unit time, or rates (*Ancey et al.*, 2008; *Einstein*, 1950); and second, these rates are contingent on the local bed elevation, encoding the property that erosion of sediment is emphasized from regions of exposure, while deposition is emphasized in regions of shelter (*Sawai*, 1987; *Wong et al.*, 2007).

Below, section 3.1 introduces the stochastic model and section 3.2 solves it with a mixture of numerical and analytical techniques. Model solutions illustrate several new features of particle activity and bed elevation statistics that result from feedbacks between the erosion and deposition rates with bed elevation change. Section 3.3 present these features, while sections 3.4 and 3.5 conclude with the implications of these features and the suggestions they raise for future research.

3.1 Stochastic model of bedload transport and bed elevations

The model in this chapter is formulated by considering a volume of downstream length L containing some number n of moving particles in the flow and some number m of stationary particles composing the bed at time t , as depicted in figure 3.1. The value m is defined relative to the mean number of grains within the control volume, so that it can be either positive or negative. n is always a positive integer including 0.

All particles are considered approximately spherical with the same diameter $2a$, so their mobility and packing characteristics are consistent. Following *Ancey et al.* (2008), basically four events can occur at any instant to modify the populations n and m . These events are characterized using probabilities per unit time (rates). These events are (1) migration of a moving particle into the volume from upstream ($n \rightarrow n+1$), (2) the entrainment (erosion) of a stationary particle into motion within the volume ($m \rightarrow m-1$ and $n \rightarrow n+1$), (3) the deposition of a moving particle to rest within the volume ($m \rightarrow m+1$ and $n \rightarrow n-1$), and (4) the migration of a moving particle out of the volume to downstream ($n \rightarrow n-1$). The four events

are depicted as arrows in figure 3.1. As the events occur at random intervals, they set up a joint stochastic evolution of the populations n and m characterized by a joint probability distribution $P(n, m, t)$ for the number of particles in motion and rest in the volume at t .

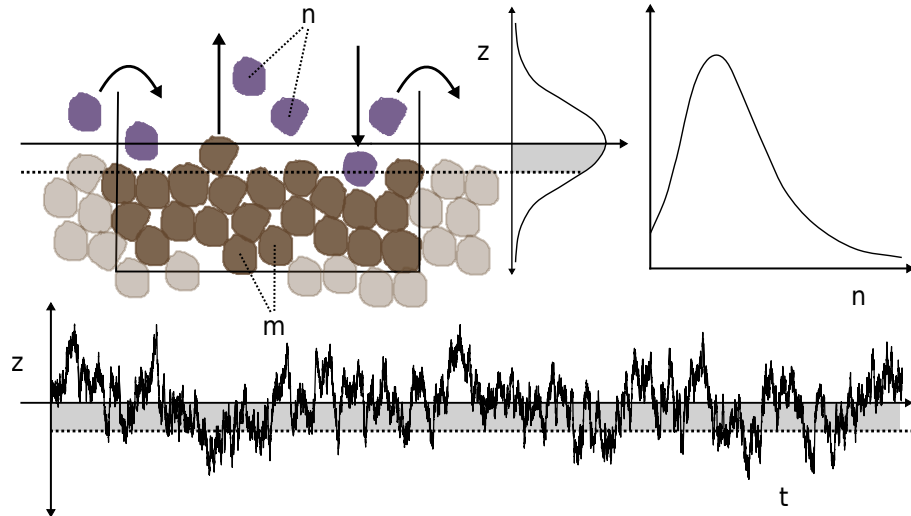


Figure 3.1: Definition sketch of a control volume containing n moving grains and m resting grains. Migration, entrainment, and deposition are represented by arrows, and the instantaneous bed elevation is depicted by dotted lines. The bed is displayed in a degraded state, where $m < 0$. The marginal distributions of n and m are indicated in the upper right panel, while the bottom panel is a realized time-series of bed elevations computed from m using (3.1).

The populations n and m provide the volumetric bedload flux Φ and the local bed elevation z . The mean transport rate is given by $\Phi = u_s \langle n \rangle / L$, where u_s is the characteristic velocity of moving bedload and $\langle n \rangle = \sum_{n,m} n P(n, m)$ is the mean number of grains in motion (Ancey *et al.*, 2008; Charru *et al.*, 2004; Furbish *et al.*, 2012b). The bed elevation is related to m through the packing geometry of the bed. This relationship depends on the packing fraction ϕ of grains in the bed (Bennett, 1972). Considering the bed as two-

dimensional (*Einstein*, 1950; *Paintal*, 1971), the deviation from the mean bed elevation can be expressed as

$$z(m) = \frac{\pi a^2}{\phi L} m = z_1 m. \quad (3.1)$$

The constant $z_1 = \pi a^2 / (\phi L)$ is an important scale in the problem. z_1 is the magnitude of bed elevation change in an average sense across the control volume associated with the addition or removal of a single grain.

Bed elevation changes modify the likelihood of entrainment and deposition in a negative feedback (*Sawai*, 1987; *Wong et al.*, 2007). Aggradation increases the likelihood of entrainment, while degradation increases the likelihood of deposition. *Wong et al.* (2007) concluded that bed elevation changes induce an exponential variation in entrainment and deposition probabilities, while *Sawai* (1987) concluded that the variation is linear. For simplicity, this chapter utilizes the scaling of *Sawai* (1987). This scaling is equivalent to the *Wong et al.* (2007) scaling when bed elevation changes are small. Because experimental distributions of bed elevations are often symmetrical, (*Crickmore and Lean*, 1962; *Martin et al.*, 2014; *Pender et al.*, 2001; *Wong et al.*, 2007), the erosion and deposition feedbacks are considered to have the same strength. As bed elevation changes drive up (down) erosion rates, so they drive down (up) deposition rates to the same degree.

Merging these ideas with those of *Ancey et al.* (2008) produces expressions for the four possible transitions with local bed elevation-dependent entrainment and deposition rates:

$$R_{MI}(n+1|n) = \nu \quad \text{migration in,} \quad (3.2)$$

$$R_E(n+1, m-1|n, m) = (\lambda + \mu n)[1 + \kappa m], \quad \text{entrainment,} \quad (3.3)$$

$$R_D(n-1, m+1|n, m) = \sigma n[1 - \kappa m], \quad \text{deposition.} \quad (3.4)$$

$$R_{MO}(n-1|n) = \gamma n \quad \text{migration out.} \quad (3.5)$$

In equations (3.3) and (3.4), κ is a coupling constant between bed elevations and the entrainment and deposition rates. κ is referred to as a coupling con-

stant since it controls the strength of this feedback. I will later demonstrate the relationship

$$\kappa \approx \left(\frac{z_1}{2l}\right)^2 \quad (3.6)$$

where l is a characteristic length scale of bed elevation change that can be interpreted as the active layer depth (*Church and Haschenburger*, 2017; *Wong et al.*, 2007). ν is the rate of migration into the control volume, λ is the conventional entrainment rate, μ is the collective entrainment rate, σ is the deposition rate, and γ is the rate of migration out of the control volume. At $m = 0$, these equations reduce to those of the *Ancey et al.* (2008) model. Away from this elevation, entrainment and deposition are alternatively suppressed or enhanced depending on the sign of m , constituting a feedback between bed elevations and erosion / deposition.

All four rates are independent of the past history of the populations and depend only on the current populations (n, m) . As a result, the model is Markovian (*Cox and Miller*, 1965; *Van Kampen*, 2007), meaning time intervals between any two subsequent transitions are exponentially distributed (*Gillespie*, 2007).

The master equation for the probability flow can be written using the Komogorov equation $\partial P(n, m; t)/\partial t = \sum_{n', m'} [R(n, m|n', m')P(n', m'; t) - R(n', m'|n, m)P(n, m; t)]$ (*Ancey et al.*, 2008; *Cox and Miller*, 1965; *Gillespie*, 1992) as

$$\begin{aligned} \frac{\partial P}{\partial t}(n, m; t) &= \nu P(n-1, m; t) + [\lambda(m+1) + \mu(n-1)][1 + \kappa(m+1)]P(n-1, m+1; t) \\ &\quad + \sigma(n+1)[1 - \kappa(m-1)]P(n+1, m-1; t) + \gamma(n+1)P(n+1, m; t) \\ &\quad - \{\nu + \lambda + \mu(n+1) + \sigma(n-1) + \gamma(n+1)\}P(n, m; t). \end{aligned} \quad (3.7)$$

The joint distribution $P(n, m; t)$ that solves this equation fully characterizes the statistics of n and m – proxies for the bedload flux and local bed elevation.

The average entrainment and deposition rates E and D over all bed elevations are $E = \lambda + \mu\langle n \rangle$ and $D = \sigma\langle n \rangle$. The solutions of (3.7) should be expected to adjust from whatever initial conditions toward a steady-

state distribution $P_s(n, m)$ – independent of time – if the constant factors in the transition rates are representative of equilibrium transport conditions. Equilibrium requires $E = D$, meaning there is no net change in elevation, and $\nu = \gamma\langle n \rangle$, meaning mass is conserved in the control volume (inflow = outflow). This Master equation describes a two-species stochastic birth-death model (*Cox and Miller*, 1965) of a type well-known in population ecology (*Pielou*, 1977; *Swift*, 2002) and chemical physics (*Gardiner*, 1983). In context of this chapter, the two populations are the moving and stationary grains in the control volume.

3.2 Model solutions

Unfortunately, equation (3.7) does not admit an analytical solution unless $\kappa = 0$ (but see *Swift* (2002) for the generating function method which fails in this case). The difficulty originates from the product terms between n and m representing the bed elevation dependence of collective entrainment and deposition rates.

Because the model is Markovian, it is nevertheless possible to numerically simulate equation (3.7) with the Gillespie algorithm (*Gillespie*, 1977, 1992, 2007). In conditions when the coupling constant κ between the entrainment/deposition rates and the bed elevation is weak, it is also possible to solve the master equation approximately with mean field and Fokker-Planck approaches (*Gardiner*, 1983; *Haken*, 1978). The Gillespie simulation algorithm is described below in 3.2.1, while these analytical approximations are described in 3.2.2.

3.2.1 Numerical study of the joint model

The Gillespie algorithm takes advantage of the defining property of a Markov process: when transition rates are independent of history, time intervals between transitions are exponentially distributed (*Cox and Miller*, 1965).

As a result, to step the Markov process through a single transition, one can draw a first random value from the exponential distribution of transition intervals to determine the time of the next transition, then draw a second

random value to choose the type of transition that occurs using relative probabilities formed from equations (3.2-3.5). The transition is enacted by shifting t , n and m by the appropriate values to the type of transition (that is, entrainment is $m \rightarrow m - 1$ and $n \rightarrow n + 1$, and so on). This procedure can be iterated to form an exact realization of the stochastic process (*Gillespie*, 2007). The appendix chapter C provides additional background on the stochastic simulation method.

Using this method, I simulated 4 transport conditions with 13 different values of l taken across a range from $l = a$ (a single radius) to $l = 10a$ (10 radii). These values include the range exhibited by the available experimental data on bed elevation timeseries (*Martin et al.*, 2014; *Singh et al.*, 2009; *Wong et al.*, 2007).

For the migration, entrainment, and deposition parameters representing bed-load transport at each flow condition $(\nu, \lambda, \mu, \sigma, \gamma)$, I used the values measured by *Ancey et al.* (2008) in a series of flume experiments: these are summarized in table 3.1. Flow conditions are labeled (a), (g), (i), and (l), roughly in order of increasing bedload flux (see *Ancey et al.* (2008) for more details). In all simulations, I

took the packing fraction $\phi = 0.6$ – a typical value for a pile of spheres (e.g., *Bennett*, 1972), and I set $L = 22.5\text{cm}$ and $a = 0.3\text{cm}$, values from the original *Ancey et al.* (2008) experiments. Each simulation was run for 250 hours of virtual time, a period selected to ensure convergence of particle activity and bed elevation statistics.

Table 3.1: Migration, entrainment, and deposition rates at $z(m) = 0$ from *Ancey et al.* (2008). Units are s^{-1} (probability/time). Bed elevation changes modulate these rates in accord with (3.2-3.5).

flow	ν	λ	μ	σ	γ
(a)	5.45	6.59	3.74	4.67	0.77
(g)	7.74	8.42	4.34	4.95	0.56
(i)	15.56	22.07	3.56	4.52	0.68
(l)	15.52	14.64	4.32	4.77	0.48

3.2.2 Approximate solutions of the joint model

The n and m dynamics in equation (3.7) can be approximately decoupled using the inequality $l \gg z_1$ (equivalently $\kappa \ll 1$) which holds for large values of the active layer depth l . These inequalities mean many entrainment or deposition events are required for an appreciable change in the entrainment or deposition rates. Concentrating on steady state conditions $\partial P / \partial t = 0$, one can introduce the exact decomposition $P(n, m) = A(n|m)M(m)$ to equation (3.7), with the new distributions normalized as $\sum_m M(m) = 1$ and $\sum_n A(n|m) = 1$ (e.g. *Haken*, 1978). This provides the steady state equation

$$0 = \nu A(n-1|m)M(m) + [\lambda + \mu(n-1)][1 + \kappa(m+1)]A(n-1|m+1)M(m+1) \\ + \sigma(n+1)[1 - \kappa(m-1)]A(n+1, m-1)M(m-1) + \gamma(n+1)A(n+1|m)M(m) \\ - \{\nu + [\lambda + \mu n](1 + \kappa m) + \sigma n(1 - \kappa m) + \gamma n\}A(n, m)M(m). \quad (3.8)$$

Summing this equation over n provides a still exact description of the distribution of bed elevations $M(m)$ in terms of the conditional mean particle activity $\langle n|m \rangle = \sum_n nA(n|m)$:

$$0 = [\lambda + \mu \langle n|m+1 \rangle][1 + \kappa(m+1)]M(m+1) \\ + \sigma \langle n|m-1 \rangle[1 - \kappa(m-1)]M(m-1) \\ - \{[\lambda + \mu \langle n|m \rangle](1 + \kappa m) + \sigma \langle n|m \rangle(1 - \kappa m)\}M(m). \quad (3.9)$$

Unfortunately, these two equations are no easier to solve than the original master equation, since the amount of coupling between n and m is not reduced in equation (3.8).

The simplest approximation to these equations holds that κ is so small that the dynamics of n are totally independent of m : $A(n|m) = A(n)$. Taking this limit in equation (3.8), summing over m , and using $\langle m \rangle = 0$ reproduces the *Ancey et al.* (2008) particle activity model. As shown in section 1.1.13, this has solution

$$A(n) = \frac{\Gamma(r+n)}{\Gamma(r)n!} p^r (1-p)^n. \quad (3.10)$$

which is a negative binomial distribution for the particle activity with parameters $r = (\nu + \lambda)/\mu$ and $p = 1 - \mu/(\sigma + \gamma)$. This result implies $\langle n|m \rangle = \langle n \rangle$, so with the definitions of E and D and the equilibrium condition $E = D$, equation (3.9) provides

$$0 \approx [1 + \kappa(m + 1)]M(m + 1) + [1 - \kappa(m - 1)]M(m - 1) - 2M(m). \quad (3.11)$$

This mean field equation matches the discrete Ornstein-Uhlenbeck model of bed elevation changes developed by *Martin et al.* (2014). The independent bed elevation and particle activity models of *Martin et al.* (2014) and *Ancey et al.* (2008) derive from the model equation 3.7 in a mean field approximation when κ is insignificant.

In the supplementary information I show that the Fokker-Planck approximation (*Gardiner*, 1983) formed by expanding $M(m \pm 1)$ to second order in m within equation (3.11) provides the solution $M(m) \propto \exp(-\kappa m^2)$: this is a normal distribution of bed elevations with variance $\sigma_m^2 \propto \frac{1}{2\kappa}$. As I will demonstrate in section 3.3, and as I have already suggested with equation (3.6), this is a poor approximation to the bed elevation variance. Nevertheless, this approximation does capture the Gaussian shape of the bed elevation distribution. The essential issue with this mean field approach is that the conditional mean particle activity $\langle n|m \rangle$ varies significantly with m in actuality, especially when collective entrainment contributes to the mean entrainment rate E . I will discuss these points subsequently when developing more refined approximations and presenting numerical results.

A more careful approximate solution to equation (3.9) can be obtained by prescribing a phenomenological equation for $\langle n|m \rangle$ into equation (3.9) in order to close the equation for m without solving equation (3.8). From numerical simulations we determine that

$$\langle n|m \rangle \approx \langle n \rangle \left(1 - \frac{2\kappa m}{1 - \mu/\sigma} \right) \quad (3.12)$$

captures the general features of the conditional mean particle activity. As I show in the supplementary information, introducing this closure equation

to (3.9), making the Fokker-Planck approximation, and neglecting terms of $O(\kappa^2)$ provides

$$M(m) \approx M_0 e^{-2\kappa m^2}, \quad (3.13)$$

representing a Gaussian distribution with variance $\sigma_m^2 = \frac{1}{4\kappa}$ – smaller than the former mean field theory by a factor of two and in agreement with the result posited in equation (3.6). M_0 is a normalization constant. This closure equation approach shows good correspondence with numerical solutions of equation (3.7), at least for the flow parameters in table 3.1.

3.3 Results

From the initial conditions, all simulations show a rapid attainment of steady-state stochastic dynamics of n and m which support a time-independent joint distribution $P(n, m)$. The bottom panel of figure 3.1 shows an elevation time-series. In order to describe the implications of coupling bedload transport to bed elevation changes, the numerical and analytical results for the probability distributions of bedload transport and bed elevations are presented in section 3.3.1 and the statistical moments of these quantities in section 3.3.2. The effects of collective entrainment on bed elevation changes are studied in section 3.3.3, and the resting times of sediment undergoing burial are evaluated in section 3.3.4.

3.3.1 Probability distributions of bedload transport and bed elevations

The joint distribution is computed numerically by counting occurrences of the states (n, m) in the simulated time series. From this joint distribution the marginal distributions $P(n)$ and $P(m)$ are obtained by summing over m and n respectively. A representative subset of these marginal distributions is displayed in figure 3.2 alongside the approximate results of equations (3.10) and (3.13). The mean field equation (3.10) for the particle activity n closely represents the numerical results, and while there are small differences between numerical and analytical results for the relative number m of resting particles, the numerical solutions approximately match equation (3.13), hav-

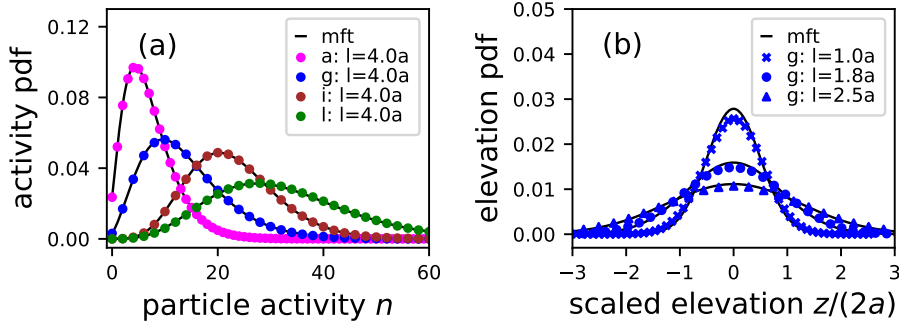


Figure 3.2: Panel (a) presents the probability distribution of particle activity n and panel (b) presents the probability distribution of the relative number of particles m for a representative subset of simulations. These distributions represent different flows from table 3.1, distinguished by color, and different values of the active layer depth l (equivalently the coupling constant κ), distinguished by the marker style. The mean field theories (mft) of equations (3.10) and (3.13) are displayed as solid black lines.

ing Gaussian profiles consistent with the assumption of a symmetric scaling of erosion and deposition rates with bed elevation changes.

3.3.2 Statistical moments of bed elevation and the particle activity

The moments of n and m are calculated by summing over $P(n, m)$. The j th order unconditional moment of the particle activity n derives from

$$\langle n^j \rangle = \sum_n n^j P(n), \quad (3.14)$$

while the j th order moment of n held conditional on m is

$$\langle n^j | m \rangle = \sum_n n^j P(n, m). \quad (3.15)$$

The moments of m show no dependence on the value of n . The mean elevation is always $\langle m \rangle = 0$ due to the initial assumption of symmetry in the entrainment and deposition rate scaling with m .

Figure 3.3 demonstrates that the variance of bed elevations is approximately $\sigma_z^2 = z_1^2 \sigma_m^2 = \frac{1}{4\kappa} = l^2$, agreeing with the approximation in equation (3.13); this result suggests that l is a characteristic length scale of bed elevation fluctuations. The close correspondence between the mean field approximation and the numerical simulations in figure (3.2a) suggests the unconditional moments of n correspond closely with the Ancey *et al.* (2008) result. They appear to be identical within numerical uncertainty.

The coupling between bed elevation changes and the erosion and deposition rates develop a strong dependence of the particle activity on m . Figure (3.4) displays the mean shift $[\langle n|m \rangle - \langle n \rangle]/\langle n \rangle$ and the variance shift $[\text{var}(n|m) - \text{var}(n)]/\text{var}(n)$ of the particle activity due to departures of the bed elevation from its mean position. Figure (3.4a) demonstrates that the flow conditions in table 3.1 support departures of the mean particle activity by as much as 60% from the overall mean value when the bed is in a degraded state $z \approx -3l$, and the activity can be decreased by 20% when the bed is in an aggraded state. The closure model (3.12) used to derive the approximate bed elevation distribution (3.13) is plotted behind the conditional mean profiles in figure (3.4a), where it appears to be crude approximation, as it does not capture the asymmetry. Nevertheless, figure 3.3 demonstrates the variance $1/(4\kappa)$ derived from this closure equation is representative of

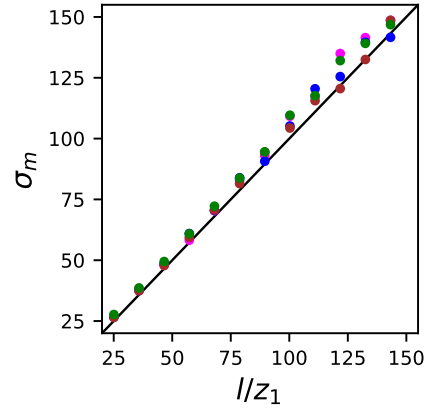


Figure 3.3: Data from all simulations demonstrating that the active layer depth l characterizes bed elevation changes as posited in equation (3.6): $\sigma_m^2 \approx (l/z_1)^2$.

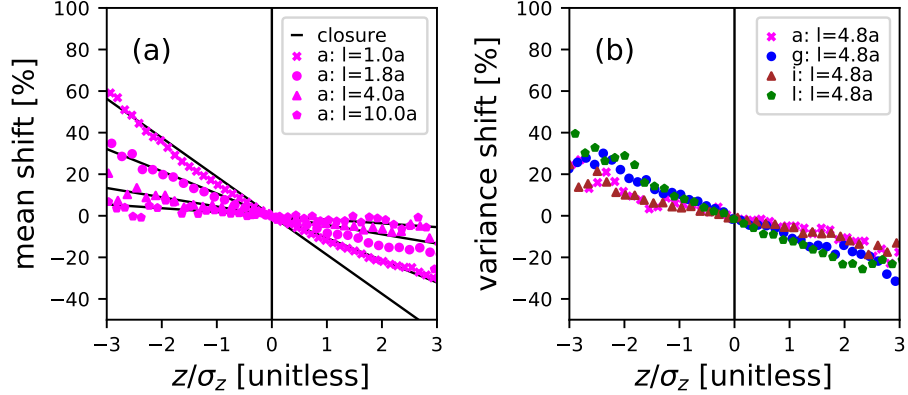


Figure 3.4: The shifts between particle activity moments conditioned on instantaneous elevations and their over-all mean values. Panel (a) indicates the mean particle activity shift versus the bed elevation measured in units of $\sigma_z = l$. This shift displays asymmetric dependence on m at the flow conditions of the Ancey *et al.* (2008) experiments, and departures of the bedload transport mean can be as much as 60% when the bed is in a severely degraded state with $z \approx -3l$. The closure equation (3.12) is plotted in panel (a). Panel (b) demonstrates a more symmetrical variance shift with some dependence on flow conditions displaying shifts of up to 20% with bed elevations. These results indicate that bedload statistics measurements on short timescales could be severely biased by departures from the mean bed elevation.

the numerical relationship. For the parameters of the Ancey *et al.* (2008) experiments, figure (3.4b) displays a variance shift with bed elevation changes that is less severe than the mean shift but is nevertheless appreciable, with bed elevations changing the magnitude of bedload activity fluctuations by as much as 20%. The summary is that bed elevation changes regulate the particle activity moments, with a moment suppression effect when the bed is aggraded, and a moment enhancement effect when the bed is degraded.

3.3.3 Collective entrainment and bedload activity fluctuations

Noting that bed elevations regulate the particle activity moments, the next step is to study the influence of collective entrainment on this effect by modifying the relative proportion of the individual to collective contributions in the mean entrainment rate $E = \lambda + \sigma\langle n \rangle$. The equilibrium condition $E = D$ implies that the fraction of entrainment due to the collective process is $f = \mu\langle n \rangle/E = \mu/\sigma$. This fraction can be used to hold E constant and modify the prevalence of the collective entrainment process by setting $\lambda = E(1 - f)$ and $\mu = \sigma f$. Interpolating f between zero and one interpolates the particle activity component of the master equation 3.7 from a purely Poissonian model to a negative binomial model, isolating the effect of collective entrainment on the particle activity statistics over a dynamic sedimentary bed. Figure 3.5 depicts the modification of the particle activity mean and variance as the importance of collective entrainment is tuned (through λ and μ) with all other parameters fixed. When $f = 0$, the bed elevation ceases to influence the particle activity mean or variance, while larger fractions increasingly enable the moment regulation effect identified in section 3.3.2.

3.3.4 Resting times of sediment undergoing burial

Resting times for sediment undergoing burial are obtained from analyzing the return times from above in the time-series of m (e.g., Redner, 2007). Following Voepel *et al.* (2013) and Martin *et al.* (2014), we concentrate on a particular bed elevation m' , and find all time intervals separating deposition events at $m = m'$ from erosion events at $m = m' + 1$. These are the return times from above of the sedimentary bed conditional to the elevation m' . Binning these conditional return times (using logarithmically-spaced bins to reduce computational load) and counting the occurrences in each bin, we obtain an exceedance distribution of return times t_r held conditional to the elevation m' : $P(T > t_r | m')$. Using the marginal probability distribution of bed elevations $P(m)$ (figure 3.2(b)), we derive the unconditional exceedance

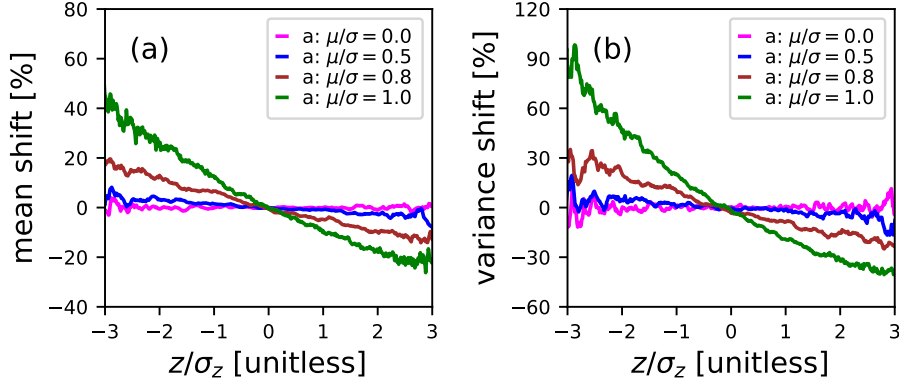


Figure 3.5: The shift of the mean particle activity in panel (a) and its fluctuations in panel (b) with departures of the bed elevation from its mean. All simulations are at flow condition (g) from table 3.1 except λ and μ are modified to shift the fraction $f = \mu/\sigma$ of the over-all entrainment rate E due to collective entrainment. Clearly, collective entrainment drives strong departures of the bedload statistics away from the mean field model (3.10) at large departures from the mean bed elevation. Panel (b) shows particle activity fluctuations suppressed by 90% when $z \approx -3l$ and collective entrainment is the dominant process. When collective entrainment is absent, meaning $\mu/\sigma = 0$, this moment regulation effect vanishes: it is a consequence of collective entrainment.

distribution of resting times as a sum over all elevations (*Martin et al., 2014; Nakagawa and Tsujimoto, 1980; Voepel et al., 2013; Yang and Sayre, 1971*):

$$P(T > t_r) = \sum_{m'} P(m') P(T > t_r | m'). \quad (3.16)$$

A representative subset of these results are displayed in figure 3.6. Comparing panels 3.6(a) and 3.6(c) shows two separate variations with input parameters: first, the distributions vary with the flow conditions, and second, they vary with the standard deviation of bed elevations (l). However, as shown in panels 3.6(b) and 3.6(d), a characteristic timescale T_0 is found

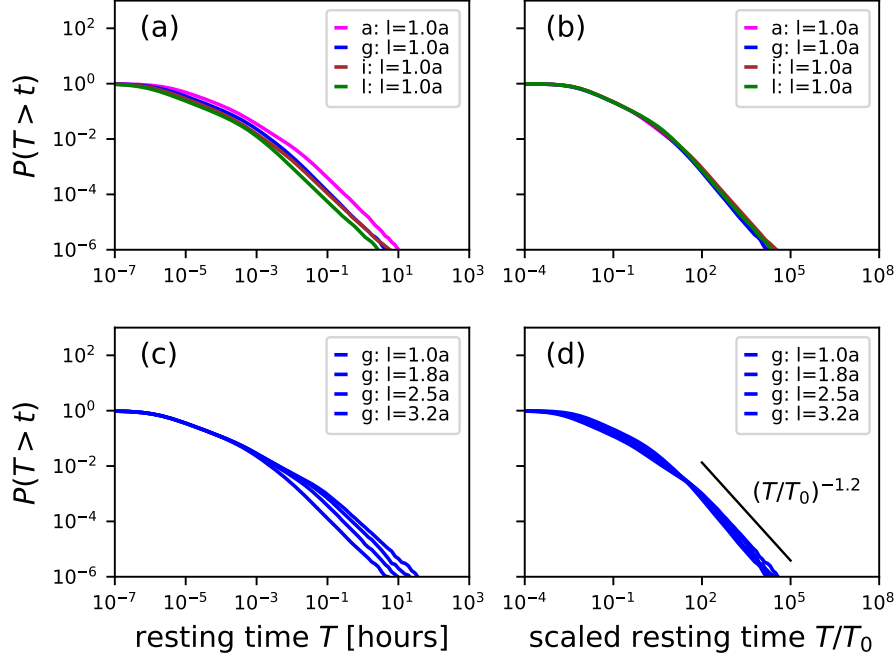


Figure 3.6: Resting time statistics scale differently with transport conditions and the bed elevation variance. Panel (a) shows differing flow conditions at a fixed l value, while panel (c) shows fixed flow conditions at differing l . When scaled by T_0 (3.17), both types of difference collapse in the tails of the distributions, as shown in panels (b) and (d). In panels (b) and (d), the black dotted lines indicate a power law decay of the collapsed tails having parameter $\alpha \approx 1.18$.

to collapse away both variations. We obtained this T_0 heuristically by considering the characteristic speed of bed elevation change. This is the mean number of grains leaving the bed per unit time is E , and the removal of a single grain changes the bed elevation by z_1 (3.1). Therefore, bed elevations change with a characteristic speed $v = z_1 E$. Since the range of elevation deviations is l (figure 3.3), the time required for the bed to shift through

this characteristic distance is l/v , or equivalently

$$T_0 = \frac{l}{z_1 E}. \quad (3.17)$$

When scaling the resting time by this T_0 , we obtain the collapse shown in figure 3.6. Using the log-likelihood estimation technique described by *Newman* (2005), we estimate the scaled resting time non-exceedance distributions decay as a heavy tailed power law with parameter $\alpha = 1.18 \pm 0.32$ for all return times satisfying $T/T_0 > 10^3$. These distributions are sufficiently heavy tailed to violate the central limit theorem and drive anomalous super-diffusion of bedload, a result which supports the earlier conclusions of *Voepel et al.* (2013) and *Martin et al.* (2014).

3.4 Discussion

3.4.1 Context of the research

Einstein developed the first stochastic models of bedload tracer diffusion (*Einstein*, 1937) and the bedload flux (*Einstein*, 1950), and his ideas can be viewed as the nexus of an entire paradigm of research that extends into the present day (e.g., *Ancey et al.*, 2008; *Hassan et al.*, 1991; *Hubbell and Sayre*, 1964; *Nakagawa and Tsujimoto*, 1976; *Wu et al.*, 2019a). These models aim to predict bedload transport characteristics from stochastic concepts of individual particle motions. With some exceptions (*Nakagawa and Tsujimoto*, 1980; *Pelosi et al.*, 2014; *Wu et al.*, 2019a,b; *Yang and Sayre*, 1971), existing descriptions are spatially one-dimensional, concentrating on the motion of grains in the downstream direction without including the vertical dimension wherein local bed elevation changes imply sediment burial (*Martin et al.*, 2014; *Voepel et al.*, 2013) and change the mobility of surface grains (*Nakagawa and Tsujimoto*, 1980; *Yang and Sayre*, 1971).

3.4.2 New contributions

This chapter has modified the birth-death approach to describe sediment transport in a control volume. This model was applied to study the interplay between bedload transport and bed elevation fluctuations and to investigate resting time distributions of sediment undergoing burial. This model is the first description of bedload transport and bed elevations as a coupled stochastic population model based on individual grains. Numerical solutions and analytical approximations provided negative binomial distributions of bedload activity and normal distributions of bed elevations. Although experiments under more natural conditions with segregation processes, migrating bedforms, or sediment supply perturbations have shown particle activity distributions with heavier tails (*Dhont and Ancey*, 2018; *Saletti et al.*, 2015) and non-Gaussian bed elevations (*Aberle and Nikora*, 2006; *Singh et al.*, 2012), our results reproduce the key features of the most controlled bed elevation (*Martin et al.*, 2014; *Wong et al.*, 2007) and bedload transport (*Ancey et al.*, 2008; *Heyman et al.*, 2016) experiments in the literature.

The inclusion of coupling between the bed elevation and entrainment and deposition rates revealed a novel dependence of particle activity on bed elevation changes, highlighting a new consequence of the collective entrainment process (*Ancey et al.*, 2008; *Lee and Jerolmack*, 2018). This coupling develops a significant variation of the particle activity moments with deviations of the bed from its mean elevation. These particle activity variations with bed elevation changes disappear in the absence of collective entrainment.

Finally, the model allowed resolution of resting times for sediment undergoing burial within the sedimentary bed. These timescales were obtained by analyzing return times from above in the bed elevation timeseries. This analysis produces heavy-tailed power-law resting times with tail parameters sufficient to drive anomalous diffusion of bedload at long timescales. The power-law tails were found to collapse across flow conditions using a timescale formed from the mean erosion rate and the active layer depth.

As the model in this chapter builds on earlier works describing particle

activity and bed elevation changes independently, it also reduces to these works in simplified limits when the coupling between the particle activity and the local bed elevation vanishes. With the mean field approach in section 3.2.2, the *Martin et al.* (2014) Ornstein-Uhlenbeck model for bed elevations and the *Ancey et al.* (2008) birth-death model for the particle activity were derived as simplified limits of the coupled model developed in this chapter. While the mean field description of bed elevations over-predicts the bed elevation variance by approximately a factor of two, it does capture the Gaussian shape of the bed elevation distribution, and its conclusions on the tail characteristics of resting time distributions for sediment undergoing burial are identical to the model in this chapter within the numerical uncertainty. *Martin et al.* (2014) described a power-law distribution with tail parameter $\alpha \approx 1$ which falls neatly within the estimation $\alpha = 1.18 \pm 0.32$ presented here.

3.4.3 Next steps for research

The model presented in this chapter computes statistical characteristics of the bedload particle activity and bed elevation within a control volume by assuming all particles on the bed surface have similar mobility characteristics while sediment transport and bed topography are in equilibrium. In actuality, particles span a range of sizes, and spatial organization occurs both in the forces imparted to particles by the flow (*Amir et al.*, 2014; *Shih et al.*, 2017) and in the mobility characteristics of particles on the bed surface (*Charru et al.*, 2004; *Hassan et al.*, 2007; *Nelson et al.*, 2014). Together, these factors may generate spatial correlations in particle activities that models concentrating on a single control volume will be unable to capture. Models chaining multiple control volumes together have shown spatial correlations in the particle activity as a result of collective entrainment (*Ancey et al.*, 2015; *Heyman et al.*, 2014), and similar approaches have also been applied to study correlations in turbulent flows (*Gardiner*, 1983). In light of this work, the model presented in this chapter is considered a preliminary step toward a multiple-cell model of particle activities and bed elevation

changes with potential to express spatial correlations between longitudinal profile and particle activity statistics.

Like the theory developed by *Martin et al.* (2014), the model 3.7 produces heavy-tailed power-law resting times for sediment undergoing burial by treating bed elevation changes as an unbounded random walk with a mean reverting tendency. This result suggests sediment burial can explain the heavy-tailed rests seen in field data (*Bradley*, 2017; *Olinde and Johnson*, 2015; *Pretzlav*, 2016). The resting time distributions derived in section 3.3.4 show a divergent variance and possibly a divergent mean, since this occurs for $\alpha < 1$ (*Sornette*, 2006) which is within range of the results.

Divergent mean resting time distributions present a paradox, since they imply all particles should eventually be immobile, violating the equilibrium transport assumption. *Voepel et al.* (2013) demonstrated that a bounded random walk for bed elevations provides a power-law distribution that eventually transitions to a faster thin-tailed decay, allowing for power-law scaling like our result and *Martin et al.* (2014) without this divergent mean paradox. One resolution to this issue could come from a spatially distributed model with multiple cells. Neighboring locations might bound excessive local elevation changes through granular relaxations from gradients above the angle of repose. In this interpretation, divergent mean power law resting time distributions may be relics of single cell models for bed elevation changes. We should always expect a maximum depth to which the bed can degrade relative to neighboring locations; this could temper the power law tail without required the reflecting boundaries used by *Voepel et al.* (2013).

Finally, this chapter presented the probability distribution functions and first and second moments of the particle activity and bed elevation, indicating novel coordination between the statistical characteristics of these quantities which deserve experimental testing. Some relatively recent particle tracking experiments have demonstrated joint resolution of bed elevations and bedload transport (*Heyman et al.*, 2016; *Martin et al.*, 2014). A suitably designed experiment using this methodology could test the prediction that bed elevations regulate particle activity statistics, as essentially represented in figures 3.4 and 3.5.

Many other statistical characteristics of bedload transport have been left for future studies. For example, the dependence of bedload transport (*Saletti et al.*, 2015; *Singh et al.*, 2009) and bed elevation statistics (*Aberle and Nikora*, 2006; *Singh et al.*, 2009, 2012) on the spatial and temporal scales over which they are observed is an emerging research topic which was previously referenced in section 1.1.14. Whether bed elevation distributions are also scale-dependent like the sediment flux distribution of chapter 2 is an interesting question for future research.

3.5 Summary

This chapter presented a stochastic model for particle activity and local bed elevations including feedbacks between elevation changes and sediment transport. This model includes collective entrainment, whereby moving particles tend to destabilize stationary ones. The model was analyzed using a mixture of numerical and analytical methods, and two key results were presented:

1. Resting times for sediment undergoing burial lie on a heavy-tailed power law distributions with tail parameter $\alpha \approx 1.2$;
2. Collective entrainment generates a statistical regulation effect, whereby bed elevation changes modify the mean and variance of the particle activity by as much as 90%: this effect vanishes when collective entrainment is absent.

These results imply measurements of bedload transport statistics could be biased at observation timescales smaller than adjustments of the bed elevation timeseries when collective entrainment occurs. The next step is to generalize the model in this chapter to a multi-cell framework to study channel morphodynamics in a stochastic framework.

Chapter 4

Burial-induced three-range diffusion in sediment transport

Many environmental problems including channel morphology (*Hassan and Bradley*, 2017), contaminant transport (*Macklin et al.*, 2006), and aquatic habitat restoration (*Gaeuman et al.*, 2017) rely on our ability to predict the diffusion characteristics of coarse sediment tracers in river channels. Diffusion is quantified by the time dependence of the positional variance σ_x^2 of a group of tracers. With the scaling $\sigma_x^2 \propto t$, the diffusion is said to be normal, since this is found in the classic problems (*Taylor*, 1920). However, with the scaling $\sigma_x^2 \propto t^\gamma$ with $\gamma \neq 1$, the diffusion is said to be anomalous (*Sokolov*, 2012), with $\gamma > 1$ defining super-diffusion and $\gamma < 1$ defining sub-diffusion (*Metzler and Klafter*, 2000). *Einstein* (1937) developed one of the earliest models of bedload diffusion to describe a series of flume experiments (*Ettema and Mutel*, 2004). Interpreting individual bedload trajectories as a sequence of random steps and rests, Einstein originally concluded that a group of bedload tracers undergoes normal diffusion.

More recently, Nikora et al. realized coarse sediment tracers can show either normal or anomalous diffusion depending on the length of time they have been tracked (*Nikora et al.*, 2001b, 2002). From numerical simulations

and experimental data, Nikora et al. discerned “at least three” scaling ranges $\sigma_x^2 \propto t^\gamma$ as the observation time increased. They associated the first range with “local” timescales less than the interval between subsequent collisions of moving grains with the bed, the second with “intermediate” timescales less than the interval between successive resting periods of grains, and the third with “global” timescales composed of many intermediate timescales. Nikora et al. proposed super-diffusion in the local range, anomalous or normal diffusion in the intermediate range, and sub-diffusion in the global range. They attributed these ranges to “differences in the physical processes which govern the local, intermediate, and global trajectories” of grains (Nikora et al., 2001b), and they called for a physically based model to explain the diffusion characteristics (Nikora et al., 2002).

Experiments support the Nikora et al. conclusion of multiple scaling ranges (Fathel et al., 2016; Martin et al., 2012), but they do not provide consensus on the expected number of ranges or their scaling properties. This lack of consensus probably stems from resolution issues. For example, experiments have tracked only moving grains, resolving the local range (Fathel et al., 2016; Furbish et al., 2012a, 2017); grains resting on the bed surface between movements, resolving the intermediate range (Einstein, 1937; Nakagawa and Tsujimoto, 1976; Yano, 1969); grains either moving or resting on the bed surface, likely resolving local and intermediate ranges (Martin et al., 2012); or grains resting on the surface after floods, likely resolving the global range (Bradley, 2017; Phillips et al., 2013). At long timescales, a significant fraction of tracers bury under the bed surface (Ferguson et al., 2002; Haschenburger, 2013; Hassan et al., 1991, 2013; Papangelakis and Hassan, 2016), meaning burial dominates long term diffusion characteristics (Bradley, 2017; Martin et al., 2014; Voepel et al., 2013), possibly at global or even longer “geomorphic” timescales (Hassan and Bradley, 2017) than Nikora et al. originally considered. As a result, three diffusion ranges can be identified by patching together multiple datasets (Nikora et al., 2002; Zhang et al., 2012), but they are not resolved by any one dataset.

Newtonian bedload trajectory models also show multiple diffusion ranges, although they also do not provide consensus on the expected number of

ranges or their scaling properties. The majority of these models predict two ranges of diffusion (local and intermediate) without predicting a global range. Among these, *Nikora et al.* (2001b) used synthetic turbulence (*Kraichnan*, 1970) with a discrete element method for the granular phase (*Cundall and Strack*, 1979); *Bialik et al.* (2012) used synthetic turbulence with a random collision model (*Sekine and Kikkawa*, 1992); and *Fan et al.* (2016) used a Langevin equation with probabilistic rests. To our knowledge, only *Bialik et al.* (2015) have claimed to capture all three ranges from a Newtonian approach. They incorporated a second resting mechanism into their earlier model (*Bialik et al.*, 2012), implicitly suggesting that three diffusion ranges could result from two distinct timescales of sediment rest. However, Newtonian approaches have not evaluated the effect of sediment burial on tracer diffusion, probably due to the long simulation timescales required.

Random walk bedload diffusion models constructed in the spirit of *Einstein* (1937) provide an alternative to the Newtonian approach and can include a second timescale of rest by incorporating sediment burial. Einstein originally modeled bedload trajectories as instantaneous steps interrupted by durations of rest lying on statistical distributions (*Hassan et al.*, 1991), but this generates only one range of normal diffusion (*Einstein*, 1937; *Hubbell and Sayre*, 1964; *Nakagawa and Tsujimoto*, 1976). Recently, researchers have generalized Einstein's model in a few different ways to describe multiple diffusion ranges. *Lisle et al.* (1998) and *Lajeunesse et al.* (2017) promoted Einstein's instantaneous steps to motion intervals with random durations and a constant velocity, providing two diffusion ranges – local and intermediate. *Wu et al.* (2019a) retained Einstein's instantaneous steps but included the possibility that grains can become permanently buried as they rest on the bed, also providing two diffusion ranges – intermediate and global. These earlier works suggest the minimal required components to model three bedload diffusion ranges: (1) exchange between motion and rest intervals and (2) the sediment burial process.

In this study, I incorporate these two components into Einstein's original approach to describe three diffusion ranges with a physically based model, as called for by *Nikora et al.* (2002). Einstein was a giant in river geophysics

and fostered an entire paradigm of research leveraging and generalizing his stochastic methods (*Gordon et al.*, 1972; *Hubbell and Sayre*, 1964; *Nakagawa and Tsujimoto*, 1976; *Paintal*, 1971; *Yang and Sayre*, 1971; *Yano*, 1969). Einstein’s model can be viewed as a pioneering application of the continuous time random walk (CTRW) developed by *Montroll* (1964) in condensed matter physics to describe the diffusion of charge carriers in solids. To incorporate motion intervals and sediment burial, I utilize the multi-state CTRW formalism developed by *Weiss* (1976, 1994) that extends the CTRW of *Montroll* (1964). Below, I develop and solve the model in section 4.1. Then, I discuss the predictions of this model, present its implications for local, intermediate, and global ranges of bedload diffusion, and suggest next steps for bedload diffusion research in sections 4.2 and 4.3.

4.1 Bedload trajectories as a multi-state random walk

4.1.1 Assumptions of the burial model

Particle trajectories are formulated as a three-state random walk where the states are motion, surface rest, and burial. These states are labelled as $i = 2$ (motion), $i = 1$ (rest), and $i = 0$ (burial). The target is the probability distribution $p(x, t)$ to find a grain at position x and time t if it is known to have started with the initial distribution $p(x, 0) = \delta(x)$. Times spent moving or resting on the surface are characterized by exponential distributions $\psi_2(t) = k_2 e^{-k_2 t}$ and $\psi_1(t) = k_1 e^{-k_1 t}$, since numerous experiments show thin-tailed distributions for these quantities (*Ancey et al.*, 2006; *Einstein*, 1937; *Fathel et al.*, 2015; *Martin et al.*, 2012; *Roseberry et al.*, 2012). The end results will not be contingent on the specific distributions chosen, since all thin-tailed distributions provide similar diffusion characteristics in random walks (*Weeks and Swinney*, 1998; *Weiss*, 1994). Grains in motion are considered to have a characteristic velocity V (*Lajeunesse et al.*, 2017; *Lisle et al.*, 1998), and burial is modelled as long lasting enough to be effectively permanent (*Wu et al.*, 2019a), with grains resting on the surface having

a probability per unit time κ to become buried. This means $\Phi(t) = e^{-\kappa t}$ represents the probability that a grain is not buried after resting for a time t , while $1 - \Phi(t)$ represents the probability that it is buried. The initial conditions are specified with probabilities θ_1 and θ_2 to be in rest or motion at $t = 0$. Normalization requires $\theta_1 + \theta_2 = 1$.

4.1.2 Governing equations

With these assumptions, the governing equations for the set of probabilities $\omega_{ij}(x, t)$ that a transition occurs from state i to state j at position x and time t can be derived using the statistical physics approach to multi-state random walks (*Schmidt et al.*, 2007; *Weeks and Swinney*, 1998; *Weiss*, 1994). Denoting by $g_{ij}(x, t)$ the probability for a particle to displace by x in a time t within the state i before it transitions to the state j , the transition probabilities $\omega_{ij}(x, t)$ sum over all possible paths to the state i from previous locations and times:

$$\omega_{ij}(x, t) = \theta_i g_{ij}(x, t) + \sum_{k=0}^2 \int_0^x dx' \int_0^t dt' \omega_{ki}(x', t') g_{ij}(x - x', t - t'). \quad (4.1)$$

Defining another set of probabilities $G_i(x, t)$ that a particle displaces by a distance x in a time t within the state i and possibly remains within the state, a similar sums over paths for the probabilities to be in the state i at x, t produces:

$$p_i(x, t) = \theta_i G_i(x, t) + \sum_{k=0}^2 \int_0^x dx' \int_0^t dt' \omega_{ki}(x', t') G_i(x - x', t - t'). \quad (4.2)$$

Finally, the overall probability to be at position x at time t is

$$p(x, t) = \sum_{k=0}^2 p_k(x, t) \quad (4.3)$$

This joint density is completely determined from the solutions of equations (4.1-4.2) given specification of the distributions g_{ij} and G_i .

4.1.3 Joint probability distribution of particle position with burial

These distributions can be constructed from the assumptions described in section 4.1.1. Since particles resting on the bed surface bury in a time t with probability $\Phi(t)$, and resting times are distributed as $\psi_1(t)$, these assumptions obtain $g_{12}(x, t) = \delta(x)k_1 e^{-k_1 t} e^{-\kappa t}$ and $g_{10}(x, t) = \delta(x)k_1 e^{-k_1 t}(1 - e^{-\kappa t})$. Since motions have velocity v for times distributed as $\psi_2(t)$, the assumptions provide $g_{21}(x, t) = \delta(x - vt)k_2 e^{-k_2 t}$. Since burial is quasi-permanent, all other $g_{ij} = 0$. The G_i are constructed in the same way except using the cumulative probabilities $\int_t^\infty dt' \psi_i(t') = e^{-k_i t}$, since these characterize motions and rests that are ongoing (Weiss, 1994). Using the cumulative probabilities provides $G_1(x, t) = \delta(x)e^{-k_1 t}$ and $G_2(x, t) = \delta(x - vt)e^{-k_2 t}$.

Equations (4.1-4.2) with these g_{ij} and G_i are solved using Laplace transforms in space and time ($x, t \rightarrow \eta, s$). This method, similar to Weeks and Swinney (1998), unravels the convolution structure of these equations, eventually producing

$$\tilde{p}(\eta, s) = \frac{1}{s} \frac{(s + \kappa + k')s + \theta_1(s + \kappa)\eta v + \kappa k_2}{(s + \kappa + k_1)\eta v + (s + \kappa + k')s + \kappa k_2}, \quad (4.4)$$

where $k' = k_1 + k_2$. Inverting this result using known Laplace transforms (Arfken, 1985; Prudnikov et al., 1992) obtains

$$\begin{aligned} p(x, t) &= \theta_1 \left[1 - \frac{k_1}{\kappa + k_1} \left(1 - e^{-(\kappa+k_1)t} \right) \right] \delta(x) \\ &\quad + \frac{1}{v} e^{-\Omega\tau-\xi} \left(\theta_1 \left[k_1 \mathcal{I}_0(2\sqrt{\xi\tau}) + k_2 \sqrt{\frac{\tau}{\xi}} \mathcal{I}_1(2\sqrt{\xi\tau}) \right] \right. \\ &\quad \left. + \theta_2 \left[k_1 \delta(\tau) + k_2 \mathcal{I}_0(2\sqrt{\xi\tau}) + k_1 \sqrt{\frac{\xi}{\tau}} \mathcal{I}_1(2\sqrt{\xi\tau}) \right] \right) \\ &\quad + \frac{1}{v} \frac{\kappa k_2}{\kappa + k_1} e^{-\kappa\xi/(\kappa+k_1)} \left[(\theta_1/\Omega) \mathcal{Q}_2(\xi/\Omega, \Omega\tau) + \theta_2 \mathcal{Q}_1(\xi/\Omega, \Omega\tau) \right] \end{aligned} \quad (4.5)$$

for the joint distribution that a tracer is found at position x at time t . This result generalizes the earlier results of Lisle et al. (1998) and Ein-

stein (1937) to include sediment burial. This equation uses the short-hand notations $\xi = k_2x/v$, $\tau = k_1(t - x/v)$, and $\Omega = (\kappa + k_1)/k_1$ (c.f. Lisle *et al.*, 1998). The \mathcal{I}_ν are modified Bessel functions of the first kind and the \mathcal{Q}_μ are generalized Marcum Q-functions defined by $\mathcal{Q}_\mu(x, y) = \int_0^y e^{-z-x}(z/x)^{(\mu-1)/2} \mathcal{I}_{\mu-1}(2\sqrt{xz}) dz$ and originally devised for radar detection theory (Marcum, 1960; Temme, 1996). The Marcum Q-functions derive from the burial process. Because resting grains can become buried with an exponential probability, while the probability that particles rest follows a modified Bessel distribution (Einstein, 1937; Lisle *et al.*, 1998), evaluating the probability that particles rest and become buried generates the Q-function convolution structure.

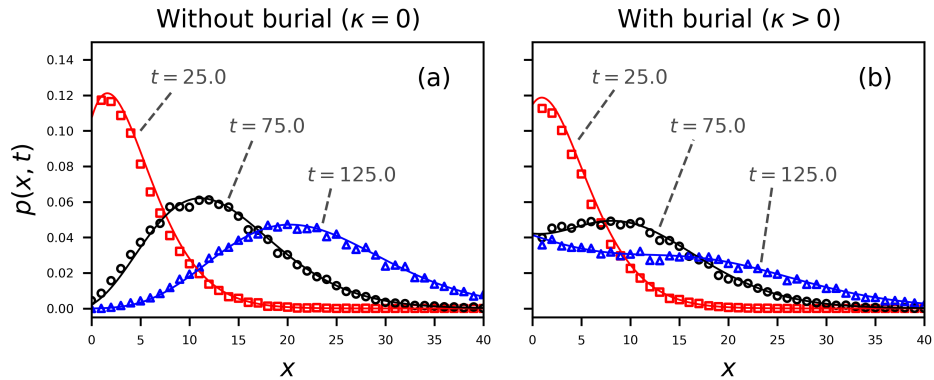


Figure 4.1: Joint distributions for a grain to be at position x at time t are displayed for the choice $k_1 = 0.1$, $k_2 = 1.0$, $v = 2.0$. Grains are considered initially at rest ($\theta_1 = 1$, $\theta_2 = 0$). The solid lines are the analytical distribution in equation (4.5), while the points are numerically simulated, showing the correctness of our derivations. Colors pertain to different times. Units are unspecified, since the aim is to demonstrate the general characteristics of $p(x, t)$. Panel (a) shows the case $\kappa = 0$ – no burial. In this case, the joint distribution tends toward Gaussian at large times (Einstein, 1937; Lisle *et al.*, 1998). Panel (b) shows the case when grains have rate $\kappa = 0.01$ to become buried while resting. Because of burial, the joint distribution tends toward a more uniform distribution than Gaussian.

Figure 4.1 depicts the distribution (4.5) alongside simulations generated by a direct method based on evaluating the cumulative transition probabilities between states on a small timestep (*Barik et al.*, 2006). When grains do not become buried, as in panel (a) of figure 4.1, the distribution becomes Gaussian-like at relatively large observation times, exemplifying normal diffusion and satisfying the central limit theorem. When grains become buried, as in panel (b) of figure 4.1, the Q-function terms prevent the distribution from approaching a Gaussian at large timescales, exemplifying anomalous diffusion (*Weeks and Swinney*, 1998) and violating the central limit theorem (*Metzler and Klafter*, 2000; *Schumer et al.*, 2009).

4.1.4 Downstream diffusion

To obtain an analytical formula for tracers diffusing downstream while they gradually become buried, the first two moments of position are derived by taking derivatives with respect to η of the Laplace space distribution (4.4) using an approach similar to *Shlesinger* (1974) and *Weeks and Swinney* (1998). These moments produce the positional variance $\sigma_x^2 = \langle x^2 \rangle - \langle x \rangle^2$. The first two moments are

$$\langle x(t) \rangle = A_1 e^{(b-a)t} + B_1 e^{-(a+b)t} + C_1, \quad (4.6)$$

$$\langle x^2(t) \rangle = A_2(t) e^{(b-a)t} + B_2(t) e^{-(a+b)t} + C_2, \quad (4.7)$$

so the variance is

$$\sigma_x^2(t) = A(t) e^{(b-a)t} + B(t) e^{-(a+b)t} + C(t). \quad (4.8)$$

In these equations, $a = (\kappa + k_1 + k_2)/2$ and $b = \sqrt{a^2 - \kappa k_2}$ are effective rates having dimensions of inverse time, while the A , B , and C factors are provided in table 4.1.

The positional variance (4.8) is plotted in figure 4.2 for conditions $\theta_1 = 1$ and $k_2 \gg k_1 \gg \kappa$. The notation “ \gg ” is interpreted in this context to mean “of at least an order of magnitude greater”. These conditions are most relevant to tracers in gravel-bed rivers, since they represent that grains

Table 4.1: Abbreviations used in the expressions of the mean (4.6), second moment (4.7) and variance (4.8) of bedload tracers.

$A_1 = \frac{v}{2b} \left[\theta_2 + \frac{k_1 + \theta_2 \kappa}{b - a} \right]$
$B_1 = -\frac{v}{2b} \left[\theta_2 - \frac{k_1 + \theta_2 \kappa}{a + b} \right]$
$C_1 = -\frac{v}{2b} \left[\frac{k_1 + \theta_2 \kappa}{b - a} + \frac{k_1 + \theta_2 \kappa}{a + b} \right]$
$A_2(t) = \frac{v^2}{2b^3} \left[(bt - 1)[k_1 + \theta_2(2\kappa + k_1 + b - a)] + \theta_2 b + \frac{(\kappa + k_1)(\theta_2 \kappa + k_1)}{(b - a)^2} [(bt - 1)(b - a) - b] \right]$
$B_2(t) = \frac{v^2}{2b^3} \left[(bt + 1)[k_1 + \theta_2(2\kappa + k_1 - a - b)] + \theta_2 b - \frac{(\kappa + k_1)(\theta_2 \kappa + k_1)}{(a + b)^2} [(bt + 1)(a + b) + b] \right]$
$C_2 = \frac{v^2}{2b^3} (\kappa + k_1)(\theta_2 \kappa + k_1) \left[\frac{2b - a}{(b - a)^2} + \frac{a + 2b}{(a + b)^2} \right]$
$A(t) = A_2(t) - 2A_1 C_1 - A_1^2 \exp[(b - a)t]$
$B(t) = B_2(t) - 2B_1 C_1 - B_1^2 \exp[-(a + b)t]$
$C(t) = C_2 - C_1^2 - 2A_1 B_1 \exp[-2at]$

are initially at rest (*Hassan et al.*, 1991; *Wu et al.*, 2019a), motions are typically much shorter than rests (*Einstein*, 1937; *Hubbell and Sayre*, 1964), and burial requires a much longer time than typical rests (*Ferguson and Hoey*, 2002; *Haschenburger*, 2013; *Hassan and Church*, 1994). Figure 4.2 demonstrates that under these conditions the variance (4.8) shows three diffusion ranges with approximate power law scaling ($\sigma_x^2 \propto t^\gamma$) that are identified as the local, intermediate, and global ranges proposed by Nikora et al., followed by a fourth range of no diffusion ($\sigma_x^2 = \text{const}$) stemming from the burial of all tracers. Following *Hassan and Bradley* (2017) I suggest to call the fourth range geomorphic, since any further transport in this range can occur only if scour re-exposes buried grains to the flow (*Martin et al.*, 2014; *Nakagawa and Tsujimoto*, 1980; *Voepel et al.*, 2013; *Wu et al.*, 2019b).

4.1.5 Diffusion exponents and three range scaling

Two limiting cases of equation (4.8) provide the scaling exponents γ of the diffusion $\sigma_x^2 \propto t^\gamma$ in each range. Limit (1) represents times so short a negligible amount of sediment burial has occurred, $t \ll 1/\kappa$, while limit

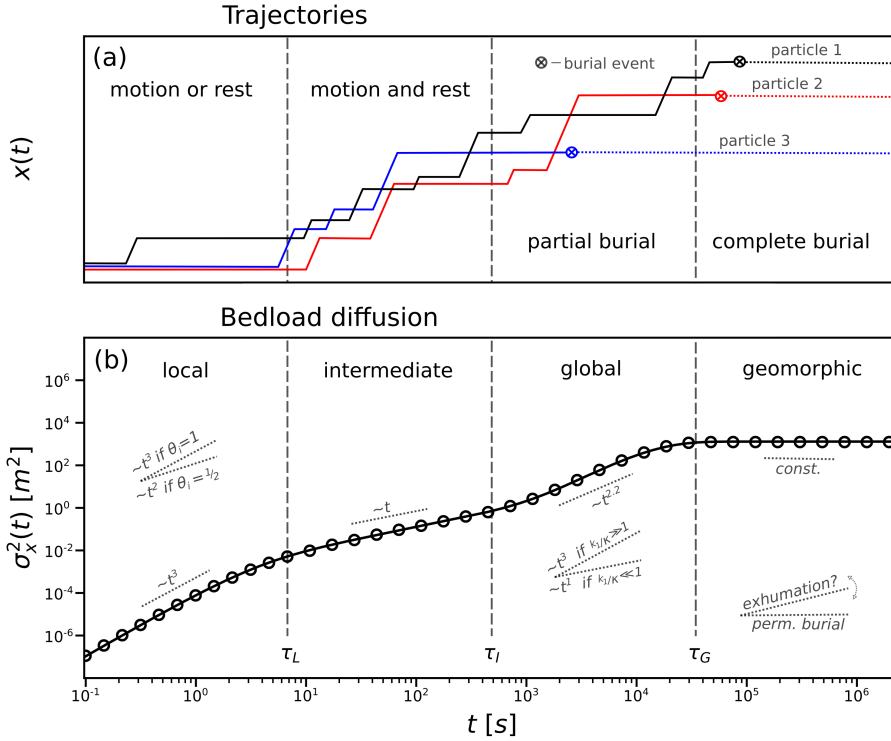


Figure 4.2: Panel (a) sketches conceptual trajectories of three grains, while panel (b) depicts the variance (4.8) with mean motion time 1.5 s, resting time 30.0 s, and movement velocity 0.1 m/s – values comparable to laboratory experiments transporting small (5 mm) gravels (Lajeunesse *et al.*, 2010; Martin *et al.*, 2012). The burial timescale is 7200.0s (two hours), and grains start from rest ($\theta_1 = 1$). The solid line is equation (4.8), and the points are numerically simulated. Panel (b) demonstrates four distinct scaling ranges of σ_x^2 : local, intermediate, global, and geomorphic. The first three are diffusive. Three crossover times τ_L , τ_I , and τ_G divide the ranges. Within each range, a slope key demonstrates the scaling $\sigma_x^2 \propto t^\gamma$. Panel (a) demonstrates that different mixtures of motion, rest, and burial states generate the ranges. At local timescales, grains usually either rest or move; at intermediate timescales, they transition between rest and motion; at global timescales, they transition between rest, motion, and burial; and at geomorphic timescales, all grains bury. Additional slope keys in the local and global ranges of panel (b) illustrate the effect of initial conditions and rest/burial timescales on the diffusion, while the additional slope key within the geomorphic range demonstrates the expected scaling when burial is not permanent, as discussed in section 4.2.

(2) represents times so long motion intervals appear as instantaneous steps of mean length $l = v/k_2$, $1/k_2 \rightarrow 0$ while $v/k_2 = \text{constant}$. Limit (1) provides local exponent $2 \leq \gamma \leq 3$ depending on the initial conditions θ_i , and intermediate exponent $\gamma = 1$. If grains start in motion or rest exclusively, meaning one $\theta_i = 0$, the local exponent is $\gamma = 3$, while if grains start in a mixture of motion and rest states, meaning neither θ_i is zero, the local exponent is $\gamma = 2$. Limit (2) provides global exponent $1 \leq \gamma \leq 3$ depending on the relative importance of κ and k_1 . The extreme $k_1/\kappa \ll 1$ produces $\gamma = 1$ in the global range, while the opposite extreme $k_1/\kappa \rightarrow \infty$ produces $\gamma = 3$. To summarize, when $k_2 \gg k_1 \gg \kappa$ so all three diffusion ranges exist, equation (4.8) implies:

1. local range super-diffusion with $2 < \gamma < 3$ depending on whether grains start from purely motion or rest ($\gamma = 3$) or from a mixture of both states ($\gamma = 2$),
2. intermediate range normal diffusion $\gamma = 1$ independent of model parameters, and
3. global range super-diffusion $1 < \gamma < 3$ depending on whether burial happens relatively slowly ($\gamma \rightarrow 1$) or quickly ($\gamma \rightarrow 3$) compared to surface resting times.

Finally, the burial of all tracers generates a geomorphic range of no diffusion.

4.2 Discussion

4.2.1 Local and intermediate ranges with comparison to earlier work

This chapter extended *Einstein* (1937) by including motion, rest, and burial processes in a multi-state random walk (*Weeks and Swinney*, 1998; *Weiss*, 1994) to demonstrate that a group of bedload tracers moving downstream while gradually becoming buried will generate a super-diffusive local range (*Fathel et al.*, 2016; *Martin et al.*, 2012; *Witz et al.*, 2019), a normal-diffusive

intermediate range (*Nakagawa and Tsujimoto*, 1976; *Yano*, 1969), and a super-diffusive global range (*Bradley*, 2017; *Bradley et al.*, 2010), before the diffusion eventually terminates in a geomorphic range (*Hassan and Bradley*, 2017). *Nikora et al.* (2002) highlighted the need for such a physical description, although they suggested to use a two-state random walk between motion and rest states with heavy-tailed resting times, and they did not discuss sediment burial. However, other works have demonstrated that a two-state walk with heavy-tailed rests provides two diffusion ranges – not three (*Fan et al.*, 2016; *Weeks et al.*, 1996), and although heavy-tailed resting times have been documented for surface particles (*Fraccarollo and Hassan*, 2019; *Liu et al.*, 2019), they are more often associated with buried particles (*Martin et al.*, 2012, 2014; *Olinde and Johnson*, 2015; *Pelosi et al.*, 2014; *Pierce and Hassan*, 2020a; *Voepel et al.*, 2013), while surface particles retain light-tailed resting times (*Ancey et al.*, 2006; *Einstein*, 1937; *Nakagawa and Tsujimoto*, 1976; *Yano*, 1969). Accordingly, I developed a random walk model of bedload trajectories with light-tailed surface resting times that incorporates sediment burial.

The local and intermediate range diffusion characteristics resulting from this model correspond closely to the original Nikora et al. concepts, while the global range has a different origin than Nikora et al. envisioned. *Nikora et al.* (2001b) explained that local diffusion results from the non-fractal (smooth) characteristics of bedload trajectories between subsequent interactions with the bed, while intermediate diffusion results from the fractal (rough) characteristics of bedload trajectories after many interactions with the bed. This chapter represents these conclusions: non-fractal (and super-diffusive) bedload trajectories exist on timescales short enough that each grain is either resting or moving, while fractal (and normal-diffusive) bedload trajectories exist on timescales when grains are actively switching between motion and rest states. I conclude that local and intermediate ranges stem from the interplay between motion and rest timescales, as demonstrated by earlier two-state random walk models (*Lajeunesse et al.*, 2017; *Lisle et al.*, 1998) and by all Newtonian models that develop sequences of motions and rests (*Bialik et al.*, 2012; *Nikora et al.*, 2001b), even those including heavy-tailed

rests (*Fan et al.*, 2016).

4.2.2 Global and geomorphic ranges with next steps for research

Nikora et al. explained that divergent resting times generate a sub-diffusive global range. However, studies have demonstrated that divergent resting times can generate super-diffusion in asymmetric random walks (*Weeks and Swinney*, 1998; *Weeks et al.*, 1996), and both experiments (*Bradley*, 2017; *Bradley et al.*, 2010) and models (*Pelosi et al.*, 2014; *Wu et al.*, 2019a,b) of bedload tracers undergoing burial have demonstrated global range super-diffusion. While my own results also show global range super-diffusion, they do not necessarily refute the Nikora et al. conclusion of sub-diffusion at long timescales. I assumed sediment burial was a permanent condition which developed a non-diffusive geomorphic range. In actuality, burial is a temporary condition, because bed scour can exhume buried sediment back into transport (*Wu et al.*, 2019b), probably after heavy-tailed intervals (*Martin et al.*, 2014; *Voepel et al.*, 2013). A generalization of the model in this chapter to include heavy-tailed timescales between burial and exhumation might develop four ranges of diffusion, where the long-time decay of the exhumation time distribution would dictate the geomorphic range diffusion characteristics as depicted in figure 4.2. If cumulative exhumation times decay faster than $T^{-1/2}$, as suggested in chapter 3, other equilibrium transport models (*Martin et al.*, 2014; *Voepel et al.*, 2013), and laboratory experiments (*Martin et al.*, 2012, 2014), the geomorphic range is expected to be super-diffusive (*Weeks and Swinney*, 1998). However, if they decay slower than $T^{-1/2}$, as implicitly suggested by the data of *Olinde and Johnson* (2015), the geomorphic range is expected to be genuinely sub-diffusive (*Weeks and Swinney*, 1998), leaving Nikora et al. with the final word on long-time sub-diffusion.

The analytical solution of bedload diffusion in equation (4.8) reduces exactly to the analytical solutions of the *Lisle et al.* (1998) and *Lajeunesse et al.* (2017) models in the limit without burial ($\kappa \rightarrow 0$), the *Wu et al.* (2019a) model in the limit of instantaneous steps ($k_2 \rightarrow \infty$ and $l = v/k_2$), and the original *Einstein* (1937) model in the limit of instantaneous steps without

burial. These reductions demonstrate that the majority of recent bedload diffusion models, whether developed from Exner-type equations (*Pelosi and Parker*, 2014; *Pelosi et al.*, 2014; *Wu et al.*, 2019a) or advection-diffusion equations (*Lajeunesse et al.*, 2017; *Lisle et al.*, 1998), can be viewed equivalently as continuous-time random walks applied to individual bedload trajectories. Within random walk theory, sophisticated descriptions of transport with variable velocities (*Masoliver and Weiss*, 1994; *Zaburdaev et al.*, 2008), correlated motions (*Escaff et al.*, 2018; *Vicsek and Zafeiris*, 2012), and anomalous diffusion (*Fa*, 2014; *Masoliver*, 2016; *Metzler et al.*, 2014) have been developed. Meanwhile, in bedload transport research, variable velocities (*Furbish et al.*, 2012a; *Heyman et al.*, 2016; *Lajeunesse et al.*, 2010), correlated motions (*Heyman et al.*, 2014; *Lee and Jerolmack*, 2018; *Saletti and Hassan*, 2020), and anomalous diffusion (*Bradley*, 2017; *Fathel et al.*, 2016; *Schumer et al.*, 2009) constitute open research issues. I believe further developing the linkage between existing bedload models and random walk concepts could rapidly progress our understanding.

4.3 Summary

In this chapter, I developed a random walk model to describe sediment tracers transporting through a river channel as they gradually become buried, providing a physical description of the local, intermediate, and global diffusion ranges identified by *Nikora et al.* (2002). Pushing their ideas somewhat further, I followed *Hassan and Bradley* (2017) to propose a geomorphic range to describe diffusion characteristics at timescales larger than the global range when burial and exhumation both moderate downstream transport. At base level, this work demonstrates that (1) durations of sediment motions, (2) durations of sediment rest, and (3) the sediment burial process are sufficient to develop three diffusion ranges that terminate when all tracers become buried. This work provides a complementary perspective on the three range diffusion exhibited in chapter 2. A next step is to incorporate exhumation to better understand the geomorphic range. Ultimately, the multi-state random walk formalism used in this chapter has been demonstrated to implicitly underlies

most existing bedload diffusion models. The random walk formalism is an alternative perspective on the Langevin approaches used elsewhere in this thesis, and it provides a powerful tool for researchers targeting landscape-scale understanding from statistical concepts of the underlying grain-scale dynamics.

Chapter 5

Collisional Langevin model of bedload sediment velocity distributions

5.1 Introduction

Bed load transport rates show wide and frequent fluctuations which originate from coupling between the fluid and granular phases. Owing to these fluctuations, measured transport rates often show slow convergence through time (*Dhont and Ancey*, 2018; *Turowski*, 2010), and predicted rates can deviate from measured values by several orders of magnitude (*Martin*, 2003; *Recking et al.*, 2012). These challenges limit numerous ecological and engineering applications that rely on sediment transport predictions (*Gaeuman et al.*, 2017; *Malmon et al.*, 2005). In recent decades, stochastic formulations of the bed load flux have become increasingly popular for their potential to predict the mean transport rates required by applications while also predicting the magnitude of transport fluctuations and quantifying the dependence of measurements on the observation scale (secs. 1.1.13-1.1.14). Recent indications that sediment transport fluctuations might explain longstanding open problems in alluvial channel stability, such as channel width mainte-

nance (*Abramian et al.*, 2019, 2020) and bedform initiation (*Bohorquez and Ancey*, 2016; *Jerolmack and Mohrig*, 2005) provide additional motivation to develop these stochastic approaches. One subset of stochastic methods expresses downstream transport rates as a sum over the instantaneous streamwise velocities of all particles in motion within a control volume (sec. 1.1.13). This formulation requires the instantaneous velocity distributions of sediment particles (*Lajeunesse et al.*, 2010), although understanding of these distributions remains limited. There is as of yet no consensus on the shape of the bedload velocity distribution, and although the models described in section 1.1.5 of the introduction have described some extreme end-member distributions (e.g. *Ancey and Heyman*, 2014; *Fan et al.*, 2014), no models have been developed that describe the full range of experimental observations (*Fathel et al.*, 2015; *Heyman et al.*, 2016; *Houssais and Lajeunesse*, 2012; *Lajeunesse et al.*, 2010; *Liu et al.*, 2019). In this chapter, I develop a stochastic model of particle velocities which addresses this shortcoming.

High-speed video experiments have measured different streamwise particle velocity distributions without indicating why one distribution or another appears in a given set of hydraulic and sedimentary conditions. One set of studies has shown exponential particle velocity distributions (*Charru et al.*, 2004; *Fathel et al.*, 2016, 2015; *Lajeunesse et al.*, 2010; *Roseberry et al.*, 2012; *Seizilles et al.*, 2014). These experiments involve uniformly-sized small sands or glass beads (0.05 – 2mm) in turbulent and subcritical flows, but not always; the experiments of *Lajeunesse et al.* (2010) were supercritical, while the experiments of *Charru et al.* (2004) and *Seizilles et al.* (2014) were viscous. A second set of studies have shown Gaussian particle velocity distributions (*Ancey and Heyman*, 2014; *Heyman et al.*, 2016; *Martin et al.*, 2012). In these experiments, particles are typically larger (2 – 8mm) uniformly-sized gravels or glass beads, and flows are generally turbulent and super-critical. Other experiments display velocity distributions that are intermediate between exponential and Gaussian extremes that appear visually more like a Gamma distribution (*Houssais and Lajeunesse*, 2012; *Liu et al.*, 2019). The *Houssais and Lajeunesse* (2012) experiments involved a binomial distribution of glass beads with diameters 0.7mm and 2.2mm in turbulent

and supercritical flow conditions, while the *Liu et al.* (2019) experiments used sand having median diameter 1.1mm. Flows were again turbulent and subcritical. From this experimental record, the velocity distribution shape apparently does not consistently relate to super or sub-critical flow conditions, whether sediment grains are natural (sand, gravel) or synthetic (glass beads), or whether the flow is laminar or turbulent. However there is a loose trend within the particle size. Smaller particles tend to show more exponential-like distributions (e.g. *Fathel et al.*, 2015), while larger ones show Gaussian distributions (e.g. *Heyman et al.*, 2016). This summary suggests that the shape of streamwise bed load velocity distribution could be controlled by the particle size.

Existing models of streamwise bed load velocities can be divided into computational and stochastic physics categories. Computational models numerically integrate some approximate coupled dynamics for individual grains and the fluid, generally modelling particles as spheres interacting through repulsive forces, and the flow using direct simulation of the Navier-Stokes equations or some related approximation (such as large eddy simulation or the St-Venant equations). When streamwise particle velocities have been analyzed in such simulations, they show exponential tails (*Furbish and Schmeeckle*, 2013; *González et al.*, 2017) that agree with one subset of the experimental data.

Several stochastic models have incorporated fluctuating driving and resisting terms into the Newtonian dynamics of individual grains to develop Langevin-like descriptions of bed load particle motions (sec. 1.1.5). *Fan et al.* (2014) represented turbulent drag as Gaussian white noise and included a static Coulomb friction term to model particle-bed collisions, while *Ancey and Heyman* (2014) applied an Ornstein-Uhlenbeck process which combines the fluid and driving forces were lumped into a velocity-dependent force, while Gaussian white noise represents fluctuations. Each of these models derives one end-member distribution from among the range of distributions reported in experiments. A physical description for the full range of experimentally-observed bedload velocity distributions remains an elusive target.

In this chapter I explore the possibility that the shape of the particle velocity distribution is controlled by momentum dissipation during particle-bed collisions. In the theory of granular gases, dissipative collisions are known to cause departures toward an exponential velocity distribution from the ideal Gaussian form expected from perfectly elastic collisions (*Brilliantov and Poschel*, 2004). Gas theory formulates particle-particle collisions as a nonlocal integral within the master equation for the probability distribution of particle velocity called the Boltzmann equation (*Chapman and Cowling*, 1970; *Landau and Lifshitz*, 1969). Collisions in these models involve episodic kicks to the particle momenta at random times, parameterized by billiard ball-like models of the underlying rigid body dynamics (e.g. *Brach*, 1989). In contrast, current stochastic models of bedload transport appear highly simplified, treating collisions instead with static Coulomb or velocity-dependent drag.

Taking inspiration from granular gas theory, I develop in this chapter an improved model for sediment grains in transport, including episodic particle-bed collisions. The driving motivation is to test the hypothesis that particle-bed collision characteristics can explain the range of experimentally-observed streamwise bed load particle velocity distributions. A secondary one is to introduce more realistic forces into earlier stochastic descriptions of individual bed load particle dynamics. I develop the model and explain its key assumptions in section 5.2. Then I present the analytical solution of the model and other major results in 5.3. Finally I discuss the implications of these results, summarize key findings, and suggest ideas for further research in sections 5.4 and 5.5.

5.2 Mechanistic description of particle velocities

Figure 5.1 indicates the configuration of the model in this chapter. Nearly spherical cohesionless particles of diameter d and mass m move as bed load down a slope inclined at an angle θ in a steady turbulent shear flow. The flow is just strong enough to drive grains into the rarefied transport typical in gravel-bed rivers: particles saltate downstream through a sequence of

particle-bed collisions. Moving particles collide often with stationary particles, but rarely with other moving particles.

Particles respond to turbulent drag forces $F_D(t)$ and episodic particle-bed collision forces. In contrast to the computational physics approach, I do not aim to characterize the exact timeseries of the forces on an individual particle. Instead, I model the ensemble of possible force timeseries that particles could conceivably experience. Each possibility implies a different possible velocity timeseries $u(t)$ in the downstream direction. The objective is to calculate the probability distribution $P(u)$ of this downstream velocity by averaging over the ensemble of forces. I include the most realistic particle-bed collision and fluid forces possible while still allowing for analytical solutions.

5.2.1 Episodic collisions

Collisions between bedload particles dissipate momentum, partly by converting it to vertical, lateral, or rotational momentum, partly by deforming particles and generating heat (*Schmeeckle*, 2014; *Williams and Furbish*, 2021), and partly by pressurizing the fluid (*Joseph et al.*, 2001; *Schmeeckle et al.*, 2001). The microscopic details of particle-particle collisions have been thoroughly studied (*Brach*, 1989; *Lorenz et al.*, 1997; *Montaine et al.*, 2011). Here, we introduce a simple elasticity parameter ε as a first attempt at the problem, as indicated in figure 5.1. This elasticity characterizes the fraction of downstream momentum lost in a collision. If the streamwise velocity just prior to a collision is u , just after the collision it becomes εu . The elasticity ranges from $\varepsilon = 0$, representing a completely inelastic collision, to $\varepsilon = 1$, representing a completely elastic collision.

Since the elasticity combines effects of particle shape and collision geometry and should vary from one collision to the next, the elasticity ε is interpreted as a random variable, characterized by a statistical distribution $\rho(\varepsilon)$. Some granular gas models have also included random elasticity (e.g. *Serero et al.*, 2015).

Assuming that the number of collisions per unit time is ν and that the

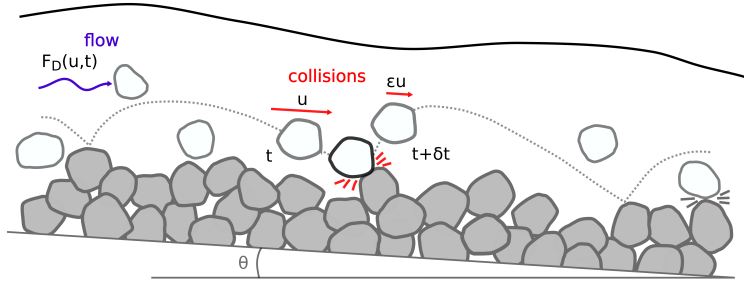


Figure 5.1: Definition sketch of rarefied sediment transport with turbulent fluid drag and particle-bed collision forces. During saltation, pre-collisional streamwise velocities u are transformed to postcollisional velocities $\varepsilon u < u$.

time intervals between subsequent particle-bed collisions are exponentially distributed (*Gordon et al.*, 1972), the collision force in the downstream direction can be written as a Poisson pulse noise (sec. 1.1.8):

$$F_C(u, t) = -mu \sum_{k=1}^{N_\nu(t)} (1 - \varepsilon_k) \delta(t - \tau_k). \quad (5.1)$$

Here, $N_\nu(t)$ is the number of collisions in time t (a Poisson random variable), the τ_k ($k = 1, 2, \dots$) are times at which collisions occur, and the ε_k are the elasticity coefficients, drawn from the distribution $\rho(\varepsilon)$ characterizing the fraction of momentum lost in each particle-bed collision. This collision force is a sequence of random impulses which are proportional to the pre-collisional streamwise momentum. This collision model should be adequate when the contact times between moving and resting particles are small compared to the times between collisions. These conditions are always satisfied for the idealized saltation trajectories depicted in figure 5.1.

5.2.2 Turbulent fluid forces

Fluid forces on a coarse particle in a viscous flow depend on the Reynolds number $\mathfrak{R}_p = dV/\nu$ defined by the particle size d , slip velocity V between particle and fluid, and kinematic viscosity ν . These forces have been calculated analytically from the Navier-Stokes equations for vanishing \mathfrak{R}_p and include acceleration, history, and velocity-dependent drag terms (*Auton*, 1987; *Hjelmfelt and Mockros*, 1966; *Maxey and Riley*, 1983). At realistic \mathfrak{R}_p , analytical results are inaccessible, so it is standard to include empirical corrections to the small \mathfrak{R}_p formulas (*Clift et al.*, 1978; *Schmeeckle et al.*, 2007). A dominant contribution to the downstream drag force F_D on nearly spherical particles at large \mathfrak{R}_p can be written $F_D = \frac{\pi}{8} \rho_f d^2 C_D(\mathfrak{R}_p) |V| V$, where ρ_f is the fluid density, d is the particle diameter, $C_D(\mathfrak{R}_p)$ is an empirical drag coefficient, and $V = U - u$ is the slip velocity between the fluid (U) and particle (u) velocities (*Coleman*, 1967; *Dwivedi et al.*, 2012; *Schmeeckle et al.*, 2007). In this study, I leave out acceleration and history terms for analytical tractability, although they are certainly relevant in coarse sediment transport (*Armenio and Fiorotto*, 2001; *Michaelides*, 1997).

Drag forces have been argued to fluctuate rapidly compared to the inertial response times of submerged grains (*Fan et al.*, 2014), and the magnitude of drag fluctuations has been observed to follow a Gaussian distribution (*Celik et al.*, 2014; *Dwivedi et al.*, 2010; *Hofland and Battjes*, 2006; *Schmeeckle et al.*, 2007). These ideas allow two major simplifications of the above drag force. First, the drag can be split into quasi-steady and fluctuating components (*Michaelides*, 1997), and second, drag fluctuations can be modelled a Gaussian white noise, where the fluctuations are symmetric, the autocorrelation time is negligible, and the strength of fluctuations is described by a diffusivity D (*Ancey and Heyman*, 2014; *Fan et al.*, 2014). Defining \bar{V} as a representative slip velocity to be specified more carefully later, \bar{C}_D as the empirical drag coefficient evaluated at this slip velocity, and $\xi(t)$ as a Gaussian white noise of mean 0 and variance 1 (*Gardiner*, 1983), the fluid drag can be written

$$F_D(t) = \Gamma + \sqrt{2D} \eta(t), \quad (5.2)$$

where $\Gamma = \frac{\pi}{8} \rho_f d^2 \bar{C}_D \bar{V}^2$ is the steady component of the drag.

5.2.3 Langevin equation for collisional bedload transport

With the above forces, the Langevin equation $m\dot{u}(t) = F_D(t) + F_C(t)$ for the sediment dynamics becomes

$$m\dot{u}(t) = \Gamma + \sqrt{2D}\eta(t) - mu(t)\xi_{\nu,\varepsilon}(t). \quad (5.3)$$

This equation replaces the steady friction terms of earlier models with an episodic term, designed to provide a more realistic representation of particle-bed collisions. Mathematically, equation 5.3 is a Langevin-like equation representing a jump-diffusion process (*Daly and Porporato*, 2006) with multiplicative Poisson noise (*Denisov et al.*, 2009; *Dubkov et al.*, 2016). Collisions introduce "jumps" in velocity while turbulent generates "diffusion". The collision term is "multiplicative" in the sense that u multiplies the Poisson noise.

Equations like 5.3 have long been studied in the stochastic physics literature (*Hanggi*, 1978; *Van Den Broeck*, 1983), but solving such equations remains extremely challenging (*Daly and Porporato*, 2010; *Dubkov and Kharcheva*, 2019; *Mau et al.*, 2014). One issue is that multiplicative white noises imply the prescription dilemma of stochastic calculus (*Gardiner*, 1983; *Risken*, 1984), meaning 5.3 is not defined without further specifying an integration rule (*Suweis et al.*, 2011). Here, the Ito interpretation (lower endpoint integration rule) is the physical choice the energy dissipated by collisions depends strictly on pre-collisional velocities, not post-collisional (e.g. *Gardiner*, 1983) since. Given this integration rule, the remaining issues are to obtain the master equation characterizing the ensemble of velocities defined by 5.3, and then to solve this equation for the velocity distribution $P(u)$.

5.2.4 Chapman-Komogorov equation and particle-bed collision integral

The equation governing the streamwise velocity distribution $P(u, t)$ is derived in appendix section D.1 with a limiting procedure, providing

$$\nu^{-1} \partial_t P(u, t) = -\tilde{\Gamma} \partial_u P(u, t) + \tilde{D} \partial_u^2 P(u, t) + I_c(u, t). \quad (5.4)$$

In this equation, I introduced the scaled parameters $\tilde{\Gamma} = \Gamma/(\nu m)$ and $\tilde{D} = D/(\nu m)$ that scale the steady and fluctuating components of the fluid force against the collision rate ν . The term

$$I_c(u, t) = -P(u, t) + \int_0^1 \frac{d\varepsilon}{\varepsilon} P\left(\frac{u}{\varepsilon}, t\right) \rho(\varepsilon) \quad (5.5)$$

is a “collision integral” term representing particle-bed collisions.

Equation 5.4 is a nonlocal extension of the Fokker-Planck equation used in earlier bed load models (*Ancey and Heyman, 2014; Fan et al., 2014*). Non-locality is introduced by the collision integral 5.5 which transfers probability from higher pre-collisional velocities u/ε to lower post-collisional velocities u . This term is analogous to the collision integral within the Boltzmann equation of kinetic theory (*Brilliantov and Poschel, 2004; Duderstadt and Martin, 1979*). Physically, it corresponds to binary collisions between particles having different masses and random restitution coefficients *Serero et al. (2015)* in the limit that the mass of one particle (here, the particle resting on the bed) diverges to infinity. Mathematically, the collision integral represents the probability distribution of the product between the elasticity ε and the downstream momentum mu (c.f. *Feller, 1967*).

Owing to its nonlocality, equation 5.4 does not admit analytical solutions as is, so further approximation is necessary. Assuming the distribution of elasticity $\rho(\varepsilon)$ is sharply peaked at some most common (mode) value ε' , which is the case in experiments of rigid body collisions (*Glielmo et al., 2014*), allows for a Kramers-Moyal type expansion of the particle-bed collision integral (*Gardiner, 1983*). Expanding all terms in the integrand except

$\rho(\varepsilon)$ provides

$$\mathcal{I}_c(u, t) = -P(u, t) + \frac{1}{\varepsilon'} P\left(\frac{u}{\varepsilon'}, t\right) + \sum_{k=1}^{\infty} \frac{\alpha_k}{k!} (\varepsilon - \varepsilon')^k \left[\frac{1}{\varepsilon} P\left(\frac{u}{\varepsilon}\right) \right]^{(k)} \Big|_{\varepsilon=\varepsilon'}, \quad (5.6)$$

where the $\alpha_k = \int_0^1 d\varepsilon \rho(\varepsilon) (\varepsilon - \varepsilon')^k$ are the central moments of ε around the mode elasticity ε' and the superscript (k) denotes the k th derivative.

In what follows, I drop all but the first two terms in this expansion to obtain the leading order contribution of particle-bed collisions to the velocity distribution. Higher orders could always be included later by perturbation theory (*Morse and Feshbach*, 1953a). I solve the resulting approximate equation in steady-state, when $\partial P(u, t)/\partial t = 0$. Equation 5.4 indicates that this solution will be a good approximation to the time-dependent problem when particle motions generally survive multiple collisions ($t \gg \nu^{-1}$).

5.3 Results

5.3.1 Derivation of the bedload velocity distribution

Hereafter I drop the prime on the most common streamwise restitution coefficient ε' . With the truncation to two terms, equation 5.4 gives

$$0 = -\tilde{\Gamma} \partial_u P(u) + \tilde{D} \partial_u^2 P(u) - P(u) + \frac{1}{\varepsilon} P\left(\frac{u}{\varepsilon}\right), \quad (5.7)$$

which is an advanced functional differential equation. This equation is “functional” in the sense that it is nonlocal in velocity due to the last term on the right hand side, and it is “advanced” in that u/ε is advanced beyond the argument u involved in the rest of this equation (since $0 < \varepsilon < 1$). Such equations seen some attention in the mathematics literature, where they are sometimes called pantograph equations (*Hall and Wake*, 1989; *Kim*, 1998; *Zaidi et al.*, 2015).

In the appendix section D.2 I solve equation 5.7 using Laplace trans-

forms, providing

$$P(u) = \frac{\theta(-u)}{K_+} \sum_{l=0}^{\infty} \frac{\varepsilon^{-l} e^{\lambda_+ \varepsilon^{-l} u}}{\prod_{m=1}^l (-\tilde{D} \lambda_+^2 \varepsilon^{-2m} + \tilde{\Gamma} \lambda_+ \varepsilon^{-m} + 1)} \\ + \frac{\theta(u)}{K_-} \sum_{l=0}^{\infty} \frac{\varepsilon^{-l} e^{\lambda_- \varepsilon^{-l} u}}{\prod_{m=1}^l (-\tilde{D} \lambda_-^2 \varepsilon^{-2m} + \tilde{\Gamma} \lambda_- \varepsilon^{-m} + 1)}. \quad (5.8)$$

The factors λ_{\pm} are defined in appendix equations D.11. They are proportional to $\tilde{\Gamma}/\tilde{D}$. The normalization factors are K_{\pm} are

$$K_{\pm} = \tilde{D}(\lambda_+ - \lambda_-) \prod_{l=1}^{\infty} (-\tilde{D} \lambda_{\pm}^2 \varepsilon^{2l} + \tilde{\Gamma} \lambda_{\pm} \varepsilon^l + 1). \quad (5.9)$$

Although this velocity distribution has a complex mathematical structure, one can verify that this is a normalized probability distribution ($\int du P(u) = 1$) which has very simple limiting behaviors as the mode elasticity ε approaches fully elastic ($\varepsilon = 1$) and inelastic ($\varepsilon = 0$) values. The complexity of this result is not surprising given how few analytical solutions are available in granular gas theories with similar nonlocal collision integrals (e.g. *Brilliantov and Poschel, 2004*).

It is possible to derive the moments of this probability distribution by multiplying 5.7 by u , integrating, and then solving the resulting moment evolution equations (c.f. *Cox and Miller, 1965*). These calculations are provided in appendix section D.3, where the mean bedload velocity is derived as

$$\langle u \rangle = \frac{\Gamma}{\nu(1-\varepsilon)} = \frac{\gamma}{1-\varepsilon}. \quad (5.10)$$

This result scales linearly with the mean fluid drag and nonlinearly with the rate and typical elasticity of collisions, indicating a strong influence of particle collisions on bedload velocities. The second moment is

$$\langle u^2 \rangle = 2 \frac{d + \gamma \langle u \rangle}{1 - \varepsilon^2}, \quad (5.11)$$

leading to the velocity variance ($\sigma_u^2 = \langle u^2 \rangle - \langle u \rangle^2$)

$$\sigma_u^2 = \frac{2d + \gamma^2}{1 - \varepsilon^2}. \quad (5.12)$$

This result demonstrates that velocity fluctuations originate from both the steady and fluctuating components of the flow forces, yet the variance is linear in these factors and is therefore relatively insensitive to the fluid flow. This is consistent with the remarkable similarities sometimes visible between viscous and turbulent flow experiments (e.g. *Charru et al.*, 2004; *Lajeunesse et al.*, 2010). In contrast, particle velocity fluctuations in equation 5.12 depend sharply on the parameters representing particle-bed collisions, suggesting collisions are the leading control on particle velocity fluctuations.

Figure 5.2 depicts the velocity characteristics of particles for different realizations of the fluid and collisional forces. This figure reveals an apparent transition from exponential-like to Gaussian-like velocity distributions as collisions vary from more inelastic ($\varepsilon \rightarrow 0$) to more elastic ($\varepsilon \rightarrow 1$). In between, the full distribution 5.8 resembles a Gamma distribution, although it is represented by equation 5.8, not a Gamma distribution.

5.3.2 Exponential and Gaussian regimes: limits to earlier work

In fact, the apparent transition from exponential to Gaussian in figure 5.2 can be demonstrated from equation 5.8. Despite its complex appearance, simple Gaussian and exponential forms derive from this equation as exact mathematical limits. When particle-bed collisions are completely inelastic ($\neq 0$), 5.8 becomes an exponential distribution, and when they are completely elastic ($\nu = 1$), 5.8 becomes Gaussian. Figure 5.3 demonstrates in detail the approach of the distribution toward these limits.

The exponential limit of 5.8 as $\varepsilon \rightarrow 0$ is easy to see. Taking $\varepsilon \rightarrow 0$ in 5.8, all terms in the series except for that with $l = 0$ become exponentially small, leaving behind the same two-sided exponential distribution derived

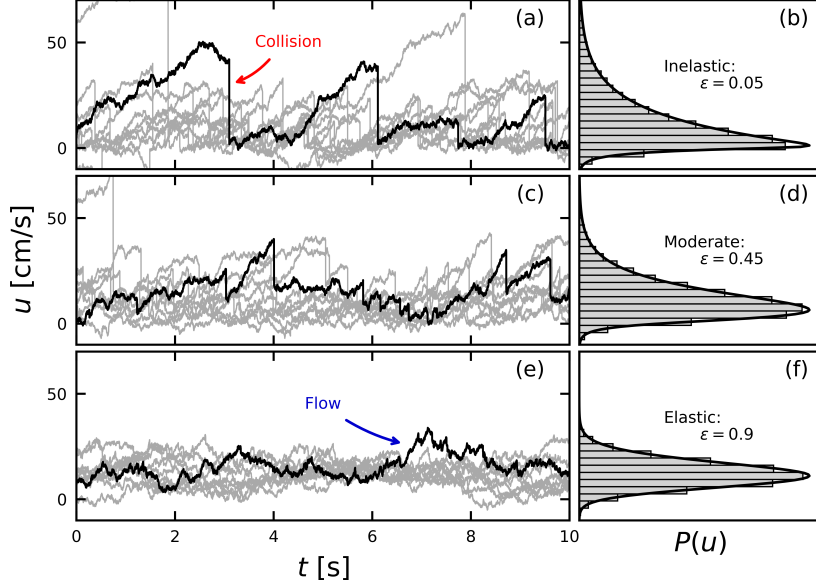


Figure 5.2: Left and right panels are paired. Left panels show velocity realizations as gray traces. Velocities are calculated from Monte Carlo simulations. Individual realizations are singled out as black traces. Particle-bed collisions imply sudden downward-velocity jumps. Flow forces generate fluctuating positive accelerations between collisions. Right panels show simulated histograms of particle velocities and exact solutions from equation 5.8. As elasticity ε varies, the particle velocity distributions interpolate between exponential (inelastic) and Gaussian (elastic) forms.

by *Fan et al.* (2014) up to differences in notation:

$$P(u) = \frac{d}{\sqrt{\gamma^2 + 4d}} e^{\frac{\gamma u - \sqrt{\gamma^2 + 4d}|u|}{2d}}. \quad (5.13)$$

Thus, for bed load transport conditions with typically very inelastic particle-bed collisions, we can expect exponential-like velocities and large deviations from a Gaussian behavior.

The Gaussian limit as $\varepsilon \rightarrow 1$ of 5.8 is more difficult to evaluate. The

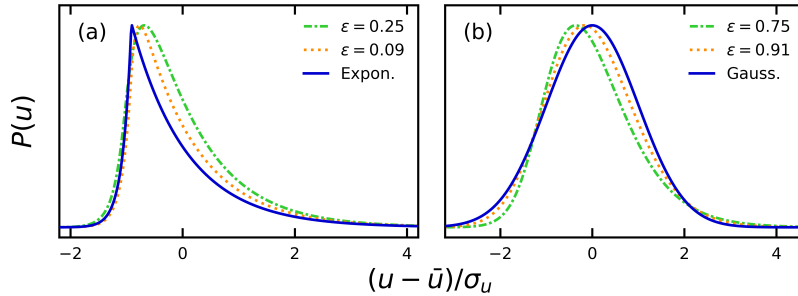


Figure 5.3: The particle velocity distribution approaches an exponential distribution in (a) as particle-bed collisions become extremely elastic ($\varepsilon \rightarrow 1$), and it approaches a Gaussian in (b) as they become extremely inelastic ($\varepsilon \rightarrow 0$). On the abscissa, the mean sediment velocity is standardized by its mean \bar{u} and standard deviation σ_u .

challenge is that the statistical moments 4.6 and 5.12 diverge at the same time as the denominator factors of the distribution 5.8. In the appendix section D.4 I return instead to the original equation 5.7 to evaluate the completely elastic limit, obtaining

$$P(u) = \frac{1}{\sqrt{2\pi\sigma_u^2}} e^{-\frac{(u-\bar{u})^2}{2\sigma_u^2}}. \quad (5.14)$$

This result is identical to the velocity distribution derived by *Ancey and Heyman* (2014), up to notation.

5.3.3 Comparison with experimental data

A variety of velocity distributions have been observed in bedload transport experiments, ranging from exponential to Gaussian in shape. This section compares these with the theoretical result eq. 5.8. Comparing eq. 5.8 with experimental data requires values for the steady component of the drag force Γ , the particle mass m , the magnitude of turbulent drag fluctuations D , the rate of particle-bed collisions ν , and the mode elasticity of collisions ε .

This section compares eq. 5.8 with the results of six different exper-

iments. In each case, the particle mass is computed from experimental parameters assuming spherical sediment as $m = \pi \rho_s d^3 / 6$, where ρ_s is the sediment density and d is the particle diameter. The steady component of the drag force is estimated as

$$\Gamma = \frac{\pi}{8} \rho C_D(Re_p) d^2 u_*^2, \quad (5.15)$$

where ρ is the fluid density and $C_D(Re_p)$ is the drag coefficient, given as (*Clift et al.*, 1978; *González et al.*, 2017)

$$C_D = \frac{24}{Re_p} (1 + 0.194 Re_p^{0.631}). \quad (5.16)$$

Particle Reynolds numbers are estimated using the shear velocity: $Re_p = u_* d / \nu$.

The magnitude D of turbulent fluctuations is eliminated with the mean and variance of the particle velocity. The remaining coefficients in the model, the dissipation per collision ε and the collision rate ν , are treated as calibration parameters and are tuned to provide best fit between the distribution 5.8 and the experimental data.

The parameters for each experiment and the best-fit calibration parameters are collated in table 5.1, while the results of fitting the model to the available experimental data are shown in figure 5.4. In every case, good agreement is obtained between the theoretical and empirical velocity distributions, suggesting that the Langevin model 5.3 captures the essential physics.

5.4 Discussion

In this final chapter I developed a Langevin description of bed load sediment transport which includes episodic collisions between particles and the bed. The model relates the shape of the instantaneous streamwise particle velocity distribution to the elasticity of particle-bed collisions. This work generalizes earlier approaches available in the literature which did not treat episodic collisions (*Ancey and Heyman*, 2014; *Fan et al.*, 2014), and

Experiment	d [mm]	u_* [cm/s]	Re_p [-]	St [-]	Fr [-]	ε [-]	ν [s^{-1}]
(a) Fathel <i>et al</i>	0.5	2.0	9.97	2.9	0.3	0.08	24.
(b) Lajeau. <i>et al</i>	2.2	4.4	99.	29.	1.5	0.21	2.6
(c) Liu <i>et al</i>	1.1	8.6	94.	29.	0.3	0.28	34.
(d) Heyman <i>et al</i>	6.4	9.7	620.	180.	1.3	0.96	13.
(e) Ancey <i>et al</i>	8.0	7.4	590.	170.	2.1	0.92	4.8
(f) Martin <i>et al</i>	7.1	5.8	410.	120.	3.7	0.89	2.1

Table 5.1: Parameters used to fit the distributions in figure 5.4. The first five columns involve data from the experiments for particle diameter d , shear velocity u_* , particle Reynolds number Re_p , Stokes number St , and Froude number Fr . The final two columns involve values that were tuned to fit the theoretical distribution 5.8 to the experimental data, the dissipation ε and the collision rate ν . Units are indicated in square brackets. One can see a generally increasing relationship between particle size and elasticity, and likewise a decreasing relationship between particle size and collision frequency.

provides a new physical explanation for the different streamwise sediment velocity distributions resolved in experiments.

Although in reality, the turbulent forces on moving sediment particles vary in a complex spatio-temporal way, I have approximated the fluid forces on bed load particles as spatially uniform Gaussian white noise. Even though the non-Gaussian and history-dependent aspects of fluid turbulence certainly do impact sediment entrainment (Cameron *et al.*, 2020; Celik *et al.*, 2014), this flow model appears more or less justified since sediment transport experiments provide similar velocity distributions regardless of whether the flow is viscous or turbulent (Charru *et al.*, 2004; Lajeunesse *et al.*, 2010), and since particle relaxation times are typically long compared to the timescales of turbulent fluctuations (Hofland and Battjes, 2006; Nakagawa and Tsujimoto, 1981; Schmeeckle *et al.*, 2007).

The model developed in this chapter described particle-bed collision forces as a sequence of instantaneous impulses in an approach that is reminiscent of the kinetic theory of gases (Landau and Lifshitz, 1969). The

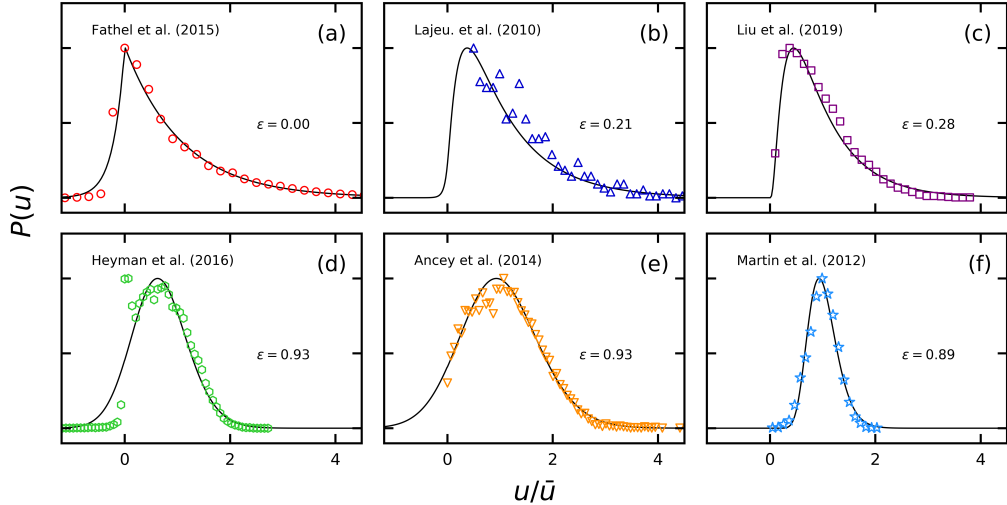


Figure 5.4: This figure compares the available experimental data on velocity distributions and the theoretical velocity distribution 5.8 with parameters ν , ε , and D treated as calibration parameters. In all cases there is good agreement, indicating that the model is capable of the range of distributions exhibited by the experimental data.

effect of each collision on the streamwise particle velocities was described by a simple elasticity-like coefficient. Although such approximate descriptions of particle-particle collisions are common in the theory of granular gases, the elasticity coefficient introduced here is not equivalent to the “coefficient of restitution” typically applied in granular gas theory. The coefficient of resitution is defined normal to the contact plane of two particles during a collision, and it characterizes energy loss due to deformation of the colliding particles in the absence of a viscous fluid (Brach and Dunn, 1992; Ismail and Stronge, 2008).

In bedload transport, colliding particles are submerged in a viscous fluid, and this introduces additional damping processes besides particle deformation (Joseph et al., 2001; Schmeeckle et al., 2001; Yang and Hunt, 2006). The model developed here did not consider these viscous forces, nor did it explicitly model the geometry of collisions, as ε was defined as a parameter

applying to the downstream velocity only. Thus, although I have included episodic particle-bed collisions in a stochastic sediment transport model for the first time, the key parameter (ε) in this formulation has a rather heuristic character and is not clearly related to the coefficient of restitution from granular gas theory. Future studies should formulate particle-bed collisions in stochastic sediment transport models considering more details of collision geometry (*Sekine and Kikkawa*, 1992), fluid-particle interactions (*Marshall*, 2011), and traditional restitution (*Brach*, 1989) using the present study as a starting point.

5.4.1 Does the velocity distribution depend on particle size?

Several researchers have considered why particle velocity distributions differ from one experiment to the next. One prevailing view is that it relates to flow hydraulics (*Wu et al.*, 2020). Many of the experiments producing Gaussian velocity distributions were conducted in supercritical flows (e.g. *Ancey and Heyman*, 2014; *Heyman et al.*, 2016; *Martin et al.*, 2012), whereas many producing exponential distributions were conducted in subcritical flows (e.g. *Charru et al.*, 2004; *Fathel et al.*, 2015; *Seizilles et al.*, 2014). However several experiments run counter to this hypothesis. The experiments of *Lajeunesse et al.* (2010) produced distinctly exponential velocity distributions in flows well within the supercritical regime ($Fr = 1.5$), whereas *Liu et al.* (2019) produced Gamma-like distributions in the subcritical regime ($Fr = 0.3$).

An alternative viewpoint, formulated in this chapter, is that the shape of the velocity distribution originates from granular interactions. Particle size enters the Langevin model 5.3 explicitly within the steady component of the drag, but it may also enter implicitly through the elasticity parameter ε . The analytical velocity distribution 5.8 was fit to six different experimental datasets in figure 5.4, and the best fit parameters required to for these fits were presented in table 5.1. These fit parameters suggest collisions are generally less elastic for smaller particle sizes, whereas they are more elastic for larger particle sizes. This suggests that the amount of momentum dissipated by collisions may depend on particle size.

Because the elasticity ε lumps together collision geometry and dissipation effects, it is challenging to attribute the increasing relationship between elasticity and particle size evident in table 5.1 directly to particle size. Yet this would be consistent with experiments of idealized particle collisions in viscous fluids. These demonstrate that momentum dissipation varies sharply with particle size, being more elastic for large particles, and less elastic for small particles (*Joseph et al.*, 2001; *Schmeeckle et al.*, 2001; *Yang and Hunt*, 2006), exactly like the trend in the table. A definite conclusion that particle size controls the shape of the bedload velocity distribution requires additional experimental and theoretical study. This chapter nevertheless produces suggestive ideas.

5.5 Summary

This chapter has presented a Langevin description of individual bedload particles saltating downstream through episodic collisions. The model suggests that episodic particle-bed collisions control the shape of the particle velocity distribution, and it is the first model to describe the full range of bedload velocity distributions that have been reported in experimental studies.

This work hints that particle size, and not flow hydraulics, may be primarily responsible for the different bedload velocity distributions obtained in experiments, although future study is required for a definite conclusion. The next step is to build up the episodic collision model presented in this chapter to include the geometric details of particle-bed collisions. Such an effort would produce additional insight into the controls of transverse, vertical, and rotational movements on the downstream velocities of individual grains.

Chapter 6

Summary and future work

This thesis has described bedload transport from the statistical physics of individual grains. The work has improved upon earlier descriptions. It describes the movements of grains along a wider range of timescales than before, highlights Langevin equations, master equations, and random walks as the common threads of stochastic sediment transport modelling, and provides more realistic descriptions of bedload transport. In particular, I have

1. developed the linkage between sediment flux probability distributions and individual particle trajectories (ch. 2),
2. described particle trajectories alternating through motion and rest with fluctuating velocities (ch. 2),
3. evaluated the control of bed elevation changes over sediment transport rates (ch. 3),
4. characterized how long particles can remain buried within the sedimentary bed (ch. 3),
5. incorporated the process of sediment burial in a description of downstream particle movement (ch. 4), and
6. formulated the velocity distributions of sediment particles including episodic particle-bed collisions (ch. 5).

These developments improve understanding of sediment transport in streams.

6.1 Overall methodology of the thesis

6.1.1 Langevin and master equations

The overarching strategy in all of these developments has been to identify control and response variables, represent control variables by idealized noises (entrainment and deposition events, particle burial events, turbulent forces, or particle-bed collisions), and then formulate dynamical equations relating the response variables to these stochastic control variables. This strategy phrases sedimentary dynamics in terms of Langevin-like equations, stochastic analogues of Newton's $F = ma$, where the acceleration a is swapped for the response variable of interest in the problem and the force F is a stochastic combination of the control variables.

Once the stochastic dynamical equations were written for a given problem, its solutions were averaged over realizations of the control variables to produce a master equation, an integro-differential equation governing the probability distributions of the response variables.

The solutions of the master equation in a given problem produce the probability distribution for the response variable of interest, which in the thesis has included at different points the bedload particle position (chs. 2 and 4), the particle velocity (ch. 5), the bed elevation (ch. 3), and the sediment transport rate (ch. 2). The same stochastic strategy should be applicable to a wide range of problems in geomorphology where phenomena can built up from component parts with apparently noisy characteristics.

6.1.2 Idealized noises and their combinations

A major challenge in this research is that only a handful of noises in statistical physics are comprehensively understood (*Horsthemke and Lefever, 1984*), so the available options in stochastic modelling are constrained. The noises used in this thesis include white Gaussian, Poisson, and dichotomous noises, representing erratic fluctuations, sequences of spikes, and random

switches respectively (*Van Den Broeck*, 1983). Turbulence was described using Gaussian noise, while instantaneous steps, particle arrivals to a control surface, and particle-bed collisions were described with Poisson noise. Alternation between motion and rest was represented with dichotomous noise. Whenever these processes acted in combination, the dynamical equations describing the response variable included multiple sources of idealized noise as required. This inclusion of multiple noise sources has not yet to my knowledge been pursued in any earlier stochastic models of sediment transport.

River science offers no guarantee that these idealized white noises which we happen to understand best are sufficient to describe its phenomena. White noises are an idealization which is probably never realized in nature (*Gardiner*, 1983; *Kubo et al.*, 1978). In contrast, colored noises in which fluctuations have favoured frequencies are well-known to occur in many fluid and granular physics phenomena, most famously in context of fluid turbulence (*Kolmogorov*, 1941; *Nikora and Goring*, 2002) and granular collapse (*Bak et al.*, 1987; *Jensen*, 1998). In river science, many phenomena exhibit colored spectra, like the size distributions of bedforms (*Guala et al.*, 2014; *Nikora et al.*, 1997), the fluid forces on bed particles (*Amir et al.*, 2014; *Dwivedi et al.*, 2011), the roughness characteristics of gravel beds (*Aberle and Nikora*, 2006; *Singh et al.*, 2012), and sediment flux timeseries (*Chartrand and Furbish*, 2021; *Dhont and Ancey*, 2018). It will be problematic if these phenomena require colored noise for their description. Dynamical equations driven by colored noise can be extremely challenging to solve (*Hanggi*, 1978; *Hänggi and Jung*, 2007; *Luczka*, 2005). Even if white noise models like those developed in this thesis are not exactly accurate, they remain necessary as a basis for comparison when formulating and solving colored noise models (*Fox*, 1986; *Moss and McClintock*, 1989).

6.2 Key contributions

6.2.1 Calculation of the probability distribution of the sediment flux from micromechanics of particle transport

The first major contribution of this thesis is in chapter 2. Here, I formulated the probability distribution of the sediment flux from the trajectories of individual particles moving downstream. This work unifies the sediment trajectory models originating from Einstein (secs. 1.1.2-1.1.3) with the renewal approach to calculate the sediment flux (sec. 1.1.14). The striking feature of this formulation is that, as a result of the particle dynamics, the mean bedload flux becomes scale-dependent, whereby the expected magnitude of the flux depends on the time-period over which it is observed.

Ballio et al. (2018) explained that scale-dependence originates from individual particle trajectories, but this had not been described in a mathematical model until now. Descriptions of the mean sediment flux from the movement characteristics of individual grains have existed now for a long time (sec. 1.1.8), and an emerging body of research has producing  full probability distribution of the flux, but without referencing individual movement characteristics (secs. 1.1.13-1.1.14). This work unifies these two research themes and presents a statistical mechanics formulation of bed load sediment transport based on individual particle trajectories.

6.2.2 Inclusion of velocity fluctuations into Einstein's model of individual particle trajectories

Second, in chapter 2 I developed the first analytical description of sediment trajectories through motion and rest including velocity fluctuations within the motion state. Einstein originally formulated sediment transport as a sequence of instantaneuous steps and rests (sec. 1.1.2), and this was later improved to include the duration of motion (sec. 1.1.3). Until this thesis, movement velocities in analytical models were considered constant which contrasts with reality. Although some numerical models have described mo-

tion/rest cycles with velocity fluctuations (*Bialik et al.*, 2012; *Fan et al.*, 2016; *Schmeeckle*, 2014), they had not resolved the novel three-range diffusion characteristics these dynamics imply.

This description predicts multiple-range diffusion across local, intermediate, and global scales as a result of particle velocity fluctuations within the motion state; it introduces a dimensionless Peclet number as an important characteristic of bedload sediment transport; and it relates the timescales at which transitions between local, intermediate, and global timescales occur to the movement characteristics of individual grains. These developments constitute a new understanding of bedload movement across its timescales.

6.2.3 Quantification of the control of bed elevation fluctuations over sediment transport fluctuations

Third, chapter 3 modified the birth-death description of bedload transport (sec. 1.1.13) to include feedbacks between the local bed elevation and the entrainment and deposition rates. This allowed for a mathematical investigation of (1) how bed elevation changes affect sediment transport rates and (2) how bed elevation changes control the residence times of particles buried in the bed. Sediment transport fluctuations have come under increasing scrutiny with the resurgence of stochastic modelling in sediment transport, while the burial times of particles are crucial for using sediment tracers to predict sediment transport. Earlier birth-death models had generally considered that entrainment and deposition rates of particles remain constant even though these processes imply bed degradation and aggradation respectively, which are known to modify the entrainment and deposition rates in a negative feedback.

This work demonstrates that this negative feedback buffers bedload transport fluctuations whenever collective entrainment occurs, meaning the magnitude of bedload transport fluctuations depends on the rate of bed elevation change. The residence times of buried particles are random variables that lie on heavy-tailed power-law distributions. These distributions allow for arbitrarily long resting times, which poses challenging implications for researchers attempting to predict the downstream sediment flux in applica-

tions by tracking sediment tracer particles.

6.2.4 Characterization of how sediment burial affects the downstream transport of sediment particles

Fourth, chapter 4 presenting a model of sediment trajectories through motion, rest, and burial, describing sediment transport across local, intermediate, global, and geomorphic ranges (), and producing new understanding of how exactly the distinct spreading characteristics of particles within each of these ranges arise (e.g *Pretzlav et al.*, 2021).

Until this work, the mechanisms which produce the different spreading rates of particles across the scaling ranges identified by Nikora and coworkers had been uncertain for several decades, and earlier works had included what were believed to be the required features without describing three or more scaling ranges. The work ultimately demonstrates that many approaches to describe individual particle motions are reformulations of the continuous time random walk formalism from physics, indicating underlying unity within a diverse body of research and bringing powerful tools from statistical physics to the sediment transport problem.

6.2.5 Description of how particle-bed collisions control movement velocities of grains

Finally, chapter 5 displayed a new theoretical model of individual grains saltating downstream in a turbulent flow through a sequence of particle-bed collisions. This work provides the first comprehensive description of all bedload velocity distributions observed in experiments (sec. 5.3.3), while earlier works had described only particular end-member distributions (sec. 1.1.5).

6.3 Limitations and future research directions

This thesis has produced new understanding of how to describe bedload transport using statistical physics, but its approach has many limitations deserving of future research attention. In some cases these are specific to

the models produced in the thesis, but in others, they are shared in common with a majority of models in the stochastic sediment transport research paradigm (*Ancey*, 2020a; *Furbish and Doane*, 2021).

6.3.1 Landscape dynamics and channel morphology

The first limitation concerns the assumption, implicit in every chapter of this thesis, that sediment transport characteristics are steady and uniform in time and space. This assumption contrasts with conditions in real gravel-bed rivers, where riffles, bars, and steps coordinate the movements of individual grains (*Ashmore and Church*, 1998; *McDowell and Hassan*, 2020), sediment is supplied in episodic bursts from mass movements (*Benda*, 1990; *Müller and Hassan*, 2018), woody debris coordinates sediment movement (*Eaton et al.*, 2012; *Reid et al.*, 2019), and variable flow conditions modify bed texture and sediment availability (*Mao*, 2012; *Phillips et al.*, 2018).

To date, very little work has concentrated on stochastic sediment transport models in unsteady conditions (e.g. *Bohorquez and Ancey*, 2016). The most obvious scheme to address unsteadiness is to introduce time and space dependence to movement velocities, diffusivities, or entrainment and deposition rates, but how exactly one should express these rates in terms of time and space is a matter for speculation, and would be contingent on a given context given our limited understanding of how these parameters relate to the flow hydraulics (e.g. *Heyman et al.*, 2016).

Future studies might investigate in more depth the linkage between flow hydraulics, the geometric arrangement of grains on the bed, and the bed topography with the entrainment and deposition rates of individual particles to develop the foundational knowledge to incorporate temporally or spatially variable flow and sedimentary conditions into stochastic models of sediment transport.

6.3.2 Grain size distributions

The second major limitation of this work concerns grain size. In actuality, sediments in rivers spans a range of sizes, and differential mobility based

on particle size produces spatial sorting, both vertically as in bed armoring (*Aberle and Nikora*, 2006; *Parker and Klingeman*, 1982; *Wilcock and Southard*, 1989), and laterally as patch, particle cluster, or riffle development (*Nelson et al.*, 2014; *Venditti et al.*, 2017).

There have been a few works on stochastic modelling of sediment transport with multiple grain sizes (*Parker et al.*, 2002; *Sun and Donahue*, 2000), but these approaches are not spatially distributed, so there is as yet no stochastic method to understand sorting processes.

Future studies should revisit the stochastic framework applied to multiple grain sizes. Simplified experimental geometries based on bimodal sediment beds (e.g. *Houssais and Lajeunesse*, 2012) would be a great context to revisit these issues. Extending the motion-rest model of chapter 3 to two grain sizes with a matrix formulation, then calibrating its parameters to experiments would be a nice place to start.

6.3.3 The full range of geophysical flows

The final limitation I will mention is that all of the efforts in this thesis were concentrated on weak bedload transport, where densities of moving particles are low enough that they may interact with the static bed but never with each other. This assumption is justified because weak bedload transport conditions are typical of gravel bed rivers (*Ashworth and Ferguson*, 1989; *Warburton*, 1992), but it is nonetheless a limitation given the diversity of processes which move sediment over Earth's surface.

Earth's landforms are shaped by numerous transport phenomena from booming debris flows (*Iverson*, 1997) to barely perceptible hillslope creep (*Deshpande et al.*, 2021). Different phenomena are basically distinguished by the relative importance of fluid, granular, and gravitational forces in sustaining them (*Jerolmack and Daniels*, 2019).

Weak bedload transport is characterized by fluid forces small in comparison to gravity, and collision forces comparable to gravity. Viewed in this way, the work in this thesis targets a minute region of the vast parameter space spanned by Earth's geophysical flows, and geomorphology requires

characterization of them all. Future studies should continue the effort (*Furbish and Doane, 2021*) to describe these processes as different expressions of the same basic statistical mechanics building blocks.

6.4 Conclusion

This thesis described the movements of individual grains along streambeds using probabilistic methods. The research has related the overall sediment transport rates responsible for channel evolution to the movements of individual grains. At base level, the thesis embraces variability as an intrinsic part of Earth surface dynamics, and it produces descriptions which predict mean values as well as the magnitude of their fluctuations.

The founders of process geomorphology always acknowledged the role of variability in landscape evolution (*Horton, 1945; Langbein and Leopold, 1964; Strahler, 1952*), although their main efforts were to develop strategies to describe landscapes without including it, like averaged shear stresses to avoid fluid turbulence (*Bagnold, 1954; Meyer-Peter and Müller, 1948*), competent conditions to replace climate fluctuations (*Wolman and Gerson, 1978; Wolman and Miller, 1960*), and representative grain sizes to avoid evolving grain size distributions (*Andrews, 1983; Parker and Klingeman, 1982*).

The stochastic descriptions of sediment transport developed in this thesis hint toward a methodology to step beyond averaged descriptions of landscape evolution, propagate noises through the equations governing landscape change, and revisit the old question in geomorphology: How does variability shape Earth's surface?

Bibliography

Abbott, J. E., and J. R. Francis, Saltation and suspension trajectories of solid grains in a water stream., *Philos. Trans. R. Soc.*, *284*, 225–254, 1977. → page 9

Aberle, J., and V. Nikora, Statistical properties of armored gravel bed surfaces, *Water Resources Research*, *42*, 1–11, 2006. → pages 69, 72, 109, 114

Abramian, A., O. Devauchelle, G. Seizilles, and E. Lajeunesse, Boltzmann Distribution of Sediment Transport, *Physical Review Letters*, *123*, 14,501, 2019. → page 89

Abramian, A., O. Devauchelle, and E. Lajeunesse, Laboratory rivers adjust their shape to sediment transport, *Physical Review E*, *102*, 2020. → page 89

Allen, B., and A. Kudrolli, Granular bed consolidation, creep, and armoring under subcritical fluid flow, *Physical Review Fluids*, *7*, 1–13, 2018. → pages 2, 17

Amir, M., V. I. Nikora, and M. T. Stewart, Pressure forces on sediment particles in turbulent open-channel flow: A laboratory study, *Journal of Fluid Mechanics*, *757*, 458–497, 2014. → pages 2, 70, 109

Ancey, C., Bedload transport: a walk between randomness and determinism. Part 1. The state of the art, *Journal of Hydraulic Research*, *58*, 1–17, 2020a. → pages 2, 26, 29, 32, 44, 46, 49, 113

Ancey, C., Bedload transport: a walk between randomness and determinism. Part 2. Challenges and prospects, *Journal of Hydraulic Research*, *58*, 18–33, 2020b. → pages 3, 29

- Ancey, C., and J. Heyman, A microstructural approach to bed load transport: Mean behaviour and fluctuations of particle transport rates, *Journal of Fluid Mechanics*, 744, 129–168, 2014. → pages 12, 13, 25, 29, 30, 32, 33, 36, 46, 89, 90, 94, 96, 101, 102, 105
- Ancey, C., and I. Pascal, Estimating Mean Bedload Transport Rates and Their Uncertainty, *Journal of Geophysical Research: Earth Surface*, 125, 1–29, 2020. → pages 2, 16, 24, 33
- Ancey, C., T. Böhm, M. Jodeau, and P. Frey, Statistical description of sediment transport experiments, *Physical Review E - Statistical, Nonlinear, and Soft Matter Physics*, 74, 1–14, 2006. → pages 10, 17, 23, 24, 25, 32, 46, 50, 51, 52, 76, 84
- Ancey, C., A. C. Davison, T. Böhm, M. Jodeau, and P. Frey, Entrainment and motion of coarse particles in a shallow water stream down a steep slope, *Journal of Fluid Mechanics*, 595, 83–114, 2008. → pages xii, xviii, 16, 24, 29, 33, 46, 52, 53, 54, 55, 56, 58, 59, 60, 63, 64, 68, 69, 70, 169
- Ancey, C., P. Bohorquez, and J. Heyman, Stochastic interpretation of the advection-diffusion, *Journal of Geophysical Research : Earth Surface*, 120, 325–345, 2015. → page 70
- Andrews, E. D., Entrainment of gravel from naturally sorted riverbed material., *Geological Society of America Bulletin*, 94, 1225–1231, 1983. → page 115
- Arfken, G., *Mathematical methods for physicists*, Academic Press, Inc., 1985. → pages 7, 78, 152, 153, 154, 155, 156, 158, 159, 160, 161
- Armanini, A., *Principles of river hydraulics*, Springer, Cham, 2017. → page 18
- Armanini, A., V. Cavedon, and M. Righetti, A probabilistic/deterministic approach for the prediction of the sediment transport rate, *Advances in Water Resources*, 81, 10–18, 2015. → page 18
- Armenio, V., and V. Fiorotto, The importance of the forces acting on particles in turbulent flows, *Physics of Fluids*, 13, 2437–2440, 2001. → page 94
- Ashmore, P. E., and M. Church, Sediment transport and river morphology: A paradigm for study, in *Gravel-bed Rivers in the Environment*, pp.

115–148, Water Resources Publications, Highlands Ranch, CO, 1998. → page 113

Ashworth, P. J., and R. I. Ferguson, Size-selective entrainment of bed load in gravel bed streams, *Water Resources Research*, 25, 627–634, 1989. → page 114

Auton, T. R., The lift force on a spherical body in a rotational flow, *Journal of Fluid Mechanics*, 183, 199–218, 1987. → page 94

Bagnold, R. A., Experiments on a gravity-free dispersion of large solid spheres in a Newtonian fluid under shear, *Proceedings of the Royal Society of London. Series A. Mathematical and Physical Sciences*, 225, 49–63, 1954. → pages 16, 115

Bagnold, R. A., The flow of cohesionless grains in fluids, *Philosophical Transactions of the Royal Society of London. Series A, Mathematical and Physical Sciences*, 249, 235–297, 1956. → pages 2, 16

Bagnold, R. A., An Approach to the Sediment Transport Problem from General Physics, *Tech. Rep. 4*, U.S. Geological Survey, Washington, DC, 1966. → page 16

Bagnold, R. A., The nature of saltation and of 'bed-load' transport in water, *Proc. Roy. Soc. London, Series a*, 332, 473–504, 1973. → page 16

Bak, P., C. Tang, and K. Wiesenfeld, Self-organized criticality: An explanation of the 1/f noise, *Physical Review Letters*, 59, 381–384, 1987. → page 109

Balakrishnan, V., On a simple derivation of master equations for diffusion processes driven by white noise and dichotomic Markov noise, *Pramana*, 40, 259–265, 1993. → pages 7, 9, 150, 151

Ballio, F., V. Nikora, and S. E. Coleman, On the definition of solid discharge in hydro-environment research and applications, *Journal of Hydraulic Research*, 52, 173–184, 2014. → page 15

Ballio, F., D. Pokrajac, A. Radice, and S. A. Hosseini Sadabadi, Lagrangian and Eulerian Description of Bed Load Transport, *Journal of Geophysical Research: Earth Surface*, 123, 384–408, 2018. → pages 14, 23, 110

- Banerjee, T., S. N. Majumdar, A. Rosso, and G. Schehr, Current fluctuations in noninteracting run-and-tumble particles in one dimension, *Physical Review E*, 101, 1–16, 2020. → page 36
- Barik, D., P. K. Ghosh, and D. S. Ray, Langevin dynamics with dichotomous noise; Direct simulation and applications, *Journal of Statistical Mechanics: Theory and Experiment*, 2006. → pages xvi, 40, 80
- Barry, J. J., J. M. Buffington, and J. G. King, A general power equation for predicting bed load transport rates in gravel bed rivers, *Water Resources Research*, 40, 1–22, 2004. → page 2
- Bateman, H., and A. Erdelyi, *Higher Transcendental Functions*, McGraw-Hill, New York, 1953. → page 154
- Bathurst, J. C., Effect of coarse surface layer on bed-load transport, *Journal of Hydraulic Engineering*, 133, 1192–1205, 2007. → page 2
- Benavides, S. J., E. A. Deal, M. Rushlow, J. G. Venditti, K. Kamrin, and J. T. Perron, The impact of intermittency on bed load sediment transport, *Unpublished*, pp. 1–18, 2021. → page 46
- Benda, L., The influence of debris flows on channels and valley floors in the Oregon coast range, USA, *Earth Surface Processes and Landforms*, 15, 457–466, 1990. → page 113
- Bennett, C. H., Serially deposited amorphous aggregates of hard spheres, *Journal of Applied Physics*, 43, 2727–2734, 1972. → pages 54, 58
- Berezhkovskii, A. M., and G. H. Weiss, Detailed description of a two-state non-Markov system, *Physica A: Statistical Mechanics and its Applications*, 303, 1–12, 2002. → page 158
- Bialik, R. J., V. I. Nikora, and P. M. Rowiński, 3D Lagrangian modelling of saltating particles diffusion in turbulent water flow, *Acta Geophysica*, 60, 1639–1660, 2012. → pages 75, 84, 111
- Bialik, R. J., V. I. Nikora, M. Karpiński, and P. M. Rowiński, Diffusion of bedload particles in open-channel flows: distribution of travel times and second-order statistics of particle trajectories, *Environmental Fluid Mechanics*, 15, 1281–1292, 2015. → page 75

- Böhm, T., C. Ancey, P. Frey, J. L. Reboud, and C. Ducottet, Fluctuations of the solid discharge of gravity-driven particle flows in a turbulent stream, *Physical Review E - Statistical Physics, Plasmas, Fluids, and Related Interdisciplinary Topics*, 69, 13, 2004. → page 23
- Böhm, T., C. Ancey, P. Frey, M. Jodeau, and J. L. Reboud, Experiments on gravity-driven particle flows in a turbulent stream, *Powders and Grains 2005 - Proceedings of the 5th International Conference on Micromechanics of Granular Media*, 2, 1001–1004, 2005. → page 32
- Bohorquez, P., and C. Ancey, Particle diffusion in non-equilibrium bedload transport simulations, *Applied Mathematical Modelling*, 40, 7474–7492, 2016. → pages 89, 113
- Brach, R. M., Rigid body collisions, *American Society of Mechanical Engineers (Paper)*, 56, 133–138, 1989. → pages 91, 92, 105
- Brach, R. M., and P. F. Dunn, A mathematical model of the impact and adhesion of microspheres, *Aerosol Science and Technology*, 16, 51–64, 1992. → page 104
- Bradley, D. N., Direct Observation of Heavy-Tailed Storage Times of Bed Load Tracer Particles Causing Anomalous Superdiffusion, *Geophysical Research Letters*, 44, 12,227–12,235, 2017. → pages 5, 51, 71, 74, 84, 85, 86
- Bradley, D. N., G. E. Tucker, and D. A. Benson, Fractional dispersion in a sand bed river, *Journal of Geophysical Research*, 115, F00A09, 2010. → pages 84, 85
- Brilliantov, N. V., and T. Poschel, *Kinetic theory of granular gases*, 1st ed., Oxford University Press, Oxford, 2004. → pages 30, 47, 91, 96, 98
- Cameron, S. M., V. I. Nikora, and M. J. Witz, Entrainment of sediment particles by very large-scale motions, *Journal of Fluid Mechanics*, 888, 2020. → pages 4, 46, 103
- Campagnol, J., A. Radice, and F. Ballio, Scale-based statistical analysis of sediment fluxes, *Acta Geophysica*, 60, 1744–1777, 2012. → page 24
- Cardy, J., Reaction-diffusion processes, in *Non-equilibrium statistical physics and turbulence*, edited by S. Nazarenko and O. V. Zaboronski, pp. 108–161, Cambridge University Press, Cambridge, 2008. → page 47

- Celik, A. O., P. Diplas, C. L. Dancey, and M. Valyrakis, Impulse and particle dislodgement under turbulent flow conditions, *Physics of Fluids*, 22, 1–13, 2010. → page 50
- Celik, A. O., P. Diplas, and C. L. Dancey, Instantaneous pressure measurements on a spherical grain under threshold flow conditions, *Journal of Fluid Mechanics*, 741, 60–97, 2014. → pages 2, 4, 31, 94, 103
- Chapman, S., and T. G. Cowling, *Mathematical theory of non-uniform gases*, Cambridge University Press, Cambridge, 1970. → pages 47, 91
- Charru, F., Selection of the ripple length on a granular bed sheared by a liquid flow, *Physics of Fluids*, 18, 1–9, 2006. → pages 19, 20
- Charru, F., H. Mouilleron, and O. Eiff, Erosion and deposition of particles on a bed sheared by a viscous flow, *Journal of Fluid Mechanics*, 519, 55–80, 2004. → pages 2, 4, 19, 20, 31, 54, 70, 89, 99, 103, 105
- Chartrand, S., and D. J. Furbish, The transport of sediment mixtures examined with a birth-death model for grain-size fractions, *Preprint*, 2021. → page 109
- Chartrand, S. M., A. M. Jellinek, M. A. Hassan, and C. Ferrer-Boix, Morphodynamics of a Width-Variable Gravel Bed Stream: New Insights on Pool-Riffle Formation From Physical Experiments, *Journal of Geophysical Research: Earth Surface*, 123, 2735–2766, 2018. → page 24
- Cheng, N. S., Analysis of bedload transport in laminar flows, *Advances in Water Resources*, 27, 937–942, 2004. → page 18
- Church, M., Continental drift, *Earth Surface Processes and Landforms*, 30, 129–130, 2005. → page 1
- Church, M., Bed material transport and the morphology of alluvial river channels, *Annual Review of Earth and Planetary Sciences*, 34, 325–354, 2006. → page 2
- Church, M., The trajectory of geomorphology, *Progress in Physical Geography*, 34, 265–286, 2010. → page 1
- Church, M., and J. K. Haschenburger, What is the "active layer"? , *Water Resources Research*, 53, 5–10, 2017. → page 56

- Clark, A. H., M. D. Shattuck, N. T. Ouellette, and C. S. O'Hern, Onset and cessation of motion in hydrodynamically sheared granular beds, *Physical Review E - Statistical, Nonlinear, and Soft Matter Physics*, 92, 1–28, 2015. → page 11
- Clark, A. H., M. D. Shattuck, N. T. Ouellette, and C. S. O'Hern, Role of grain dynamics in determining the onset of sediment transport, *Physical Review Fluids*, 2, 2017. → pages 11, 17
- Clift, R., J. R. Grace, and M. E. Weber, Bubbles, Drops, and Particles, 1978. → pages 94, 102
- Coleman, N. L., A theoretical and experimental study of drag and lift forces acting on a sphere resting on a hypothetical streambed, in *International Association for Hydraulic Research Congress*, pp. 185–192, Littleton, CO, 1967. → page 94
- Coleman, S. E., and V. I. Nikora, Exner equation: A continuum approximation of a discrete granular system, *Water Resources Research*, 45, 1–8, 2009. → page 23
- Cox, D. R., *Renewal Theory*, Methuen, London, 1962. → page 26
- Cox, D. R., and H. D. Miller, *The theory of stochastic processes*, Wiley, New York, 1965. → pages 18, 24, 25, 39, 42, 56, 57, 98, 165, 169
- Crickmore, M., and G. Lean, The measurement of sand transport by the time-integration method with radioactive tracers, *Proceedings of the Royal Society of London. Series A. Mathematical and Physical Sciences*, 270, 27–47, 1962. → page 55
- Cudden, J. R., and T. B. Hoey, The causes of bedload pulses in a gravel channel: The implications of bedload grain-size distributions, *Earth Surface Processes and Landforms*, 28, 1411–1428, 2003. → page 23
- Cundall, P. A., and O. D. Strack, A discrete numerical model for granular assemblies, *Geotechnique*, 29, 47–65, 1979. → pages 11, 75
- Daly, E., and A. Porporato, Probabilistic dynamics of some jump-diffusion systems, *Physical Review E - Statistical, Nonlinear, and Soft Matter Physics*, 73, 1–7, 2006. → page 95
- Daly, E., and A. Porporato, Effect of different jump distributions on the dynamics of jump processes, *Physical Review E - Statistical, Nonlinear, and Soft Matter Physics*, 81, 1–10, 2010. → page 95

- Denisov, S. I., W. Horsthemke, and P. Hänggi, Generalized Fokker-Planck equation: Derivation and exact solutions, *European Physical Journal B*, **68**, 567–575, 2009. → page 95
- Deshpande, N. S., D. J. Furbish, P. E. Arratia, and D. J. Jerolmack, The perpetual fragility of creeping hillslopes, *Nature Communications*, **12**, 1–7, 2021. → page 115
- Dey, S., and S. Z. Ali, Advances in modeling of bed particle entrainment sheared by turbulent flow, *Physics of Fluids*, **30**, 2018. → page 19
- Dhont, B., and C. Ancey, Are Bedload Transport Pulses in Gravel Bed Rivers Created by Bar Migration or Sediment Waves?, *Geophysical Research Letters*, **45**, 5501–5508, 2018. → pages 23, 32, 33, 46, 48, 52, 69, 88, 109
- Drake, T. G., R. L. Shreve, W. E. Dietrich, P. J. Whiting, and L. B. Leopold, Bedload transport of fine gravel observed by motion-picture photography, *Journal of Fluid Mechanics*, **192**, 193–217, 1988. → page 9
- Dubkov, A. A., and A. A. Kharcheva, Steady-state probability characteristics of Verhulst and Hongler models with multiplicative white Poisson noise, *European Physical Journal B*, **92**, 1–6, 2019. → page 95
- Dubkov, A. A., O. V. Rudenko, and S. N. Gurbatov, Probability characteristics of nonlinear dynamical systems driven by δ -pulse noise, *Physical Review E*, **93**, 1–7, 2016. → page 95
- Duderstadt, J. J., and W. R. Martin, *Transport Theory*, 1st ed., Wiley Interscience, New York, 1979. → page 96
- Dwivedi, A., B. Melville, and A. Y. Shamseldin, Hydrodynamic forces generated on a spherical sediment particle during entrainment, *Journal of Hydraulic Engineering*, **136**, 756–769, 2010. → page 94
- Dwivedi, A., B. W. Melville, A. Y. Shamseldin, and T. K. Guha, Analysis of hydrodynamic lift on a bed sediment particle, *Journal of Geophysical Research: Earth Surface*, **116**, 2011. → pages 50, 109
- Dwivedi, A., B. Melville, A. J. Raudkivi, A. Y. Shamseldin, and Y. M. Chiew, Role of turbulence and particle exposure on entrainment of large spherical particles in flows with low relative submergence, *Journal of Hydraulic Engineering*, **138**, 1022–1030, 2012. → pages 2, 94

- Eaton, B. C., M. A. Hassan, and S. L. Davidson, Modeling wood dynamics, jam formation, and sediment storage in a gravel-bed stream, *Journal of Geophysical Research F: Earth Surface*, 117, 1–18, 2012. → page 113
- Eaton, B. C., L. G. MacKenzie, and W. H. Booker, Channel stability in steep gravel–cobble streams is controlled by the coarse tail of the bed material distribution, *Earth Surface Processes and Landforms*, 45, 3639–3652, 2020. → page 2
- Einstein, H. A., Bed load transport as a probability problem, Ph.D. thesis, ETH Zurich, 1937. → pages xix, 4, 5, 7, 9, 17, 28, 29, 32, 40, 48, 50, 51, 68, 73, 74, 75, 76, 78, 79, 81, 83, 84, 85
- Einstein, H. A., Formulas for the transport of bed sediment, *Trans. Am. Soc. Civ. Eng.*, 107, 561–574, 1942. → page 17
- Einstein, H. A., *The bedload function for sediment transportation in open channel flows*, technical ed., Soil Conservation Service, Washington, DC, 1950. → pages 17, 19, 32, 50, 51, 52, 53, 55, 68
- Elghannay, H., and D. Tafti, LES-DEM simulations of sediment transport, *International Journal of Sediment Research*, 33, 137–148, 2018. → page 12
- Elgueta-Astaburuaga, M. A., and M. A. Hassan, Sediment storage, partial transport, and the evolution of an experimental gravel bed under changing sediment supply regimes, *Geomorphology*, 330, 1–12, 2019. → page 23
- Engelund, F., and J. Fredsoe, A sediment transport model for straight alluvial channels., *Nordic Hydrology*, 7, 293–306, 1976. → page 17
- Escaff, D., R. Toral, C. Van Den Broeck, and K. Lindenberg, A continuous-time persistent random walk model for flocking, *Chaos*, 28, 1–11, 2018. → pages 47, 86
- Ettema, R., and C. F. Mutel, Hans Albert Einstein: Innovation and compromise in formulating sediment transport by Rivers, *Journal of Hydraulic Engineering*, 130, 477–487, 2004. → pages 5, 73
- Exner, F. M., Über die Wechselwirkung zwischen Wasser und Geschiebe in Flüssen, *Sitzungsberichte der Akademie der Wissenschaften in Wien. Mathem.-naturw. Klasse, Abteilung 2a*, pp. 165–207, 1925. → page 22

- Fa, K. S., Uncoupled continuous-time random walk model: Analytical and numerical solutions, *Physical Review E - Statistical, Nonlinear, and Soft Matter Physics*, *89*, 1–9, 2014. → page 86
- Fan, N., D. Zhong, B. Wu, E. Foufoula-Georgiou, and M. Guala, A mechanistic-stochastic formulation of bed load particle motions: From individual particle forces to the Fokker-Planck equation under low transport rates, *Journal of Geophysical Research: Earth Surface*, *119*, 464–482, 2014. → pages 12, 30, 32, 89, 90, 94, 96, 100, 102
- Fan, N., A. Singh, M. Guala, E. Foufoula-Georgiou, and B. Wu, Exploring a semimechanistic episodic Langevin model for bed load transport: Emergence of normal and anomalous advection and diffusion regimes, *Water Resources Research*, *52*, 2789–2801, 2016. → pages 75, 84, 85, 111
- Fathel, S., D. Furbish, and M. Schmeeckle, Parsing anomalous versus normal diffusive behavior of bedload sediment particles, *Earth Surface Processes and Landforms*, *41*, 1797–1803, 2016. → pages 74, 83, 86, 89
- Fathel, S. L., D. J. Furbish, and M. W. Schmeeckle, Experimental evidence of statistical ensemble behavior in bed load sediment transport, *Journal of Geophysical Research F: Earth Surface*, *120*, 2298–2317, 2015. → pages 9, 12, 22, 31, 43, 52, 76, 89, 90, 105
- Feller, W., *An Introduction to Probability Theory and its Applications*, 3rd ed., Wiley, 1967. → page 96
- Ferguson, R. I., and T. B. Hoey, Long-term slowdown of river tracer pebbles: Generic models and implications for interpreting short-term tracer studies, *Water Resources Research*, *38*, 17–1–17–11, 2002. → pages 4, 5, 29, 81
- Ferguson, R. I., D. J. Bloomer, T. B. Hoey, and A. Werritty, Mobility of river tracer pebbles over different timescales, *Water Resources Research*, *38*, 3–1–3–8, 2002. → page 74
- Ferreira, R. M. L., M. A. . Hassan, and C. Ferrer-Boix, Principles of Bedload Transport of Non-cohesive Sediment in Open-Channels, in *Rivers – Physical, Fluvial and Environmental Processes*, pp. 323–372, Springer, Cham, 2015. → page 2
- Fox, R. F., Uniform convergence to an effective Fokker-Planck equation for weakly colored noise, *Physical Review A*, *34*, 4525–4527, 1986. → page 109

- Fraccarollo, L., and M. A. Hassan, Einstein conjecture and resting-Time statistics in the bed-load transport of monodispersed particles, *Journal of Fluid Mechanics*, 876, 1077–1089, 2019. → page 84
- Francis, J. R. D., Experiments on the motion of solitary grains along the bed of a water-stream, *Proc. Roy. Soc. Lond. A.*, 332, 443–471, 1973. → page 9
- Frey, P., Particle velocity and concentration profiles in bedload experiments on a steep slope, *Earth Surface Processes and Landforms*, 39, 646–655, 2014. → page 4
- Frey, P., and M. Church, Bedload: A granular phenomenon, *Earth Surface Processes and Landforms*, 36, 58–69, 2011. → page 12
- Furbish, D. J., and T. H. Doane, Rarefied particle motions on hillslopes – Part 4 : Philosophy, *Earth Surface Dynamics*, 9, 629–664, 2021. → pages 113, 115
- Furbish, D. J., and M. W. Schmeeckle, A probabilistic derivation of the exponential-like distribution of bed load particle velocities, *Water Resources Research*, 49, 1537–1551, 2013. → page 90
- Furbish, D. J., A. E. Ball, and M. W. Schmeeckle, A probabilistic description of the bed load sediment flux: 4. Fickian diffusion at low transport rates, *Journal of Geophysical Research: Earth Surface*, 117, 1–13, 2012a. → pages 12, 15, 19, 20, 21, 22, 74, 86
- Furbish, D. J., P. K. Haff, J. C. Roseberry, and M. W. Schmeeckle, A probabilistic description of the bed load sediment flux: 1. Theory, *Journal of Geophysical Research: Earth Surface*, 117, 2012b. → pages 32, 46, 51, 52, 54
- Furbish, D. J., S. L. Fathel, and M. W. Schmeeckle, Particle motions and bedload theory: The entrainment forms of the flux and the exner equation, in *Gravel-Bed Rivers: Process and Disasters*, edited by D. Tsutsumi and J. B. Laronne, 1 ed., chap. 4, pp. 97–120, John Wiley & Sons Ltd., 2017. → pages 21, 22, 23, 34, 52, 74
- Gaeuman, D., R. Stewart, B. Schmandt, and C. Pryor, Geomorphic response to gravel augmentation and high-flow dam release in the Trinity River, California, *Earth Surface Processes and Landforms*, 42, 2523–2540, 2017. → pages 50, 73, 88

- Gardiner, C. W., *Handbook of stochastic methods for physics, chemistry and the natural sciences*, Springer-Verlag, 1983. → pages 12, 57, 60, 70, 94, 95, 96, 109, 169, 176
- Gilbert, G. K., The transportaton of debris by running water, *Tech. rep.*, U. S. Geological Survey, 1914. → page 2
- Gillespie, D. T., Exact stochastic simulation of coupled chemical reactions, *Journal of Physical Chemistry*, 81, 2340–2361, 1977. → pages 57, 165
- Gillespie, D. T., *Markov processes — an introduction for physical scientists*, 1st ed., Academic Press, Inc., 1992. → pages 56, 57, 165
- Gillespie, D. T., Stochastic simulation of chemical kinetics, *Annual Review of Physical Chemistry*, 58, 35–55, 2007. → pages 56, 57, 58, 165
- Glielmo, A., N. Gunkelmann, and T. Pöschel, Coefficient of restitution of aspherical particles, *Physical Review E - Statistical, Nonlinear, and Soft Matter Physics*, 90, 1–7, 2014. → page 96
- Goh, K. I., and A. L. Barabási, Burstiness and memory in complex systems, *Epl*, 81, 2008. → page 46
- Goldstein, H., *Classical Mechanics*, Addison-Wesley, Reading, 1997. → pages 7, 47
- Gomez, B., and M. Church, An assessment of bed load sediment transport formulae for gravel bed rivers, *Water Resources Research*, 25, 1161–1186, 1989. → page 2
- González, C., D. H. Richter, D. Bolster, S. Bateman, J. Calantoni, and C. Escauriaza, Characterization of bedload intermittency near the threshold of motion using a Lagrangian sediment transport model, *Environmental Fluid Mechanics*, 17, 111–137, 2017. → pages 12, 50, 90, 102
- Gordon, R., J. B. Carmichael, and F. J. Isackson, Saltation of plastic balls in a ‘one-dimensional’ flume, *Water Resources Research*, 8, 444–459, 1972. → pages 3, 9, 31, 76, 93
- Grass, A., Initial Instability of Fine Bed Sand, *Journal of the Hydraulics Division*, 96, 619–632, 1970. → page 19

- Guala, M., A. Singh, N. Badheartbull, and E. Foufoula-georgiou, Spectral description of migrating bed forms and sediment transport, *Journal of Geophysical Research: Earth Surface*, 119, 123–137, 2014. → pages 23, 32, 48, 109
- Haken, H., *Synergetics: An Introduction*, 2nd ed., Springer-Verlag, New York, 1978. → pages 57, 59
- Hall, A. J., and G. C. Wake, A functional differential equation arising in modelling of cell growth, *The Journal of the Australian Mathematical Society. Series B. Applied Mathematics*, 30, 424–435, 1989. → pages 97, 175
- Hamamori, A., A theoretical investigation on the fluctuations of bed load transport. Technical Report No. R4., *Tech. rep.*, Delft Hydraulics Laboratory, 1962. → pages 23, 48
- Hanggi, P., Correlation Functions and Masterequations of Generalized (Non-Markovian) Langevin Equations, *Z. Physik B*, 31, 407–416, 1978. → pages 7, 36, 95, 109
- Hanggi, P., The functional derivative and its use in the description of noisy dynamical systems, in *International School on Stochastic Processes Applied to Physics*, edited by L. Pesquera and M. A. Rodriguez, pp. 69–94, World Scientific Publishing Company, Santander, Spain, 1984. → page 7
- Hänggi, P., and P. Jung, Colored Noise in Dynamical Systems, 2007. → page 109
- Haschenburger, J. K., Vertical mixing of gravel over a long flood series, *Earth Surface Processes and Landforms*, 36, 1044–1058, 2011. → page 5
- Haschenburger, J. K., Tracing river gravels: Insights into dispersion from a long-term field experiment, *Geomorphology*, 200, 121–131, 2013. → pages 5, 74, 81
- Hassan, M. A. ., and D. N. Bradley, Geomorphic controls on tracer particle dispersion in gravel-bed rivers, in *Gravel-Bed Rivers: Process and Disasters*, edited by D. Tsutsumi and J. B. Laronne, 1st ed., pp. 159–184, John Wiley & Sons Ltd., 2017. → pages 4, 5, 29, 30, 50, 73, 74, 81, 84, 86

- Hassan, M. A., and M. Church, Vertical mixing of coarse particles in gravel bed rivers: A kinematic model, *Water Resources Research*, *30*, 1173–1185, 1994. → pages 4, 81
- Hassan, M. A., M. Church, and A. P. Schick, Distance of movement of coarse particles in gravel bed streams, *Water Resources Research*, *27*, 503–511, 1991. → pages 42, 68, 74, 75, 81
- Hassan, M. A., B. J. Smith, D. L. Hogan, D. S. Luzi, A. E. Zimmermann, and B. C. Eaton, Sediment storage and transport in coarse bed streams: scale considerations, in *Developments in Earth Surface Processes*, edited by H. Habersack, H. Piegay, and M. Rinaldi, vol. 11, chap. 18, pp. 473–496, Elsevier B.V, 2007. → pages 2, 70
- Hassan, M. A., H. Voepel, R. Schumer, G. Parker, and L. Fracarollo, Displacement characteristics of coarse fluvial bed sediment, *Journal of Geophysical Research: Earth Surface*, *118*, 155–165, 2013. → page 74
- Hernández-García, E., and C. López, Clustering, advection, and patterns in a model of population dynamics with neighborhood-dependent rates, *Physical Review E - Statistical, Nonlinear, and Soft Matter Physics*, *70*, 11, 2004. → page 47
- Heyman, J., A study of the spatio-temporal behaviour of bed load transport rate fluctuations, *PhD Dissertation*, *6256*, 116, 2014. → page 52
- Heyman, J., F. Mettra, H. B. Ma, and C. Ancey, Statistics of bedload transport over steep slopes: Separation of time scales and collective motion, *Geophysical Research Letters*, *40*, 128–133, 2013. → pages 24, 26, 29, 46, 52
- Heyman, J., H. B. Ma, F. Mettra, and C. Ancey, Spatial correlations in bed load transport : Evidence, importance, and modeling, *Journal of Geophysical Research: Earth Surface*, *119*, 1751–1767, 2014. → pages 23, 42, 52, 70, 86
- Heyman, J., P. Bohórquez, and C. Ancey, Exploring the physics of sediment transport in non-uniform super-critical flows through a large dataset of particle trajectories, *J. Geophys. Res.:Earth Surf.*, *submitted*, 2015. → page 46

- Heyman, J., P. Bohorquez, and C. Ancey, Entrainment, motion, and deposition of coarse particles transported by water over a sloping mobile bed, *Journal of Geophysical Research: Earth Surface*, 121, 1931–1952, 2016. → pages 12, 15, 31, 52, 69, 71, 86, 89, 90, 105, 113
- Hjelmfelt, A. T., and L. F. Mockros, Motion of discrete particles in a turbulent fluid, *Applied Scientific Research*, 16, 149–161, 1966. → page 94
- Hoey, T. B., Temporal variations in bedload transport in rates and sediment storage, *Progress in Physical Geography*, 16, 319–338, 1992. → pages 23, 48
- Hofland, B., and J. A. Battjes, Probability density function of instantaneous drag forces and shear stresses on a bed, *Journal of Hydraulic Engineering*, 132, 1169–1175, 2006. → pages 94, 103
- Hooke, R. L., On the history of humans as geomorphic agents, *Geology*, 28, 843–846, 2000. → page 1
- Horsthemke, W., and R. Lefever, *Noise-induced transitions: Theory and applications in physics, chemistry and biology*, 1st ed., Springer-Verlag, Berlin, 1984. → page 108
- Horton, R. E., Erosional development of streams and their drainage basins; hydrophysical approach to quantitative morphology, *GSA Bulletin*, 56, 275–370, 1945. → page 115
- Houssais, M., and E. Lajeunesse, Bedload transport of a bimodal sediment bed, *Journal of Geophysical Research: Earth Surface*, 117, 1–13, 2012. → pages 14, 89, 114
- Houssais, M., C. P. Ortiz, D. J. Durian, and D. J. Jerolmack, Onset of sediment transport is a continuous transition driven by fluid shear and granular creep, *Nature Communications*, 6, 1–8, 2015. → page 17
- Houssais, M., C. P. Ortiz, D. J. Durian, and D. J. Jerolmack, Rheology of sediment transported by a laminar flow, *Physical Review E*, 94, 1–10, 2016. → page 4
- Hubbell, D., and W. Sayre, Sand Transport Studies with Radioactive Tracers, *Journal of the Hydraulics Division*, 90, 39–68, 1964. → pages 51, 68, 75, 76, 81

- Iseya, F., and H. Ikeda, Pulsations in Bedload Transport Rates Induced by a Longitudinal Sediment Sorting: A Flume Study Using Sand and Gravel Mixtures, *Geografiska Annaler. Series A, Physical Geography*, 69, 15, 1987. → page 23
- Ismail, K. A., and W. J. Stronge, Impact of viscoplastic bodies: Dissipation and restitution, *Journal of Applied Mechanics, Transactions ASME*, 75, 0610,111–0610,115, 2008. → page 104
- Iverson, R. M., The Physics of Debris Flows, *Reviews of Geophysics*, 35, 245–296, 1997. → page 114
- Jensen, H. J., *Self-Organized Criticality*, Cambridge University Press, Cambridge, 1998. → page 109
- Jerolmack, D., and D. Mohrig, Interactions between bed forms: Topography, turbulence, and transport, *Journal of Geophysical Research: Earth Surface*, 110, 2005. → pages 3, 89
- Jerolmack, D. J., and K. E. Daniels, Viewing Earth's surface as a soft-matter landscape, *Nature Reviews Physics*, 1, 716–730, 2019. → page 115
- Ji, C., A. Munjiza, E. Avital, J. Ma, and J. J. Williams, Direct numerical simulation of sediment entrainment in turbulent channel flow, *Physics of Fluids*, 25, 2013. → page 12
- Jiang, Z., and P. K. Haff, Multiparticle simulation methods applied to the micromechanics of bed load transport, *Water Resources Research*, 29, 399–412, 1993. → page 11
- Joseph, G. G., R. Zenit, M. L. Hunt, and A. M. Rosenwinkel, Particle-wall collisions in a viscous fluid, *Journal of Fluid Mechanics*, 433, 329–346, 2001. → pages 92, 104, 106
- Kalinske, A. A., Movement of sediment as bed load in rivers, *Eos, Transactions American Geophysical Union*, 28, 615–620, 1947. → page 2
- Kim, H. K., Advanced Second Order Functional Differential Equations, Ph.D. thesis, Massey University, 1998. → page 97
- Kirchener, J. W., W. E. Dietrich, F. Iseya, and H. Ikeda, The variability of critical shear stress, friction angle, and grain protrusion in water-worked sediments, *Sedimentology*, 37, 647–672, 1990. → pages 2, 17

- Kittel, C., *Elementary statistical mechanics*, 1st ed., Wiley, New York, 1958. → page 158
- Kolmogorov, A. N., The local structure of turbulence in incompressible viscous fluid for very large Reynolds numbers, *C. R. Acad. Sci. URSS*, 30, 301–305, 1941. → page 109
- Kraichnan, R. H., Diffusion by a random velocity field, *Physics of Fluids*, 13, 22–31, 1970. → page 75
- Kubo, R., M. Toda, and N. Hashitsume, *Statistical Physics II: Nonequilibrium Statistical Physics*, 1st ed., Springer-Verlag, Berlin, 1978. → pages 7, 12, 109
- Kuhnle, R. A., and J. B. Southard, Bed load transport fluctuations in a gravel bed laboratory channel, *Water Resources Research*, 24, 247–260, 1988. → page 23
- Kumaran, V., Granular flow of rough particles in the high-Knudsen-number limit, *Journal of Fluid Mechanics*, 561, 43–72, 2006. → page 34
- Lajeunesse, E., L. Malverti, and F. Charru, Bed load transport in turbulent flow at the grain scale: Experiments and modeling, *Journal of Geophysical Research: Earth Surface*, 115, 2010. → pages xx, 9, 12, 20, 49, 82, 86, 89, 99, 103, 105
- Lajeunesse, E., O. Devauchelle, F. Lachaussée, and P. Claudin, Bedload transport in laboratory rivers: The erosion-deposition model, in *Gravel-Bed Rivers 8: Processes and Disasters*, edited by J. B. Laronne and D. Tsutsumi, pp. 415–438, Earth Surface Processes and Landforms, Kyoto and Takyama, Japan, 2015. → page 20
- Lajeunesse, E., O. Devauchelle, and F. James, Advection and dispersion of bed load tracers, *Earth Surface Dynamics*, 6, 389–399, 2017. → pages 9, 28, 30, 32, 35, 44, 48, 51, 75, 76, 84, 85, 86, 162
- Landau, L. D., and E. M. Lifshitz, *Statistical Physics. Volume 5, Course of theoretical physics*, 6th ed., Pergamon Press, Oxford, 1969. → pages 91, 103
- Langbein, W. B., and L. B. Leopold, Quasi-equilibrium states in channel morphology, *American Journal of Science*, 262, 782–794, 1964. → page 115

- Lee, D. B., and D. Jerolmack, Determining the scales of collective entrainment in collision-driven bed load, *Earth Surface Dynamics*, 6, 1089–1099, 2018. → pages 46, 52, 69, 86
- Lisle, I. G., C. W. Rose, W. L. Hogarth, P. B. Hairsine, G. C. Sander, and J. Y. Parlange, Stochastic sediment transport in soil erosion, *Journal of Hydrology*, 204, 217–230, 1998. → pages xvi, xix, 9, 10, 29, 30, 32, 35, 40, 44, 48, 75, 76, 78, 79, 84, 85, 86, 162
- Lisle, T. E., F. Iseya, and H. Ikeda, Response of a Channel with alternate bars to a decrease in supply of mixed-size bed load: A Flume Experiment, *Water Resources Research*, 29, 3623–3629, 1993. → page 23
- Liu, D., X. Liu, X. Fu, and G. Wang, Quantification of the bed load effects on turbulent open-channel flows, *Journal of Geophysical Research : Earth Surface*, 121, 767–789, 2016. → page 2
- Liu, M. X., A. Pelosi, and M. Guala, A Statistical Description of Particle Motion and Rest Regimes in Open-Channel Flows Under Low Bedload Transport, *Journal of Geophysical Research: Earth Surface*, 124, 2666–2688, 2019. → pages 14, 51, 84, 89, 90, 105
- Lorenz, A., C. Tuozzolo, and M. Y. Louge, Measurements of impact properties of small, nearly spherical particles, *Experimental Mechanics*, 37, 292–298, 1997. → page 92
- Luczka, J., Non-Markovian stochastic processes: Colored noise, *Chaos*, 15, 2005. → page 109
- Luczka, J., M. Niemiec, and E. Piotrowski, Randomly interrupted diffusion, *Physics Letters A*, 167, 475–478, 1992. → page 35
- Luczka, J., M. Niemiec, and E. Piotrowski, Linear systems with randomly interrupted Gaussian white noise, *Journal of Physics A: Mathematical and General*, 26, 4849–4861, 1993. → page 35
- Luczka, J., R. Bartussek, and P. Hanggi, White-noise-induced transport in periodic structures., *Epl*, 31, 431–436, 1995. → page 35
- Luque, R. F., and R. van Beek, Erosion and transport of bed-load sediment, *Journal of Hydraulic Research*, 14, 127–144, 1976. → page 17
- Macklin, M. G., P. A. Brewer, K. A. Hudson-Edwards, G. Bird, T. J. Coulthard, I. A. Dennis, P. J. Lechler, J. R. Miller, and J. N. Turner, A

geomorphological approach to the management of rivers contaminated by metal mining, *Geomorphology*, 79, 423–447, 2006. → pages 50, 73

Madej, M. A., D. G. Sutherland, T. E. Lisle, and B. Pryor, Channel responses to varying sediment input: A flume experiment modeled after Redwood Creek, California, *Geomorphology*, 103, 507–519, 2009. → page 23

Malmon, D. V., S. L. Reneau, T. Dunne, D. Katzman, and P. G. Drakos, Influence of sediment storage on downstream delivery of contaminated sediment, *Water Resources Research*, 41, 1–17, 2005. → pages 50, 88

Mao, L., The effect of hydrographs on bed load transport and bed sediment spatial arrangement, *Journal of Geophysical Research: Earth Surface*, 117, 1–16, 2012. → pages 23, 113

Marcum, J. I., A Statistical Theory of Target Detection By Pulsed Radar, *IRE Transactions on Information Theory*, 6, 59–267, 1960. → page 79

Marshall, J. S., Viscous damping force during head-on collision of two spherical particles, *Physics of Fluids*, 23, 2011. → page 105

Martin, R. L., Transient mechanics of bed load sediment transport, Phd dissertation, University of Pennsylvania, 2013. → page 9

Martin, R. L., D. J. Jerolmack, and R. Schumer, The physical basis for anomalous diffusion in bed load transport, *Journal of Geophysical Research: Earth Surface*, 117, 1–18, 2012. → pages xx, 12, 21, 47, 51, 74, 76, 82, 83, 84, 85, 89, 105

Martin, R. L., P. K. Purohit, and D. J. Jerolmack, Sedimentary bed evolution as a mean-reverting random walk: Implications for tracer statistics, *Geophysical Research Letters*, 41, 6152–6159, 2014. → pages 51, 55, 58, 60, 65, 66, 68, 69, 70, 71, 74, 81, 84, 85

Martin, Y., Evaluation of bed load transport formulae using field evidence from the Vedder River, British Columbia, *Geomorphology*, 53, 75–95, 2003. → page 88

Martin, Y., and M. Church, Re-examination of Bagnold's empirical bedload formulae, *Earth Surface Processes and Landforms*, 25, 1011–1024, 2000. → page 17

- Masoliver, J., Fractional telegrapher's equation from fractional persistent random walks, *Physical Review E*, 93, 1–10, 2016. → page 86
- Masoliver, J., and K. Lindenberg, Continuous time persistent random walk: a review and some generalizations, *European Physical Journal B*, 90, 2017. → page 9
- Masoliver, J., and G. H. Weiss, Telegrapher's equations with variable propagation speeds, *Physical Review E*, 49, 3852–3854, 1994. → page 86
- Masteller, C. C., N. J. Finnegan, J. M. Turowski, E. M. Yager, and D. Rickenmann, History-Dependent Threshold for Motion Revealed by Continuous Bedload Transport Measurements in a Steep Mountain Stream, *Geophysical Research Letters*, 46, 2583–2591, 2019. → page 2
- Mau, Y., X. Feng, and A. Porporato, Multiplicative jump processes and applications to leaching of salt and contaminants in the soil, *Physical Review E - Statistical, Nonlinear, and Soft Matter Physics*, 90, 1–8, 2014. → page 95
- Maurin, R., J. Chauchat, B. Chareyre, and P. Frey, A minimal coupled fluid-discrete element model for bedload transport, *Physics of Fluids*, 27, 2015. → page 11
- Maxey, M. R., and J. J. Riley, Equation of motion for a small rigid sphere in a nonuniform flow, *Physics of Fluids*, 26, 883–889, 1983. → pages 3, 94
- McDowell, C., and M. A. Hassan, The influence of channel morphology on bedload path lengths: Insights from a survival process model, *Earth Surface Processes and Landforms*, 45, 2982–2997, 2020. → page 113
- McEwan, I., and J. Heald, Discrete particle modeling of entrainment from flat uniformly sized sediment beds, *Journal of Hydraulic Engineering*, 127, 588–597, 2001. → page 11
- Mendes, L., F. Antico, P. Sanches, F. Alegria, R. Aleixo, and R. M. Ferreira, A particle counting system for calculation of bedload fluxes, *Measurement Science and Technology*, 27, 2016. → page 47
- Metzler, R., and J. Klafter, The random walk's guide to anomalous diffusion: A fractional dynamics approach, *Physics Report*, 339, 1–77, 2000. → pages 73, 80

- Metzler, R., J. H. Jeon, A. G. Cherstvy, and E. Barkai, Anomalous diffusion models and their properties: Non-stationarity, non-ergodicity, and ageing at the centenary of single particle tracking, *Physical Chemistry Chemical Physics*, 16, 24,128–24,164, 2014. → page 86
- Meyer-Peter, E., and R. Müller, Formulas for Bed-Load Transport, *Proceedings of the 2nd Meeting of the International Association of Hydraulic Research*, pp. 39–64, 1948. → pages 3, 16, 115
- Michaelides, E. E., Review—the transient equation of motion for particles, bubbles, and droplets, *Journal of Fluids Engineering, Transactions of the ASME*, 119, 233–247, 1997. → page 94
- Miller, R. L., and R. J. Byrne, the Angle of Repose for a Single Grain on a Fixed Rough Bed, *Sedimentology*, 6, 303–314, 1966. → pages 2, 4
- Montaine, M., M. Heckel, C. Kruelle, T. Schwager, and T. Pöschel, Coefficient of restitution as a fluctuating quantity, *Physical Review E - Statistical, Nonlinear, and Soft Matter Physics*, 84, 1–5, 2011. → page 92
- Montroll, E. W., Random walks on lattices, *Journal of Mathematical Physics*, 6, 193–220, 1964. → pages 6, 32, 76
- Morse, P. M., and H. Feshbach, *Methods of Theoretical Physics, Vol. II*, McGraw-Hill, New York, 1953a. → page 97
- Morse, P. M., and H. Feshbach, *Methods of Theoretical Physics, Vol I.*, McGraw-Hill, New York, 1953b. → page 41
- Moss, F., and P. V. E. McClintock (Eds.), *Noise in nonlinear dynamical systems*, vol. 1, Cambridge University Press, 1989. → pages 7, 109
- Müller, T., and M. A. Hassan, Fluvial response to changes in the magnitude and frequency of sediment supply in a 1-D model, *Earth Surface Dynamics*, 6, 1041–1057, 2018. → page 113
- Nakagawa, H., and T. Tsujimoto, On probabilistic characteristics of motion of individual sediment particles on stream beds., in *Hydraulic Problems Solved by Stochastic Methods: Second International IAHR Symposium on Stochastic Hydraulics*, pp. 293–320, Water Resources Publications, Lund, Sweden, 1976. → pages 21, 22, 51, 68, 74, 75, 76, 84

- Nakagawa, H., and T. Tsujimoto, Sand bed instability due to bed load motion, *Journal of Hydraulic Engineering*, 106, 2023–2051, 1980. → pages 66, 68, 81
- Nakagawa, H., and T. Tsujimoto, Hydrodynamic drag force acting upon a spherical particle on a rough bed composed of identical particles, *Bulletin of the Disaster Prevention Research Institute*, 31, 115–130, 1981. → pages 4, 103
- Nelson, P. A., D. Bellugi, and W. E. Dietrich, Delineation of river bed-surface patches by clustering high-resolution spatial grain size data, *Geomorphology*, 205, 102–119, 2014. → pages 70, 114
- Newman, M. E., Power laws, Pareto distributions and Zipf's law, *Contemporary Physics*, 46, 323–351, 2005. → page 68
- Nikora, V., and D. Goring, Flow turbulence over fixed and weakly mobile gravel beds, *Journal of Hydraulic Engineering*, 128, 259–361, 2002. → page 109
- Nikora, V., D. Goring, I. McEwan, and G. Griffith, Spatially averaged open-channel flow over rough bed, *Journal of Hydraulic Engineering*, 127, 123–133, 2001a. → pages 4, 43
- Nikora, V., J. Heald, D. Goring, and I. McEwan, Diffusion of saltating particles in unidirectional water flow over a rough granular bed, *Journal of Physics A: Mathematical and General*, 34, 2001b. → pages 73, 74, 75, 84
- Nikora, V., H. Habersack, T. Huber, and I. McEwan, On bed particle diffusion in gravel bed flows under weak bed load transport, *Water Resources Research*, 38, 17–1–17–9, 2002. → pages 4, 43, 73, 74, 75, 84, 86
- Nikora, V. I., A. N. Sukhodolov, and P. M. Rowinski, Statistical sand wave dynamics in one-directional water flows, *Journal of Fluid Mechanics*, 351, 17–39, 1997. → pages 24, 109
- Niño, Y., and M. García, Using Lagrangian particle saltation observations for bedload sediment transport modelling, *Hydrological Processes*, 12, 1197–1218, 1998. → pages 3, 11, 17

- Niño, Y., and M. H. Garcia, Experiments on particle-turbulence interactions in the near-wall region of an open channel flow: Implications for sediment transport, *Journal of Fluid Mechanics*, 326, 285–319, 1996. → page 17
- Olinde, L., and J. P. L. Johnson, Using RFID and accelerometer-embedded tracers to measure probabilities of bed load transport, step lengths, and rest times in a mountain stream, *Water Resources Research*, 51, 7525–7589, 2015. → pages 51, 71, 84, 85
- Pähzt, T., A. H. Clark, M. Valyrakis, and O. Durán, The Physics of Sediment Transport Initiation, Cessation, and Entrainment Across Aeolian and Fluvial Environments, *Reviews of Geophysics*, 58, 2020. → page 46
- Paintal, A. S., A stochastic model of bed load transport, *Journal of Hydraulic Research*, 9, 527–554, 1971. → pages 2, 17, 18, 19, 50, 55, 76
- Papangelakis, E., and M. A. Hassan, The role of channel morphology on the mobility and dispersion of bed sediment in a small gravel-bed stream, *Earth Surface Processes and Landforms*, 41, 2191–2206, 2016. → pages 24, 74
- Papanicolaou, A. N., A. G. Tsakiris, M. A. Wyssmann, and C. M. Kramer, Boulder Array Effects on Bedload Pulses and Depositional Patches, *Journal of Geophysical Research: Earth Surface*, 123, 2925–2953, 2018. → pages 23, 48
- Parker, G., Surface-based bedload transport relation for gravel rivers, *Journal of Hydraulic Research*, 28, 417–436, 1990. → pages 3, 16
- Parker, G., and P. C. Klingeman, On why gravel bed streams are paved, *Water Resources Research*, 18, 1409–1423, 1982. → pages 114, 115
- Parker, G., C. Paola, and S. Leclair, Probabilistic exner sediment continuity equation for mixtures with no active layer, *Journal of Hydraulic Engineering*, 128, 801, 2002. → pages 21, 22, 46, 114
- Parker, G., G. Seminara, and L. Solari, Bed load at low Shields stress on arbitrarily sloping beds: Alternative entrainment formulation, *Water Resources Research*, 39, 1–11, 2003. → page 17

- Pechenik, L., and H. Levine, Interfacial velocity corrections due to multiplicative noise, *Physical Review E - Statistical Physics, Plasmas, Fluids, and Related Interdisciplinary Topics*, 59, 3893–3900, 1999. → page 47
- Pelosi, A., and G. Parker, Morphodynamics of river bed variation with variable bedload step length, *Earth Surface Dynamics*, 2, 243–253, 2014. → page 86
- Pelosi, A., R. Schumer, G. Parker, and R. I. Ferguson, The cause of advective slowdown of tracer pebbles in rivers: Implementation of Exner-Based Master equation for coevolving streamwise and vertical dispersion, *Journal of Geophysical Research: Earth Surface*, 121, 623–637, 2014. → pages 5, 68, 84, 85, 86
- Pender, G., T. B. Hoey, C. Fuller, and I. K. McEwan, Selective bedload transport during the degradation of a well sorted graded sediment bed, *Journal of Hydraulic Research*, 39, 269–277, 2001. → page 55
- Phillips, C. B., R. L. Martin, and D. J. Jerolmack, Impulse framework for unsteady flows reveals superdiffusive bed load transport, *Geophysical Research Letters*, 40, 1328–1333, 2013. → page 74
- Phillips, C. B., K. M. Hill, C. Paola, M. B. Singer, and D. J. Jerolmack, Effect of Flood Hydrograph Duration, Magnitude, and Shape on Bed Load Transport Dynamics, *Geophysical Research Letters*, 45, 8264–8271, 2018. → page 113
- Pielou, E. C., *Mathematical Ecology*, 1 ed., John Wiley & Sons Ltd., New York, NY, 1977. → pages 24, 57
- Pierce, J. K., and M. A. Hassan, Joint Stochastic Bedload Transport and Bed Elevation Model: Variance Regulation and Power Law Rests, *Journal of Geophysical Research: Earth Surface*, 125, 1–15, 2020a. → pages v, 84
- Pierce, J. K., and M. A. Hassan, Back to Einstein: Burial-Induced Three-Range Diffusion in Fluvial Sediment Transport, *Geophysical Research Letters*, 47, 2020b. → page v
- Pretzlav, K. L., J. P. Johnson, and D. N. Bradley, Smartrock Transport From Seconds to Seasons: Shear Stress Controls on Gravel Diffusion Inferred From Hop and Rest Scaling, *Geophysical Research Letters*, 48, 1–11, 2021. → pages 4, 5, 112

- Pretzlav, K. L. G., Armor Development and Bedload Transport Processes during Snowmelt and Flash Floods Using Laboratory Experiments, Numerical Modeling, and Field-Based Motion-Sensor Tracers, Doctoral dissertation, University of Texas, 2016. → pages 51, 71
- Pretzlav, K. L. G., J. P. L. Johnson, and D. N. Bradley, Smartrock transport in a mountain stream: bedload hysteresis and changing thresholds of motion, *Water Resources Research*, 56, 1–20, 2020. → page 3
- Prudnikov, A. P., I. A. Brychkov, O. I. Marichev, and G. G. Gould, *Integrals and Series Vol. 5: Inverse Laplace Transforms*, Gordon and Breach Science Publishers, Paris, 1992. → pages 7, 78, 154, 156, 160
- Recking, A., F. Liébault, C. Peteuil, and T. Jolimet, Testing bedload transport equations with consideration of time scales, *Earth Surface Processes and Landforms*, 37, 774–789, 2012. → pages 2, 23, 32, 88
- Recking, A., G. Piton, D. Vazquez-Tarrio, and G. Parker, Quantifying the Morphological Print of Bedload Transport, *Earth Surface Processes and Landforms*, 41, 809–822, 2016. → page 2
- Redner, S., *A Guide to First-Passage Processes*, 1st ed., Cambridge University Press, Cambridge, 2007. → pages 51, 65
- Redolfi, M., W. Bertoldi, M. Tubino, and M. Welber, Bed Load Variability and Morphology of Gravel Bed Rivers Subject to Unsteady Flow: A Laboratory Investigation, *Water Resources Research*, 54, 842–862, 2018. → page 23
- Reid, D. A., M. A. Hassan, S. Bird, and D. Hogan, Spatial and temporal patterns of sediment storage over 45 years in Carnation Creek, BC, a previously glaciated mountain catchment, *Earth Surface Processes and Landforms*, 44, 1584–1601, 2019. → page 113
- Rickenmann, D., and B. W. McArdell, Continuous measurement of sediment transport in the Erlenbach stream using piezoelectric bedload impact sensors, *Earth Surface Processes and Landforms*, 32, 1362–1378, 2007. → page 24
- Risken, H., *The Fokker-Planck Equation: Methods of Solution and Applications*, 2nd ed., Springer-Verlag, Ulm, 1984. → pages 7, 13, 95

- Roseberry, J. C., M. W. Schmeeckle, and D. J. Furbish, A probabilistic description of the bed load sediment flux: 2. Particle activity and motions, *Journal of Geophysical Research: Earth Surface*, 117, 2012. → pages 23, 24, 52, 76, 89
- Rossetto, V., The one-dimensional asymmetric persistent random walk, *Journal of Statistical Mechanics: Theory and Experiment*, 2018, 2018. → page 9
- Saletti, M., and M. A. Hassan, Width variations control the development of grain structuring in steep step-pool dominated streams: insight from flume experiments, *Earth Surface Processes and Landforms*, 45, 1430–1440, 2020. → page 86
- Saletti, M., P. Molnar, A. Zimmermann, M. A. . Hassan, and M. Church, Temporal variability and memory in sediment transport in an experimental step-pool cahnnel, *Water Resources Research*, 51, 9325–3337, 2015. → pages 33, 46, 48, 52, 69, 72
- Santos, B. O., M. J. Franca, and R. M. Ferreira, Coherent structures in open channel flows with bed load transport over an hydraulically rough bed, in *Proceedings of the International Conference on Fluvial Hydraulics, RIVER FLOW 2014*, pp. 883–890, Taylor & Francis, London, 2014. → page 2
- Sawai, K., Dispersion of Bed load Particles, *Bulletin of the Disaster Prevention Research Institute*, 37, 19–37, 1987. → pages 26, 53, 55
- Schmeeckle, M. W., Numerical simulation of turbulence and sediment transport of medium sand, *Journal of Geophysical Research: Earth Surface*, 119, 1240–1262, 2014. → pages 12, 92, 111
- Schmeeckle, M. W., and J. M. Nelson, Direct numerical simulation of bedload transport using a local, dynamic boundary condition, *Sedimentology*, 50, 279–301, 2003. → page 11
- Schmeeckle, M. W., J. M. Nelson, J. Pitlick, and J. P. Bennett, Interparticle collision of natural sediment grains in water, *Water Resources Research*, 37, 2377–2391, 2001. → pages 92, 104, 106
- Schmeeckle, M. W., J. M. Nelson, and R. L. Shreve, Forces on stationary particles in near-bed turbulent flows, *Journal of Geophysical Research: Earth Surface*, 112, 1–21, 2007. → pages 3, 50, 94, 103

Schmidt, M. G., F. Sagués, and I. M. Sokolov, Mesoscopic description of reactions for anomalous diffusion: A case study, *Journal of Physics Condensed Matter*, 19, 2007. → page 77

Schumer, R., M. M. Meerschaert, and B. Baeumer, Fractional advection-dispersion equations for modeling transport at the Earth surface, *Journal of Geophysical Research: Earth Surface*, 114, 1–15, 2009. → pages 21, 80, 86

Seizilles, G., E. Lajeunesse, O. Devauchelle, and M. Bak, Cross-stream diffusion in bedload transport, *Physics of Fluids*, 26, 2014. → pages 20, 89, 105

Sekine, M., and H. Kikkawa, Mechanics of saltating grains. II, *Journal of Hydraulic Engineering*, 118, 536–558, 1992. → pages 3, 11, 75, 105

Seminara, G., L. Solari, and G. Parker, Bed load at low Shields stress on arbitrarily sloping beds: Failure of the Bagnold hypothesis, *Water Resources Research*, 38, 31–1–31–16, 2002. → page 16

Serero, D., N. Gunkelmann, and T. Pöschel, Hydrodynamics of binary mixtures of granular gases with stochastic coefficient of restitution, *Journal of Fluid Mechanics*, 781, 595–621, 2015. → pages 92, 96

Shapiro, V. E., and V. M. Loginov, "Formulae of differentiation" and their use for solving stochastic equations, *Physica A: Statistical Mechanics and its Applications*, 91, 563–574, 1978. → page 151

Shih, W. R., P. Diplas, A. O. Celik, and C. Dancey, Accounting for the role of turbulent flow on particle dislodgement via a coupled quadrant analysis of velocity and pressure sequences, *Advances in Water Resources*, 101, 37–48, 2017. → pages 2, 70

Shlesinger, M. F., Asymptotic solutions of continuous-time random walks, *Journal of Statistical Physics*, 10, 421–434, 1974. → page 80

Shobe, C. M., J. M. Turowski, R. Nativ, R. C. Glade, G. L. Bennett, and B. Dini, The role of infrequently mobile boulders in modulating landscape evolution and geomorphic hazards, *Earth-Science Reviews*, 220, 103,717, 2021. → page 23

Singh, A., K. Fienberg, D. J. Jerolmack, J. Marr, and E. Foufoula-Georgiou, Experimental evidence for statistical scaling and

- intermittency in sediment transport rates, *Journal of Geophysical Research: Earth Surface*, 114, 1–16, 2009. → pages 33, 46, 48, 52, 58, 72
- Singh, A., F. Porté-Agel, and E. Foufoula-georgiou, On the influence of gravel bed dynamics on velocity power spectra, *Water Resources Research*, 46, 1–10, 2010. → page 2
- Singh, A., E. Foufoula-Georgiou, F. Porté-Agel, and P. R. Wilcock, Coupled dynamics of the co-evolution of gravel bed topography, flow turbulence and sediment transport in an experimental channel, *Journal of Geophysical Research F: Earth Surface*, 117, 1–20, 2012. → pages 52, 69, 72, 109
- Sivan, D., K. Lambeck, R. Toueg, A. Raban, Y. Porath, and B. Shirman, Ancient coastal wells of Caesarea Maritima, Israel, an indicator for relative sea level changes during the last 2000 years, *Earth and Planetary Science Letters*, 222, 315–330, 2004. → page 1
- Slater, L., G. Villarini, S. Archfield, D. Faulkner, R. Lamb, A. Khouakhi, and J. Yin, Global Changes in 20-Year, 50-Year, and 100-Year River Floods, *Geophysical Research Letters*, 48, 1–10, 2021. → page 1
- Slaymaker, O., T. Spencer, and C. Embleton-Hamann, Recasting geomorphology as a landscape science, *Geomorphology*, 384, 107,723, 2021. → page 1
- Sokolov, I. M., Models of anomalous diffusion in crowded environments, *Soft Matter*, 8, 9043–9052, 2012. → pages 8, 11, 43, 73
- Sornette, D., *Critical Phenomena in the Natural Sciences*, Springer, Berlin, 2006. → page 71
- Strahler, A. N., Dynamic basis of geomorphology, *Bulletin of the Geological Society of America*, 63, 923–938, 1952. → page 115
- Strom, K., A. N. Papanicolaou, N. Evangelopoulos, and M. Odeh, Microforms in gravel-bed rivers: formation, disintegration, and effects on bedload transport, *Journal of Hydraulic Engineering*, 130, 554–567, 2004. → pages 23, 48
- Sumer, B. M., L. H. Chua, N. S. Cheng, and J. Fredsøe, Influence of turbulence on bed load sediment transport, *Journal of Hydraulic Engineering*, 129, 585–596, 2003. → page 2

- Sun, Z., and J. Donahue, Statistically derived bedload formula for any fraction of nonuniform sediment, *Journal of Hydraulic Engineering*, 126, 105–111, 2000. → page 114
- Suweis, S., A. Porporato, A. Rinaldo, and A. Maritan, Prescription-induced jump distributions in multiplicative Poisson processes, *Physical Review E - Statistical, Nonlinear, and Soft Matter Physics*, 83, 1–8, 2011. → page 95
- Swift, R. J., A Stochastic Predator-Prey Model, *Bulletin of the Irish Mathematical Society*, 48, 57–63, 2002. → page 57
- Szabo, J., D. Lorant, and D. Loczy (Eds.), *Anthropogenic Geomorphology: A Guide to Man-Made Landforms*, Springer, New York, 2010. → page 1
- Takayama, S., Bedload movement in torrential mountain streams, *Tokyo Geographical Paper*, 9, 169–188, 1965. → page 5
- Taylor, G. I., Diffusion by continuous movements, *Proceedings of the London Mathematical Society*, s2-20, 196–212, 1920. → pages 11, 73
- Temme, N. M., *Special Functions: An Introduction to the Classical Functions of Mathematical Physics*, John Wiley & Sons Ltd., New York, 1996. → pages 79, 160
- Tregnaghi, M., A. Bottacin-Busolin, A. Marion, and S. Tait, Stochastic determination of entrainment risk in uniformly sized sediment beds at low transport stages: 1. Theory, *Journal of Geophysical Research: Earth Surface*, 117, 1–15, 2012. → page 19
- Tsakiris, A. G., A. N. Papanicolaou, and T. J. Lauth, Signature of bedload particle transport mode in the acoustic signal of a geophone, *Journal of Hydraulic Research*, 52, 185–204, 2014. → page 47
- Tsujimoto, T., Probabilistic model of bed load processes and its application to moving bed problem (In Japanese), Ph.D. thesis, Kyoto University, 1978. → page 22
- Tucker, G. E., and D. N. Bradley, Trouble with diffusion: Reassessing hillslope erosion laws with a particle-based model, *Journal of Geophysical Research*, 115, 1–12, 2010. → page 21
- Turowski, J. M., Probability distributions of bed load transport rates: A new derivation and comparison with field data, *Water Resources Research*, 46, 2010. → pages 24, 26, 29, 32, 33, 44, 46, 88

- Valyrakis, M., P. Diplas, C. L. Dancey, K. Greer, and A. O. Celik, Role of instantaneous force magnitude and duration on particle entrainment, *Journal of Geophysical Research: Earth Surface*, 115, 2010. → pages 2, 4, 31
- Van Den Broeck, C., On the relation between white shot noise, Gaussian white noise, and the dichotomic Markov process, *Journal of Statistical Physics*, 31, 467–483, 1983. → pages 6, 7, 95, 109, 173
- Van Kampen, N. G., *Stochastic Processes in Physics and Chemistry*, 3rd ed., Elsevier B.V., 2007. → pages 13, 27, 56, 151
- van Rijn, L. C., Sediment transport, part I: Bed load transport, *Journal of Hydraulic Engineering*, 110, 1431–1456, 1984. → pages 9, 11
- Venditti, J. G., P. A. Nelson, R. W. Bradley, D. Haught, and A. B. Gitto, Bedforms, structures, patches, and sediment supply in gravel-bed rivers, *Gravel-Bed Rivers: Process and Disasters*, pp. 439–466, 2017. → pages 2, 114
- Vicsek, T., and A. Zafeiris, Collective motion, *Physics Reports*, 517, 71–140, 2012. → page 86
- Voepel, H., R. Schumer, and M. A. Hassan, Sediment residence time distributions: Theory and application from bed elevation measurements, *Journal of Geophysical Research: Earth Surface*, 118, 2557–2567, 2013. → pages 51, 65, 66, 68, 71, 74, 81, 84, 85
- Vowinckel, B., T. Kempe, and J. Fröhlich, Fluid-particle interaction in turbulent open channel flow with fully-resolved mobile beds, *Advances in Water Resources*, 72, 32–44, 2014. → pages 12, 50
- Walther, G.-r., E. Post, P. Convey, A. Menzel, C. Parmesank, T. J. C. Beebee, J.-m. Fromentin, O. H.-g. I, and F. Bairlein, Ecological response to recent climate change, *Nature*, 416, 389–395, 2002. → page 1
- Warburton, J., Observations of bed load transport and channel bed changes in a proglacial mountain stream, *Arctic & Alpine Research*, 24, 195–203, 1992. → page 114
- Weeks, E. R., and H. L. Swinney, Anomalous diffusion resulting from strongly asymmetric random walks, *Physical Review E - Statistical Physics, Plasmas, Fluids, and Related Interdisciplinary Topics*, 57, 4915–4920, 1998. → pages 51, 76, 77, 78, 80, 83, 85, 163

- Weeks, E. R., J. S. Urbach, and H. L. Swinney, Anomalous diffusion in asymmetric random walks with a quasi-geostrophic flow example, *Physica D: Nonlinear Phenomena*, 97, 291–310, 1996. → pages 84, 85
- Weiss, G. H., The two-state random walk, *Journal of Statistical Physics*, 15, 157–165, 1976. → page 76
- Weiss, G. H., *Aspects and Applications of the Random Walk.*, North Holland, Amsterdam, 1994. → pages 76, 77, 78, 83, 156, 163
- Weiss, G. H., Some applications of persistent random walks and the telegrapher's equation, *Physica A: Statistical Mechanics and its Applications*, 311, 381–410, 2002. → pages 9, 41
- Wiberg, P. L., and J. D. Smith, A theoretical model for saltating grains in water., *Journal of Geophysical Research*, 90, 7341–7354, 1985. → pages 9, 11, 50
- Wilcock, P. R., Toward a practical method for estimating sediment-transport rates in gravel-bed rivers, *Earth Surface Processes and Landforms*, 26, 1395–1408, 2001. → page 3
- Wilcock, P. R., and J. C. Crowe, Surface-based transport model for mixed-size sediment, *Journal of Hydraulic Engineering*, 129, 120–128, 2003. → page 16
- Wilcock, P. R., and B. W. McArdell, Partial transport of a sand/gravel sediment, *Water Resources Research*, 33, 235–245, 1997. → pages 5, 19
- Wilcock, P. R., and J. B. Southard, Bed load transport of mixed size sediment: Fractional transport rates, bed forms, and the development of a coarse bed surface layer, *Water Resources Research*, 25, 1629–1641, 1989. → page 114
- Williams, S., and D. Furbish, Particle energy partitioning and transverse diffusion during rarefied travel on an experimental hillslope, *Earth Surface Dynamics Discussions*, pp. 1–33, 2021. → page 92
- Willis, K. J., and S. A. Bhagwat, Biodiversity and climate change, *Science*, 326, 806–808, 2009. → page 1
- Witz, M. J., S. Cameron, and V. Nikora, Bed particle dynamics at entrainment, *Journal of Hydraulic Research*, 57, 464–474, 2019. → page 83

- Wolman, M. G., and R. Gerson, Relative scales of time and effectiveness of climate in watershed geomorphology, *Earth Surface Processes*, 3, 189–208, 1978. → page 115
- Wolman, M. G., and J. P. Miller, Magnitude and Frequency of Forces in Geomorphic Processes, *The Journal of Geology*, 68, 54–74, 1960. → page 115
- Wong, M., and G. Parker, Reanalysis and correction of bed-load relation of Meyer-Peter and Mü;ller using their own database, *Journal of Hydraulic Engineering*, 132, 1159–1168, 2006. → page 23
- Wong, M., G. Parker, P. DeVries, T. M. Brown, and S. J. Burges, Experiments on dispersion of tracer stones under lower-regime plane-bed equilibrium bed load transport, *Water Resources Research*, 43, 1–23, 2007. → pages 26, 52, 53, 55, 56, 58, 69
- Wu, Z., E. Foufoula-Georgiou, G. Parker, A. Singh, X. Fu, and G. Wang, Analytical Solution for Anomalous Diffusion of Bedload Tracers Gradually Undergoing Burial, *Journal of Geophysical Research: Earth Surface*, 124, 21–37, 2019a. → pages 42, 51, 68, 75, 76, 81, 85, 86, 163, 164
- Wu, Z., A. Singh, X. Fu, and G. Wang, Transient Anomalous Diffusion and Advective Slowdown of Bedload Tracers by Particle Burial and Exhumation, *Water Resources Research*, 55, 7964–7982, 2019b. → pages 68, 81, 85
- Wu, Z., D. Furbish, and E. Foufoula-Georgiou, Generalization of Hop Distance-Time Scaling and Particle Velocity Distributions via a Two-Regime Formalism of Bedload Particle Motions, *Water Resources Research*, 56, 1–30, 2020. → page 105
- Yalin, M. S., An expression for bed-load transportation, *J. Hydraul. Div. Am. Soc. Civ. Eng.*, 89, 221–250, 1963. → page 11
- Yalin, M. S., *Mechanics of Sediment Transport.*, (1972), Pergamon Press, 1972. → pages xiv, 16, 18
- Yang, C. T., and W. Sayre, Stochastic Model for Sand Dispersion, *Journal of the Hydraulics Division*, 97, 265–288, 1971. → pages 4, 66, 68, 76
- Yang, F. L., and M. L. Hunt, Dynamics of particle-particle collisions in a viscous liquid, 2006. → pages 104, 106

- Yano, K., Tracer Studies on the Movement of Sand and Gravel, in
Proceedings of the 12th Congress IAHR, Vol 2., pp. 121–129, IAHR,
Kyoto, Japan, 1969. → pages 51, 74, 76, 84
- Youse, A., P. Costa, and L. Brandt, Single sediment dynamics in turbulent
flow over a porous bed - Insights from interface-resolved simulations,
Journal of Fluid Mechanics, 893, 1–28, 2020. → page 12
- Zaburdaev, V., M. Schmiedeberg, and H. Stark, Random walks with
random velocities, *Physical Review E - Statistical, Nonlinear, and Soft
Matter Physics*, 78, 1–5, 2008. → page 86
- Zaidi, A. A., B. Van Brunt, and G. C. Wake, Solutions to an advanced
functional partial differential equation of the pantograph type,
*Proceedings of the Royal Society A: Mathematical, Physical and
Engineering Sciences*, 471, 2015. → page 97
- Zhang, Y., M. M. Meerschaert, and A. I. Packman, Linking fluvial bed
sediment transport across scales, *Geophysical Research Letters*, 39, 1–6,
2012. → page 74
- Zimmermann, A. E., M. Church, and M. A. Hassan, Video-based gravel
transport measurements with a flume mounted light table, *Earth Surface
Processes and Landforms*, 33, 2285–2296, 2008. → page 47

Appendix A

Calculations involved in dynamical sediment flux model

A.1 Derivation of the master equation for particle position

Here I derive the master equation 2.2 for the probability distribution of particle position from the Langevin equation 2.1. This is closely based off of the approach in *Balakrishnan* (1993).

The master equation satisfies $P(x, t) = \langle\langle \delta(x - x(t)) \rangle\rangle_\eta$, where the averages are over all realizations of the two independent noises. It is most convenient to take these averages after taking Fourier transforms and manipulating time derivatives of the resulting equations.

Integrating the Langevin equation 2.1, substituting the solution in the above definition, and taking the Fourier transform in space gives

$$\tilde{P}(g, t) = \left\langle \left\langle \exp \left[-ig \int_0^t du [V + \sqrt{2D}\xi(u)]\eta(u) \right] \right\rangle_\eta \right\rangle_\xi \quad (\text{A.1})$$

This can be rearranged as

$$\tilde{P}(g, t) = \left\langle \exp \left[igV \int_0^t du \eta(u) \right] \left\langle \exp \left[ig\sqrt{2D} \int_0^t du \xi(u) \eta(u) \right] \right\rangle_\xi \right\rangle_\eta. \quad (\text{A.2})$$

Using the classic identity for an average over white noise of an exponential (*Balakrishnan*, 1993; *Van Kampen*, 2007) gives, after recognizing that the dichotomous noise satisfies $\eta^2 = \eta$ since η is either 0 or 1,

$$\tilde{P}(g, t) = \left\langle \exp \left[(igV - g^2 D) \int_0^t du \eta(u) \right] \right\rangle_\eta. \quad (\text{A.3})$$

Now I will take time derivatives in order to apply the so-called Furutsu-Novikov formula to evaluate the ensemble average over dichotomous noise (*Shapiro and Loginov*, 1978). Applied to the dichotomous noise in figure 1.2, the Furutsu-Novikov formula is, for an arbitrary functional F of the noise,

$$\partial_t \langle \eta(t) F[\eta(t)] \rangle = \langle \eta \partial_t F \rangle + k [\langle \eta \rangle \langle F \rangle - \langle \eta F \rangle]. \quad (\text{A.4})$$

Making the shorthands $G = igV - g^2 D$ and $F = \exp G \int_0^t \eta(u) du$ and taking as time derivative of eq. A.3 gives

$$G^{-1} \partial_t \tilde{P}(g, t) = \langle \eta F \rangle. \quad (\text{A.5})$$

Taking a second time derivative opens up the possibility of using the Furutsu-Novikov formula A.4:

$$G^{-1} \partial_t \tilde{P}(g, t) = \partial_t \langle \eta F \rangle = G \langle \eta F \rangle + k [\langle \eta \rangle \tilde{P}(g, t) - G^{-1} \partial_t \tilde{P}(g, t)]. \quad (\text{A.6})$$

Applying eq. A.5 finally gives

$$\partial_t^2 \tilde{P}(g, t) = (igV - g^2 D - k) \partial_t \tilde{P} + k_E (igV - g^2 D) \tilde{P}, \quad (\text{A.7})$$

and inverse Fourier transforming provides the master equation 2.2.

A.2 Solution for the position probability distribution

The position probability distribution can be obtained from eq. 2.2 for the initial conditions $P(x, 0) = \delta(x)$ and $\partial_t P(x, 0) = \frac{k_E}{k} [D\delta''(x) - V\delta'(x)]$ using Fourier transforms in space and Laplace transforms in time. Taking these transforms provides

$$\tilde{P}(g, s) = \frac{s + k + \varphi Dg^2 - igV\varphi}{s(s + k) + (Dg^2 - igV)(s + k_E)}, \quad (\text{A.8})$$

where $\varphi = k_D/k$ is the probability a particle starts at rest.

The numerator terms encode the initial conditions. The denominator terms are where the real structure of the solution is contained. The numerator terms involving g are easily expressed as first and second derivatives with respect to x . The problem, then is to calculate the inverse Fourier integral of the denominator. This can be conducted by finding the zeros of the denominator, expanding in partial fractions, then applying the contour integral (e.g. *Arfken*, 1985)

$$\int_{-\infty}^{\infty} \frac{1}{2\pi i} \frac{e^{-igx}}{g + ic} dg = \theta(x)e^{-cx}. \quad (\text{A.9})$$

Rearranging the governing equation gives

$$\tilde{P}(g, s) = \frac{\varphi Dg^2 - igV\varphi + s + k}{D(s + k_E)} \frac{1}{g^2 - i\frac{V}{D}g + \frac{s(s+k)}{D(s+k_E)}} \quad (\text{A.10})$$

The roots of the denominator are at

$$g_{\pm} = \frac{iV}{2D} [1 \pm R], \quad (\text{A.11})$$

where

$$R = \sqrt{1 + \frac{4D}{V^2} \frac{s(s+k)}{s+k_E}} \quad (\text{A.12})$$

The partial fractions expansion is therefore

$$\frac{1}{g^2 - i\frac{V}{D}g + \frac{s(s+k)}{D(s+k_E)}} = \frac{D}{iVR} \left[\frac{1}{g - g_+} - \frac{1}{g - g_-} \right] \quad (\text{A.13})$$

Giving

$$\tilde{P}(x, s) = \frac{-\varphi D \partial_x^2 + V \varphi \partial_x + s + k}{VR(s + k_E)} \left[\int \frac{dg}{2\pi i} \frac{e^{-igx}}{g - g_+} - \int \frac{dg}{2\pi i} \frac{e^{-igx}}{g - g_-} \right] \quad (\text{A.14})$$

or eventually

$$\tilde{P}(x, s) = \frac{-\varphi D \partial_x^2 + V \varphi \partial_x + s + k}{VR(s + k_E)} \left[\theta(x) \exp\left(\frac{Vx}{2D}(1-R)\right) + \theta(-x) \exp\left(\frac{Vx}{2D}(1+R)\right) \right]. \quad (\text{A.15})$$

This simplifies slightly to

$$\tilde{P}(x, s) = \frac{-\varphi D \partial_x^2 + V \varphi \partial_x + s + k}{VR(s + k_E)} \exp\left[\frac{Vx}{2D} - \frac{V|x|}{2D}R\right], \quad (\text{A.16})$$

where as a reminder, $\varphi = k_D/k$.

Taking the inverse Laplace transform symbolically provides the desired probability density function

$$P(x, t) = \mathcal{L}^{-1} \left\{ \frac{1}{V} \left[-\varphi D \partial_x^2 + V \varphi \partial_x + k + s \right] \exp\left(\frac{Vx}{2D}\right) \frac{\exp\left(-\frac{V|x|R}{2D}\right)}{(s + k_E)R} \right\} (t). \quad (\text{A.17})$$

Using the shift property of Laplace transforms (e.g. *Arfken*, 1985), this becomes

$$P(x, t) = \frac{1}{V} e^{-k_E t} \mathcal{L}^{-1} \left\{ \left[-\varphi D \partial_x^2 + V \varphi \partial_x + k_D + s \right] \exp\left(\frac{Vx}{2D}\right) \frac{\exp\left(\frac{-V|x|R_*}{2D}\right)}{s R_*} \right\}, \quad (\text{A.18})$$

where

$$R_* = \sqrt{1 + \frac{4D(k_D - k_E)}{V^2} + \frac{4D}{V^2} \left(s - \frac{k_E k_D}{s} \right)}. \quad (\text{A.19})$$

Using the property that $\mathcal{L}^{-1}\{s\tilde{f}\} = (\delta(t) + \partial_t)f(t)$ (*Arfken*, 1985) gives

$$P(x, t) = \frac{1}{V} e^{-k_E t} [-\varphi D \partial_x^2 + V \varphi \partial_x + k_D + \delta(t) + \partial_t] \exp\left[\frac{Vx}{2D}\right] \mathcal{L}^{-1}\left\{\frac{-\exp\left[\frac{-V|x|R_*}{2D}\right]}{sR_*}\right\}(t) \quad (\text{A.20})$$

Finally, using the identity

$$\mathcal{L}^{-1}\left\{\frac{1}{s}\tilde{g}(s - a/s)\right\} = \int_0^t \mathcal{I}_0\left(2\sqrt{au(t-u)}\right)g(u)du \quad (\text{A.21})$$

from *Bateman and Erdelyi* (1953), pg. 133 (which can be derived by either u-substitution or series expansion in powers of a) provides:

$$\begin{aligned} P(x, t) &= \frac{1}{V} e^{-k_E t} [-\varphi D \partial_x^2 + V \varphi \partial_x + k_D + \delta(t) + \partial_t] \exp\left[\frac{Vx}{2D}\right] \\ &\quad \times \int_0^t du \mathcal{I}_0\left(2\sqrt{k_E k_D u(t-u)}\right) \\ &\quad \times \mathcal{L}^{-1}\left\{\frac{\exp\left[\frac{-V|x|}{2D}\sqrt{a+bs}\right]}{\sqrt{a+bs}}\right\}(u) \quad (\text{A.22}) \end{aligned}$$

where $a = 1 + 4D(k_E - k_D)/(V^2)$ and $b = 4D/V^2$ are shorthands.

Using the trick of introducing a parameter and integrating over it to remove the square root from the denominator, the remaining transform can be evaluated from standard tables (*Prudnikov et al.*, 1992), eventually giving (after integration over and setting to 1 of the fake parameter),

$$\begin{aligned} P(x, t) &= [-\varphi D \partial_x^2 + V \varphi \partial_x + k + \delta(t) + \partial_t] \int_0^t \mathcal{I}_0\left(2\sqrt{k_E k_D u(t-u)}\right) e^{-k_E(t-u)} \\ &\quad \times \sqrt{\frac{1}{4\pi Du}} \exp\left[-k_D u - \frac{(x - Vu)^2}{4Du}\right] du, \quad (\text{A.23}) \end{aligned}$$

as reported in equation 2.13.

A.3 Calculation of the scale-dependent rate function $\Lambda(T)$

The central object required to calculate the sediment flux probability distribution in equation 2.3 is

$$\Lambda(T) = \rho \int_0^\infty dx_i \int_0^\infty dx P(x + x_i, T). \quad (\text{A.24})$$

This represents the rate at which particles starts at x_i , anywhere to the left of $x = 0$, and manage to cross $x = 0$ by time T .

Again it is easiest to conduct the necessary calculus after Laplace transforming. This gives

$$\tilde{\Lambda}(s) = \rho \int_0^\infty dx_i \int_0^\infty dx \tilde{P}(x + x_i, s). \quad (\text{A.25})$$

The Laplace transform of the rate function therefore follows after integrating equation A.16 twice.

Noting that $x + x_i$ is always positive, The first integration gives

$$\begin{aligned} \tilde{\Lambda}(s) &= \rho \int_0^\infty dx_i \exp \left[\frac{V(1-R)x_i}{2D} \right] \\ &\times \left(\varphi \frac{1-R}{2R(s+k_E)} - \frac{\varphi}{R(s+k_E)} - \frac{2D(s+k)}{V^2 R(1-R)(s+k_E)} \right), \end{aligned} \quad (\text{A.26})$$

and the second integration provides

$$\begin{aligned} \tilde{\Lambda}(s) &= -\frac{\rho\varphi D}{VR(s+k_E)} + \frac{2\rho D\varphi}{VR(1-R)(s+k_E)} \\ &+ \frac{4\rho D^2(s+k)}{V^3 R(1-R)^2(s+k_E)}. \end{aligned} \quad (\text{A.27})$$

Taking the inverse transform, converting the s factor in the numerator of the last term to $\partial_t + \delta(t)$, and using the shift property gives (e.g. *Arfken*,

1985)

$$\Lambda(t) = \rho \mathcal{L}^{-1} \left\{ -\frac{\varphi D}{VR_\star s} + \frac{2D\varphi}{VR_*(1-R_\star)s} + \frac{4D^2(\bar{\partial}_t + k)}{V^3 R_\star(1-R_\star)^2 s} \right\}. \quad (\text{A.28})$$

Here the notation $\bar{\partial}_t$ means the derivative acts from the left on all terms multiplying it (as in $f(t)\bar{\partial}_tg(t) = \partial_t[f(t)g(t)]$).

After some work, using eq. A.22 and tabulated Laplace transform pairs (e.g. Arfken, 1985; Prudnikov *et al.*, 1992) to perform the inverse Laplace transforms, the net result for the rate constant is

$$\begin{aligned} \Lambda(t) = \rho \int_0^t \mathcal{I}_0 \left(2\sqrt{k_E k_D u(t-u)} \right) e^{-k_E(t-u)-k_D u} \\ \times \left[\sqrt{\frac{D}{\pi u}} \left([\bar{\partial}_t + k]u - \frac{k_D}{2k} \right) e^{-V^2 u/4D} \right. \\ \left. + \frac{V}{2} \left([\bar{\partial}_t + k]u - \frac{k_D}{k} \right) \operatorname{erfc} \left(-\sqrt{\frac{V^2 u}{4D}} \right) \right] du, \quad (\text{A.29}) \end{aligned}$$

as reported in equation 2.18.

Equation 2.18 is difficult to work with. To explore the behavior at extreme values of the observation time T , one can apply Tauberian theorems (e.g. Weiss, 1994) to invert the Laplace-transformed rate function of equation A.27 at the opposite extreme of s .

For example, at short times, expanding equation A.27 as $s \rightarrow \infty$ gives

$$\tilde{\Lambda}(s) = \frac{\rho k_E V}{2ks^2} + \frac{\rho k_E}{k} \sqrt{\frac{D}{4s^3}} \quad (\text{A.30})$$

which inverts to

$$\Lambda(t) \sim \frac{\rho k_E VT}{2k} + \frac{\rho k_E}{k} \sqrt{\frac{DT}{\pi}}, \quad (\text{A.31})$$

giving the small T behavior. This has two scaling limits within it. Provided that $T \ll 4D/V^2/\pi < 2D/V^2$, the scaling goes as $\Lambda(T) \sim T^{-1/2}$. But if $T \gg 4D/V^2/\pi$, it goes as $\Lambda(t) \sim T$.

For large times, taking $s \rightarrow 0$ gives

$$\tilde{\Lambda}(s) = \frac{\rho k_E V}{ks^2}, \quad (\text{A.32})$$

and this inverts to $\Lambda(T) = \rho k_E V T / k$ as the long time solution, providing a mean flux equivalent to the Einstein model (sec. 1.1.3). These limits are summarized in equation 2.19.

Appendix B

Calculations involved in the sediment burial model

B.1 Calculation of the distribution function

Owing to the convolution structure of manuscript equations (1-3), their solution is a formidable problem. Luckily, we have the device of Laplace transforms. These project integro-differential equations into an alternate space in which convolutions are unraveled (e.g., *Arfken*, 1985). The double Laplace transform of a joint probability distribution $p(x, t)$ is defined by

$$\tilde{p}(\eta, s) = \int_0^\infty dx e^{-\eta x} \int_0^\infty dt e^{-st} p(x, t). \quad (\text{B.1})$$

The Laplace-transformed moments of x are linked to derivatives of the double transformed distribution (B.1) (cf., *Berezkhovskii and Weiss*, 2002). Equation (B.1) implies

$$\langle \tilde{x}(s)^k \rangle = (-)^k \partial_\eta^k \tilde{p}(\eta, s) \Big|_{\eta=0}. \quad (\text{B.2})$$

The operator $\langle \circ \rangle$ denotes the ensemble average (e.g., *Kittel*, 1958). This means we can compute the variance of position as $\sigma_x^2(t) = \langle x^2 \rangle - \langle x \rangle^2 = \mathcal{L}^{-1}\{\langle \tilde{x}^2 \rangle; t\} - \mathcal{L}^{-1}\{\langle \tilde{x} \rangle; t\}^2$, where \mathcal{L}^{-1} denotes the inverse Laplace transform

(e.g., *Arfken*, 1985). This is a powerful tool, since we can use it to derive the positional variance without integrating the distribution in equation (7) of the manuscript.

Double transforming manuscript equations (1-3) using the definition (B.1) gives

$$\tilde{\omega}_{1T}(\eta, s) = \theta_1 \tilde{g}_1(\eta, s) + \tilde{\omega}_2(\eta, s) \tilde{g}_1(\eta, s) - \tilde{\omega}_{1F}(\eta, s), \quad (\text{B.3})$$

$$\tilde{\omega}_{1F}(\eta, s) = \theta_1 \tilde{g}_1(\eta, s + \kappa) + \tilde{\omega}_2(\eta, s) \tilde{g}_1(\eta, s + \kappa), \quad (\text{B.4})$$

$$\tilde{\omega}_2(\eta, s) = \theta_2 \tilde{g}_2(\eta, s) + \tilde{\omega}_{1F}(\eta, s) \tilde{g}_2(\eta, s). \quad (\text{B.5})$$

This algebraic system solves for

$$\tilde{\omega}_{1T}(\eta, s) = \frac{\theta_1 + \theta_2 \tilde{g}_2(\eta, s)}{1 - \tilde{g}_1(\eta, s + \kappa) \tilde{g}_2(\eta, s)} \{ \tilde{g}_1(\eta, s) - \tilde{g}_1(\eta, s + \kappa) \}, \quad (\text{B.6})$$

$$\tilde{\omega}_{1F}(\eta, s) = \frac{\theta_1 + \theta_2 \tilde{g}_2(\eta, s)}{1 - \tilde{g}_1(\eta, s + \kappa) \tilde{g}_2(\eta, s)} \tilde{g}_1(\eta, s + \kappa), \quad (\text{B.7})$$

$$\tilde{\omega}_2(\eta, s) = \frac{\theta_2 + \theta_1 \tilde{g}_1(\eta, s + \kappa)}{1 - \tilde{g}_1(\eta, s + \kappa) \tilde{g}_2(\eta, s)} \tilde{g}_2(\eta, s). \quad (\text{B.8})$$

Double transforming manuscript equations (4-6) gives

$$\tilde{p}_0(\eta, s) = \frac{1}{s} \tilde{\omega}_{1T}(\eta, s), \quad (\text{B.9})$$

$$\tilde{p}_1(\eta, s) = \theta_1 \tilde{G}_1(\eta, s) + \tilde{\omega}_2(\eta, s) \tilde{G}_1(\eta, s), \quad (\text{B.10})$$

$$\tilde{p}_2(\eta, s) = \theta_2 \tilde{G}_2(\eta, s) + \tilde{\omega}_{1F}(\eta, s) \tilde{G}_2(\eta, s). \quad (\text{B.11})$$

The total probability is $p(x, t) = p_0(x, t) + p_1(x, t) + p_2(x, t)$. Using equations (B.6-B.11) this becomes, in the double Laplace representation,

$$\begin{aligned} \tilde{p}(\eta, s) &= \frac{1}{s} \frac{\theta_1 + \theta_2 \tilde{g}_2(\eta, s)}{1 - \tilde{g}_1(\eta, s + \kappa) \tilde{g}_2(\eta, s)} \{ \tilde{g}_1(\eta, s) - \tilde{g}_1(\eta, s + \kappa) \} \\ &+ \frac{\theta_1 [\tilde{G}_1(\eta, s) + \tilde{g}_1(\eta, s + \kappa) \tilde{G}_2(\eta, s)] + \theta_2 [\tilde{G}_2(\eta, s) + \tilde{g}_2(\eta, s) \tilde{G}_1(\eta, s)]}{1 - \tilde{g}_1(\eta, s + \kappa) \tilde{g}_2(\eta, s)}. \end{aligned} \quad (\text{B.12})$$

Plugging the propagators outlined in manuscript equations (8-9) into equation (B.12) gives

$$\tilde{p}(\eta, s) = \frac{1}{s} \frac{(s + \kappa + k')s + \theta_1(s + \kappa)\eta v + \kappa k_2}{(s + \kappa + k_1)\eta v + (s + \kappa + k')s + \kappa k_2}. \quad (\text{B.13})$$

In this equation, $k' = k_1 + k_2$, and we have used the normalization requirement of the initial probabilities: $\theta_1 + \theta_2 = 1$. The double inverse transform of this equation provides the distribution $p(x, t)$. We invert the transform over η first. Using the results 15.103 (transform of exponential), 15.123 (transform of derivative), and 15.141 (transform of Dirac delta function) from *Arfken* (1985) provides

$$\begin{aligned} \tilde{p}(x, s) &= \theta_1 \frac{s + \kappa}{s(s + \kappa + k_1)} \delta(x) + \frac{1}{v} \left(\frac{(s + \kappa + k')s + \kappa k_2}{s(s + \kappa + k_1)} \right. \\ &\quad \left. - \frac{\theta_1(s + \kappa)[s(s + \kappa + k_1) + \kappa k_2]}{s(s + \kappa + k_1)^2} \right) \exp \left[-\frac{(s + \kappa + k')s + \kappa k_2}{s + \kappa + k_1} \frac{x}{v} \right]. \end{aligned} \quad (\text{B.14})$$

Inverting the remaining transform over s , applying results 15.152 (substitution), 15.164 (translation), and 15.175 (transform of te^{kt}) from *Arfken* (1985), and defining the shorthand notations $\tau = k_1(t - x/v)$, $\xi = k_2x/v$, and $\Omega = (\kappa + k_1)/k_1$, gives the simpler form

$$\begin{aligned} p(x, t) &= \theta_1 \left[1 - \frac{k_1}{\kappa + k_1} (1 - e^{-(\kappa + k_1)t}) \right] \delta(x) + \frac{1}{v} \exp[\Omega\tau - \xi] \\ &\times \mathcal{L}^{-1} \left\{ \left(\theta_2 + \frac{\theta_1 k_1 + \theta_2 k_2}{s} + \frac{\theta_1 k_1 k_2}{s^2} + \frac{\theta_2 \kappa k_2}{s(s - \kappa - k_1)} + \frac{\theta_1 \kappa k_1 k_2}{s^2(s - \kappa - k_1)} \right) \right. \\ &\quad \left. \times \exp \left[\frac{k_1 \xi}{s} \right]; \tau/k_1 \right\}. \end{aligned} \quad (\text{B.15})$$

Using entries 2.2.2.1, 2.2.2.8, and 1.1.1.13 from *Prudnikov et al.* (1992) in conjunction with the definition of the Marcum Q-function $\mathcal{P}_\mu(x, t)$ (e.g., *Temme*, 1996), and inserting the Heaviside functions to account for the fact that grains can neither travel backwards nor at speeds exceeding v , we finally arrive at manuscript equation (10) for the joint distribution $p(x, t)$.

B.2 Calculation of the moments

We compute the first two moments of position x and ultimately its variance using equation (B.2). The first two derivatives of the double Laplace transformed distribution (B.13) are

$$\partial_\eta \tilde{p}(\eta, s) = -v \frac{1}{s} \frac{[(s + \kappa + k')s + \kappa k_2][\theta_2(s + \kappa) + k_1]}{[\eta v(s + \kappa + k_1) + (s + \kappa + k')s + \kappa k_2]^2}, \quad (\text{B.16})$$

$$\partial_\eta^2 \tilde{p}(\eta, s) = 2v^2 \frac{1}{s} \frac{(s + \kappa + k_1)[(s + \kappa + k')s + \kappa k_2][\theta_2(s + \kappa) + k_1]}{[\eta v(s + \kappa + k_1) + (s + \kappa + k')s + \kappa k_2]^3}. \quad (\text{B.17})$$

Evaluating these at $\eta = 0$ and applying equation (B.2) provides the Laplace transformed moments

$$\frac{\langle \tilde{x}(s) \rangle}{v} = \frac{1}{s} \frac{\theta_2(s + \kappa) + k_1}{(s + \kappa + k')s + \kappa k_2} = \frac{1}{s} \frac{\theta_2(s + \kappa) + k_1}{(s + a + b)(s + a - b)}, \quad (\text{B.18})$$

$$\frac{\langle \tilde{x}^2(s) \rangle}{2v^2} = \frac{1}{s} \frac{(s + \kappa + k_1)(\theta_2(s + \kappa) + k_1)}{[(s + \kappa + k')s + \kappa k_2]^2} = \frac{1}{s} \frac{(s + \kappa + k_1)(\theta_2(s + \kappa) + k_1)}{(s + a + b)^2(s + a - b)^2}. \quad (\text{B.19})$$

The parameters $a = (\kappa + k')/2$ and $b^2 = a^2 - \kappa k_2$ were introduced to factorize the denominators. These equations can be inverted using the properties 15.164 (translation), 15.11.1 (integration), and 15.123 (differentiation) from *Arfken* (1985) after expansion in partial fractions. For the mean, the calculation is

$$\frac{2b}{v} \langle x \rangle = [\theta_2 + (k_1 + \theta_2 \kappa) \int_0^t dt] \mathcal{L}^{-1} \left\{ \frac{1}{s + a - b} - \frac{1}{s + a + b}; t \right\} \quad (\text{B.20})$$

$$= \left[\theta_2 + \frac{k_1 + \theta_2 \kappa}{b - a} \right] e^{(b-a)t} - \left[\theta_2 - \frac{k_1 + \theta_2 \kappa}{a + b} \right] e^{-(a+b)t} - \left[\frac{k_1 + \theta_2 \kappa}{b - a} + \frac{k_1 + \theta_2 \kappa}{a + b} \right]. \quad (\text{B.21})$$

This equation rearranges to manuscript equation (11). The second moment (B.19) is

$$\begin{aligned} \frac{2b^2}{v^2} \langle x^2 \rangle &= \left[\theta_2(\delta(t) + \partial_t) + (\theta_2(2\kappa + k_1) + k_1) + (\kappa + k_1)(\theta_2\kappa + k_1) \int_0^t dt \right] \\ &\times \mathcal{L}^{-1} \left\{ \frac{1}{(s+a-b)^2} + \frac{1}{(s+a+b)^2} - \frac{1}{b(s+a-b)} + \frac{1}{b(s+a+b)}; t \right\}. \end{aligned} \quad (\text{B.22})$$

This becomes

$$\begin{aligned} \frac{2b^3}{v^2} \langle x^2 \rangle &= \left[\theta_2 \partial_t + [\theta_2(2\kappa + k_1) + k_1] + (\kappa + k_1)(\theta_2\kappa + k_1) \int_0^t dt \right] \\ &\times \left((bt-1)e^{(b-a)t} + (bt+1)e^{-(a+b)t} \right) \end{aligned} \quad (\text{B.23})$$

which evaluates to manuscript equation (12). Finally, $\sigma_x^2 = \langle x^2 \rangle - \langle x \rangle^2$ derives the variance in manuscript equation (13).

B.3 Limiting behavior of the moments

We determine the diffusion exponents γ in the local, intermediate, and global ranges using the two limiting cases described in the discussion of the manuscript. Limit (1) is $\kappa \rightarrow 0$. We take this limit in equations (B.18) and (B.19) with initial condition $\theta_1 = 1$ to obtain

$$\langle \tilde{x} \rangle = v k_1 \frac{1}{s^2(s+k')}, \quad (\text{B.24})$$

$$\langle \tilde{x}^2 \rangle = 2v^2 k_1 \frac{s+k_1}{s^3(s+k')^2}. \quad (\text{B.25})$$

Inverting these equations provides the variance

$$\sigma_x^2 = 2v^2 \frac{k_1}{k'^4} \left(k_1 \left[\frac{1}{2} - k' t e^{-k' t} - \frac{1}{2} e^{-2k' t} \right] + k_2 \left[-2 + k' t + (2+k' t) e^{-k' t} \right] \right). \quad (\text{B.26})$$

This result encodes two ranges of diffusion and can also be derived from the governing equations of the *Lisle et al.* (1998) and *Lajeunesse et al.* (2017)

models. Expanding for small t provides $\sigma_x^2(t) = v^2 k_1 t^3 / 3$ – local range super-diffusion. Expanding for large t provides $\sigma_x^2(t) = 2v^2 k_1 k_2 t / k'^3$ – intermediate range normal diffusion.

We further investigate limit (1) for arbitrary initial conditions. By applying Tauberian theorems, we assert the $t \rightarrow 0$ variance is determined by the $s \rightarrow \infty$ limits of (B.18) and (B.19) (e.g., *Weeks and Swinney*, 1998; *Weiss*, 1994). Expanding these equations in powers of $1/s$ and inverting the resulting transforms gives

$$\langle x \rangle = v\theta_2 t + \frac{1}{2}v(\theta_1 k_1 - \theta_2 k_2)t^2 + O(t^3), \quad (\text{B.27})$$

$$\langle x^2 \rangle = v^2 \theta_2 t^2 + \frac{1}{3}v^2(\theta_1 k_1 - 2\theta_2 k_2)t^3 + O(t^4). \quad (\text{B.28})$$

This equation highlights the effect of initial conditions on the diffusion characteristics of the local range:

$$\sigma_x^2(t) \sim v^2 \theta_1 \theta_2 t^2 + \frac{1}{3}v^2(\theta_1 k_1 + \theta_2 k_2)t^3. \quad (\text{B.29})$$

We have taken only leading order terms for any option of θ_1 and θ_2 . Equation (B.29) shows local range exponent $\gamma = 2$ when initial conditions are mixed (both are non-zero) and $\gamma = 3$ when initial conditions are pure (one is zero).

Limit (2) is $1/k_2 \rightarrow 0$ and $v \rightarrow \infty$ while $v/k_2 = l$. Under this limit, equations (B.18) and (B.19) provide

$$\langle \tilde{x} \rangle = k_1 l \frac{1}{s(s + \kappa)}, \quad (\text{B.30})$$

$$\langle \tilde{x}^2 \rangle = 2l^2 k_1 \frac{s + \kappa + k_1}{s(s + \kappa)^2}. \quad (\text{B.31})$$

Inverting these equations and introducing the variables $c = lk_1$ (an effective velocity) and $D_d = l^2 k_1$ (a diffusivity) provides positional variance

$$\sigma_x^2(t) = \frac{2D_d(1 - e^{-\kappa t})}{\kappa} + \frac{(1 - e^{-2\kappa t} - 2e^{-\kappa t}\kappa t)c^2}{\kappa^2}. \quad (\text{B.32})$$

This is mathematically identical to the key result of *Wu et al.* (2019a).

Expanding for small t provides $\sigma_x^2(t) = 2D_dt$ – intermediate range normal diffusion, while sending $t \rightarrow \infty$ provides $\sigma_x^2 = (2D_d\kappa + c^2)/\kappa^2$ – a constant variance in the geomorphic range. The global range is characterized by competition between terms in equation (B.32), and shows $2 \leq \gamma \leq 3$ depending on the ratio k_1/κ (cf., *Wu et al.*, 2019a). Finally, both equations (B.26) and (B.32) reduce to the Einstein result $\sigma_x^2(t) = 2D_dt$ in further simplified limits.

Appendix C

Calculations involved in the bed elevation model

C.1 Numerical simulation algorithm

The Gillespie Stochastic Simulation Algorithm (SSA) generates exact realizations of a Markov random process from a sequence of random numbers. It was originally developed for chemical physics by *Gillespie* (1977) and is reviewed in *Gillespie* (1992) and *Gillespie* (2007). The SSA hinges on the defining property of a Markov process. When the transition rates from one state to another are not dependent on the distant past, the process is Markov (e.g., *Cox and Miller*, 1965). The following sections demonstrate that the time intervals τ between subsequent transitions are exponentially distributed within the model of chapter 3. The SSA follows as a consequence of this property.

C.1.1 Times between transitions of any kind

The joint description of bedload transport and bed elevation changes is characterized by a set of states (n, m) where n and m are integers. The description involves four possible transitions (migration in, entrainment, deposition, migration out) with rates given in equations (3.2-3.5).

From the state (n, m) , the rate (probability per unit time) for any transition to occur is the sum over all possibilities:

$$A(n, m) = R_{MI}(n + 1, m|n, m) + R_E(n + 1, m - 1|n, m) \\ + R_D(n - 1, m + 1|n, m) + R_{MO}(n - 1, m|n, m). \quad (\text{C.1})$$

Using this, the probability that no transition occurs from the state (n, m) in a small time interval $\delta\tau$ is $1 - A(n, m)\delta\tau$. If $Q(\tau|n, m)$ denotes the probability density that a transition of any kind occurs from the state (n, m) after a time τ , the probability density that a transition happens after a slightly larger time $\tau + \delta\tau$ can be written

$$Q(\tau + \delta\tau|n, m) = [1 - A(n, m)\delta\tau]Q(\tau|n, m). \quad (\text{C.2})$$

Taking $\delta\tau \rightarrow 0$ produces a master equation $\frac{d}{d\tau}Q(\tau|n, m) = -A(n, m)Q(\tau|n, m)$, from which it follows that the time τ between subsequent transitions is distributed as

$$Q(\tau|n, m) = A(n, m)e^{-A(n, m)\tau}. \quad (\text{C.3})$$

This equation demonstrates that the time τ to the next transition from a state (n, m) is exponentially distributed with mean value $\bar{\tau} = 1/A(n, m)$. This means if the stochastic process transitioned to the state (n, m) at a time t , the next transition will occur at a time $t + \tau$ with τ a random variable drawn from the exponential distribution C.3.

C.1.2 Selection of transitions that occur

So far, equation C.3 demonstrates how to step the time from one transition to the next, but it remains unclear how to step the state variables n and m at each transition time. There is a need to characterize the type of transition which occurs at a given transition time.

Intuitively, this will depend on the relative magnitudes of the rates from equations (3.2-3.5). The transition with the highest rate is most likely to

occur. This is formalized by generating the ratios

$$S = \left\{ \frac{R_{MI}(n+1, m|n, m)}{A(n, m)}, \frac{R_E(n+1, m-1|n, m)}{A(n, m)}, \right. \\ \left. \frac{R_D(n-1, m+1|n, m)}{A(n, m)}, \frac{R_{MO}(n-1, m|n, m)}{A(n, m)} \right\}. \quad (\text{C.4})$$

By construction, $\sum S = 1$. Forming cumulative sums of the four ratios partitions the unit interval $[0, 1]$ into four chunks, each associated with a transition – either migration in, entrainment, deposition, or migration out. The transitions with the highest rates have the largest associated chunks. Drawing a random number on $[0, 1]$ can then select the transition which occurs at a given transition time by querying which chunk it falls within.

In summary, to step the process through a single transition, the SSA draws the time interval to the next transition from the distribution (C.3), draws a uniform random from $[0, 1]$, then uses this uniform random to select the transition that occurs from the cumulative sum of the ratios in (C.4). Iterating this random number generation and selection process simulates exact realizations of the stochastic process. These are series of n and m through time from which any statistics of interest can be calculated.

C.1.3 Pseudo code for the Gillespie SSA

Simulations are initialized by the initial conditions n_0 and m_0 , the model parameters used in equations 3.2-3.5, and the desired simulation duration t_{\max} . The SSA uses these inputs to generate time series of n and m as follows:

$t = 0$	
$n = n_0$	▷ Set the initial state (n_0, m_0)
$m = m_0$	
while $t < t_{\max}$; do	▷ Simulation will go until t surpasses t_{\max}
record (n, m, t)	▷ Build time series of n and m
draw τ from eq. (C.3)	▷ Select time to next transition

```

 $t := t + \tau$ 
draw a random number  $r$  in  $[0, 1]$        $\triangleright$  Select type of transition that
occurs
compute the ratios  $r_1, r_2, r_3, r_4$  in eq. (C.4)
form the cumulative sums  $r_i = \sum_{1 \leq j \leq i} r_j$   $\triangleright$  Now enact the transition
if  $0 \leq r < r_1$  then                                 $\triangleright$  Migration in
     $n := n + 1$ 
else if  $r_1 \leq r < r_2$  then                   $\triangleright$  Entrainment
     $n := n + 1$ 
     $m := m - 1$ 
else if  $r_2 \leq r < r_3$  then                   $\triangleright$  Deposition
     $n := n - 1$ 
     $m := m + 1$ 
else if  $r_3 \leq r \leq 1$  then                 $\triangleright$  Migration out
     $n := n - 1$ 
end if
end while

```

C.2 Approximate solutions of the Master equation

C.2.1 Mean field solution of particle activity

By assuming the dynamics of the particle activity are totally independent of the bed elevation and summing equation 3.7 over all values of m obtains a mean field equation for the particle activity:

$$0 = \nu A(n-1) + [\lambda + \mu(n-1)]A(n-1) + \sigma(n+1)A(n+1) \\ + \gamma(n+1)A(n+1) - (\nu + \lambda + \mu n + \sigma n + \gamma n)A(n). \quad (\text{C.5})$$

This can be solved by introducing the generating function (*Cox and Miller*, 1965) $G(x) = \sum_n x^n A(n)$, providing

$$0 = (\nu + \lambda)(x - 1)G + [\mu x^2 + \sigma + \gamma - (\mu + \sigma + \gamma)x] \frac{\partial G}{\partial x}, \quad (\text{C.6})$$

which is separable and integrates for

$$G(x) = \left(\frac{\gamma + \sigma - \mu}{\gamma + \sigma - \mu x} \right)^{\frac{\nu + \lambda}{\mu}} \quad (\text{C.7})$$

after applying the normalization condition $G(1) = 1$. From the definition of G it follows that $A(n) = \frac{1}{n!} \frac{d^n G}{dx^n}|_{x=0}$, giving the negative binomial distribution of particle activity demonstrated by *Ancey et al.* (2008) and stated in equation 3.10 and introduced originally in section 1.1.13.

C.2.2 Mean field solution of bed elevations

The negative binomial distribution provides $\langle n|m \rangle = \langle n \rangle$, so equation 3.7 produces

$$\begin{aligned} 0 &= [\lambda + \mu\langle n \rangle][1 + \kappa(m + 1)]M(m + 1) + \sigma\langle n \rangle[1 - \kappa(m - 1)]M(m - 1) \\ &\quad - \{[\lambda + \mu\langle n \rangle](1 + \kappa m) + \sigma\langle n \rangle(1 - \kappa m)\}M(m). \end{aligned} \quad (\text{C.8})$$

Identifying $E = \lambda + \mu\langle n \rangle$ and $D = \sigma\langle n \rangle$ and incorporating $E = D$ gives equation 3.11:

$$0 = [1 + \kappa(m + 1)]M(m + 1) + [1 - \kappa(m - 1)]M(m - 1) - 2M(m). \quad (\text{C.9})$$

This can be solved using the Fokker-Planck expansion (*Gardiner*, 1983) that effectively converts this discrete Master equation for m into a diffusion equation for the quasi-continuous variable $z = z_1 m$. This works since z_1 is small. Introducing z and writing $\bar{\kappa} = \kappa/z_1$ gives

$$0 = [1 + \bar{\kappa}(z + z_1)]M(z + z_1) + [1 - \bar{\kappa}(z - z_1)]M(z - z_1) - 2M(z). \quad (\text{C.10})$$

$\bar{\kappa}$ should not depend on z_1 since the magnitude of the feedbacks between bed elevations and entrainment and deposition rates depends on elevation changes, and not on the size of grains or the length of the control volume. Expanding the entire first and second terms to second order z_1 provides the Fokker-Planck equation

$$0 = -2\bar{\kappa}z_1[zM(z)]' + z_1^2M''(z). \quad (\text{C.11})$$

Taking into account that this distribution should be normalizable, $\lim_{z \rightarrow \pm\infty} M(z) = 0$, the solution is

$$M = M_0 e^{-\kappa(z/z_1)^2} \quad (\text{C.12})$$

as provided in chapter 3.

C.2.3 Closure equation approach for bed elevations

This section produces an approximate relationship to close $\langle n|m \rangle$ in terms of m valid to first order in κ . Writing

$$\langle n|m \rangle \approx \langle n \rangle - \kappa cm, \quad (\text{C.13})$$

for the mean particle activity conditional to the elevation m into 3.7, noting $E = D$, and neglecting terms of $O(\kappa^2)$ provides

$$\begin{aligned} 0 \approx & \left[1 + \kappa(m+1) \left\{ 1 - \frac{\mu c}{E} \right\} \right] M(m+1) + \left[1 - \kappa(m-1) \left\{ 1 + \frac{\sigma c}{E} \right\} \right] \\ & - \left[2 - \kappa m \left\{ \frac{(\sigma+\mu)c}{E} \right\} \right] M(m) \end{aligned} \quad (\text{C.14})$$

At this point, c is considered an undetermined positive constant that may depend on the entrainment, migration, and deposition rates. Taking the Fokker-Planck expansion and requiring the distribution $M(m)$ to vanish at infinity for normalization yields

$$0 = 2\kappa m \left(2 + \frac{(\sigma-\mu)c}{E} \right) M(m) + \left\{ \left[2 - \kappa m \frac{(\sigma+\mu)c}{E} \right] M(m) \right\}'. \quad (\text{C.15})$$

Finally, integrating, expanding to first order in κ , and exponentiating to solve for M produces

$$M(m) = M_0 \exp \left\{ -\kappa m^2 \left[1 + \frac{(\sigma - \mu)c}{2E} \right] \right\}. \quad (\text{C.16})$$

Since the numerical solutions show $\sigma_m^2 = \frac{1}{4\kappa}$, this suggests the closure relation

$$\langle n|m \rangle = \langle n \rangle \left(1 - \frac{2\kappa m}{1 - \mu/\sigma} \right) \quad (\text{C.17})$$

corresponding to $c = 2E/(\sigma - \mu)$. This is the closure relationship provided in equation 3.12 and plotted with the numerical simulations in figure 3.4.

Appendix D

Calculations involved in the Collisional Langevin model

D.1 Derivation of Master Equation

To derive the master equation from 5.3, we temporarily consider the Gaussian white noise (GWN) $\xi(t)$ as a Poisson jump process having rate r and jumps $\sqrt{2dh}$ with h distributed as $f(h)$. We will later take a GWN limit on this noise. With this assumption, integrating 5.3 over a small time interval δt considering the Ito interpretation for the collision term provides

$$u(t + \delta t) = \begin{cases} u(t) + \gamma\delta t & \text{with probability } 1 - r\delta t - \nu\delta t \\ u(t) + \sqrt{2dh} & \text{with probability } r\delta t \\ \varepsilon u(t) & \text{with probability } \nu\delta t \end{cases} \quad (\text{D.1})$$

Considering the probability $P(u, t + \delta)$ as sum over possible paths from

$P(u, t)$ develops

$$P(u, t + \delta t) = (1 - r\delta t - \nu\delta t) \int_{-\infty}^{\infty} dw \delta(u - w - \gamma\delta t) P(w, t) \quad (\text{D.2})$$

$$+ r\delta t \int_{-\infty}^{\infty} dw \int_{-\infty}^{\infty} dh f(h) \delta(u - w - \sqrt{2d}h) P(w, t) \quad (\text{D.3})$$

$$+ \nu\delta t \int_{-\infty}^{\infty} dw \int_0^1 d\varepsilon \rho(\varepsilon) \delta(u - w\varepsilon) P(w, t). \quad (\text{D.4})$$

Evaluating all integrals over δ -functions provides

$$P(u, t + \delta t) = (1 - r\delta t - \nu\delta t) P(u - \gamma\delta t, t) \quad (\text{D.5})$$

$$+ r\delta t \int_{-\infty}^{\infty} dh f(h) P(u + \sqrt{2d}h) \quad (\text{D.6})$$

$$+ \nu\delta t \int_0^1 \frac{d\varepsilon}{\varepsilon} \rho(\varepsilon) P\left(\frac{u}{\varepsilon}\right). \quad (\text{D.7})$$

Finally, we take $\delta t \rightarrow 0$ and limit the Poisson noise involving $\sqrt{2d}$ to a Gaussian white noise by taking $r \rightarrow \infty$ as $h \rightarrow 0$ such that $h^2 r = 1$ *Van Den Broeck* (1983). This process finally obtains the master equation (5.4).

D.2 Derivation of Steady-state solution

Defining $\tilde{P}(s) = \int_{-\infty}^{\infty} du e^{ius} P(u)$ as the Fourier transform (FT) of $P(u)$ and taking the FT of 5.4 develops the recursion relation

$$\tilde{P}(s) = \frac{\tilde{P}(s\varepsilon)}{q(s)}. \quad (\text{D.8})$$

where

$$q(z) = \tilde{D}z^2 - i\tilde{\Gamma}z + 1. \quad (\text{D.9})$$

Recurring $N + 1$ times provides

$$\tilde{P}(s) = \frac{\tilde{P}(s\varepsilon^{N+1})}{q(s\varepsilon^0)q(s\varepsilon^1)\dots q(s\varepsilon^N)}. \quad (\text{D.10})$$

The polynomials $q(z)$ can always be factored as $q(z) = d(z - i\lambda_-)(z - i\lambda_+)$ where

$$\lambda_{\pm} = \frac{\tilde{\Gamma}}{2\tilde{D}} \left[1 \pm \sqrt{1 + 4\tilde{D}/\tilde{\Gamma}^2} \right]. \quad (\text{D.11})$$

Using these factors to expand $\tilde{P}(s)$ in partial fractions provides

$$\tilde{P}(s) = \tilde{P}(s\varepsilon^{N+1}) \sum_{l=0}^N \left[\frac{R_l^-}{s\varepsilon^l - i\lambda_-} + \frac{R_l^+}{s\varepsilon^l - i\lambda_+} \right] \quad (\text{D.12})$$

where the coefficients R_l^{\pm} are the residues (at least up to a constant factor) of the product $[q(s\varepsilon^0) \dots q(s\varepsilon^N)]^{-1}$:

$$R_l^{\pm} = \left. \frac{s\varepsilon^l - i\lambda_{\pm}}{q(s\varepsilon^0) \dots q(s\varepsilon^N)} \right|_{s=i\lambda_{\pm}\varepsilon^{-l}}. \quad (\text{D.13})$$

The Fourier transform (D.10) has a convenient feature as $N \rightarrow \infty$: since $0 < \varepsilon < 1$, the prefactor $\tilde{P}(s\varepsilon^{N+1})$ becomes the normalization condition $\tilde{P}(0) = 1$ for the probability distribution $P(u)$ in the limit. Taking this limit and evaluating the residues provides

$$\begin{aligned} \tilde{P}(s) &= \frac{1}{\tilde{D}(\lambda_+ - \lambda_-) \prod_{m=1}^{\infty} q(i\lambda_- \varepsilon^m)} \sum_{l=0}^{\infty} \frac{i}{(s\varepsilon^l - i\lambda_-) \prod_{m=1}^l q(i\lambda_- \varepsilon^{-m})} \\ &+ \frac{1}{\tilde{D}(\lambda_+ - \lambda_-) \prod_{m=1}^{\infty} q(i\lambda_+ \varepsilon^m)} \sum_{l=0}^{\infty} \frac{-i}{(s\varepsilon^l - i\lambda_+) \prod_{m=1}^l q(i\lambda_+ \varepsilon^{-m})} \end{aligned} \quad (\text{D.14})$$

Finally, inverting the Fourier transforms term by term with contour integration (another use of the integral given in eq. A.9), and incorporating eq. (D.9), provides the steady-state solution (5.8).

D.3 Calculation of the moments

Taking (5.4), multiplying by u^k , integrating over all space, and taking account of normalization of $P(u)$ provides a recursion relation for the moments:

$$0 = \tilde{D}k(k-1)\langle u^{k-2} \rangle + \tilde{\Gamma}k\langle u^{k-1} \rangle + (\varepsilon^k - 1)\langle u^k \rangle. \quad (\text{D.15})$$

$k = 1$ provides the mean (given in eq. 5.10)

$$\langle u \rangle = \frac{\tilde{\Gamma}}{\nu(1 - \varepsilon)} = \frac{\tilde{\Gamma}}{1 - \varepsilon} \quad (\text{D.16})$$

while $k = 2$ provides the second moment

$$\langle u^2 \rangle = 2 \frac{\tilde{D} + \tilde{\Gamma}\langle u \rangle}{1 - \varepsilon^2}, \quad (\text{D.17})$$

leading to the velocity variance

$$\sigma_u^2 = \frac{2\tilde{D} + \tilde{\Gamma}^2}{1 - \varepsilon^2} \quad (\text{D.18})$$

given in equation 5.12.

D.4 Weak and strong collision limits

Now I demonstrate that weak collisions imply a Gaussian-like distribution for sediment velocities. The limit is challenging since the steady-state distribution 5.8 and the moments above all diverge as $\varepsilon \rightarrow 1$. Following *Hall and Wake* (1989), this suggests normalizing the distribution $P(u)$ using the scaled variables

$$z = \frac{u - \langle u \rangle}{\sigma_u}, \quad (\text{D.19})$$

and

$$Q(z) = \sigma_u P(u). \quad (\text{D.20})$$

This produces a differential equation for $Q(z)$ which is well-behaved in the elastic collision limit $\varepsilon \rightarrow 1$. Incorporating this transformation into (5.4) provides a “normalized” master equation

$$(1 - \varepsilon^2) \frac{\tilde{D}}{2\tilde{D} + \tilde{\Gamma}} Q''(z) - \frac{\tilde{\Gamma}\sqrt{1 - \varepsilon^2}}{\sqrt{2\tilde{D} + \tilde{\Gamma}^2}} Q'(z) - Q(z) + \frac{1}{\varepsilon} Q \left(z + \left[\frac{1 - \varepsilon}{\varepsilon} z + \frac{\tilde{\Gamma}\sqrt{1 - \varepsilon^2}}{\varepsilon\sqrt{2\tilde{D} + \tilde{\Gamma}^2}} \right] \right) = 0 \quad (\text{D.21})$$

This equation remains exact and is only a change of variables from (5.4). Now I approximate the equation for $\varepsilon \rightarrow 1$ by expanding the final term to second order around $z = 0$ before setting $\varepsilon = 1$, obtaining

$$Q''(z) + zQ'(z) + Q(z) = 0, \quad (\text{D.22})$$

which is the classic Ornstein-Uhlenbeck Fokker-Planck equation whose solution is the standard normal distribution for $Q(z)$ (e.g. *Gardiner*, 1983). This solution provides 5.14 when transformed back to the original variables $P(u)$ and u .